DECIPHERING THE ROLE OF TET2-MEDIATED DNA METHYLCYTOSINE OXIDATION IN CANCER IMMUNOTHERAPY

A Dissertation

by

MINJUNG LEE

Submitted to the Office of Graduate and Professional Studies of
Texas A&M University
in partial fulfillment of the requirements for the degree of

DOCTOR OF PHILOSOPHY

Chair of Committee,	Yun Huang
Committee Members,	Jichao Chen
	Margie Moczygemba
	Yubin Zhou
Head of Department,	Carol Vargas

August 2020

Major Subject: Medical Sciences

ABSTRACT

Immunotherapy is one of the fastest growing fields in cancer research and treatment. It largely relies on the immune system and is impacted by tumor infiltrated immune cells, which perform an important function in the tumor environment. Although researchers report great success in cancer treatment, immunotherapy has provided few patients with a favorable prognosis.

To maximize the efficacy of current cancer immunotherapy, researchers must understand how to regulate a different T cell status and how efficacy is affected by other factors. Accumulated studies reported dynamic changes in the epigenetic landscape during T cell development. This suggests that epigenetic regulation is one of the important aspects controlling the process of generating fully functional effector T cells, followed by exhaustion and clearing.

TET family enzymes are important epigenetic regulators closely linked to various cellular processes. Tet2 is a well-known tumor suppressor in various systems, including hematopoietic stem and progenitor cells, T cells, B cells and myeloid cells. However, recent studies reported that Tet2 deficiency in immune cells, including T cells and macrophages, benefit the anti-tumor immunity.

To demonstrate how Tet2 disrupted cytotoxic T cells affect cancer immunotherapy, we established a mouse immunotherapy model and found that a strong delay of melanoma progression in mice transferred with Tet2 deleted $CD8^+$ T cells. Further transcriptome and epigenome analysis revealed that Tet2 deleted tumor

infiltrating lymphocytes (TILs) showed augmented activation of immune related pathways. For further validation of the relationship between epigenome remodeling and Tet2-mediated 5hmC generation as well as manipulating Tet2 expression to maximize its beneficial effect on immunotherapy, I developed epigenome profiling technique called sCMS-IP seq and a drug-inducible epigenome editing tool called CiDER, respectively.

In sum, we demonstrated the therapeutic potential of Tet2 inactivation in a specific immune cell type during cancer immunotherapy. It must be noted, however, that Tet2 deficiency is closely associated with various hematology disorders. Therefore, practitioners must balance the tumor promoting and immune-boosting properties of Tet2 during cancer therapy. A temporally controllable system to inactivate Tet2 in specific immune cells might be optimal for pursuing future therapeutic intervention by targeting Tet2.

DEDICATION

I would like to dedicate this dissertation to my parents, for their unconditioned love and continuous supports. I also dedicate this to my lovely husband and son, for their endless love and encouragement.

ACKNOWLEDGEMENTS

First, I would like to thank my mentor, Dr. Yun Huang. Dr. Huang offered me a great opportunity to join her lab and gave me a valuable guidance for my research. She has taught me everything to be an independent researcher, from basic experimental skills to critical thinking. She always had an open door policy to discuss anything from scientific issue to personal life, which helped me a lot in a practical way. I sincerely hope our paths cross again in the future. I would also like to thank my committee members, Dr. Moczygemba, Dr. Zhou, and Dr. Chen, for their support and guidance throughout the course of this research.

Thanks go to all the Huang lab member. Thank you all for making my time at Texas A&M IBT a wonderful experience.

Thanks also go to my family, here and there. Thank you, mom and dad, and parents-in-law for everything, and for your love and support. Thank you, my sisters and brothers. Even with so much distance between us, you all are always there for me. Thank my Houston family, Namkyoung. Our great relationship is always a strength next to me throughout my life in Houston.

Last but not least, I specially thank to my husband, Seung Yeop for everything you have done for me. I could not have completed my Ph.D. without you. Thank you, my Son, Jiho for your literally unconditioned love. You are my everything! Love you all.

CONTRIBUTORS AND FUNDING SOURCES

Contributors

This work was supervised by a dissertation committee consisting of Professors Yun Huang [advisor] and Margie Moczygemba of the Center for Infectious and Inflammatory Diseases [Home Department] and Yubin Zhou of the Center for Translational Cancer Research [Home Department] and Professor Jichao Chen of the Department of Pulmonary Medicine [Outside Department].

The data analyzed for Next generation sequencing depicted in Chapter 3 was provided by Dr. Jianfang Li of the Center for Epigenetics and Disease Prevention.

All other works conducted for the dissertation was completed by the student, under the advisement of Dr. Yung Huang.

Funding Sources

Graduate study was supported by a fellowship from Texas A&M University.

This work was also made possible in part by grants from National Institute of Health grants [R01HL134780 and R01HL146852], the American Cancer Society [RSG-18-043-01-LIB], and by an allocation from the Texas A&M University start-up fund.

NOMENCLATURE

WT	Wild-type
CTLs	Cytolytic T Lymphocytes
IRs	Inhibitory Receptors
PD-1	Programmed cell Death 1
CTLA-4	Cytotoxic T Lymphocyte Antigen-4
RCC	Renal Cell Carcinoma
NSCLC	Non-Small Cell Lung Carcinoma
PI3K	Phosphatidylinositol 3-kinase
TILs	Tumor-Infiltrating Lymphocytes
TME	Tumor Microenvironment
Treg	Regulatory T cells
MDSCs	Myeloid-Derived Suppressor Cells
DNMTs	DNA methyltransferases
HSC	Hematopoietic Stem Cell
TCR	T-Cell Receptor
TSSs	Transcription Start Sites
5mC	5-methylcytosine
5hmC	5-hydroxymethylcytosine
TET	Ten-Eleven Translocation
MBP1	Methyl-CpG-Binding Protein

TDG	Thymine DNA Glycosylase
mESCs	Mouse Embryonic Stem Cells
MDS	Myelodysplastic Syndrome
MDSCs	Myeloid-Derived Suppressor Cells
CMML	Chronic Myelomonocytic Leukemia
AML	Acute Lymphocytic Leukemia
ALL	Acute Myeloid Leukemia
CAR	Chimeric Antigen Receptor
LOF	Loss-of-function
CD	Catalytic Domain
CMS	Cytosin 5-Methylenesulphonate
t-SNE	t-Distributed Stochastic Neighbor Embedding
DSBH	Double-Stranded Beta-Helix
FKBP12	FK506 Binding Protein 12
FRB	FKBP Rapamycin Binding domain
HEK293T	Human Embryonic Kidney 293T
DHMRs	Differentially Hydroxymethylated genomic Regions
ATAC-seq	Assay for Transposase-Accessible Chromatin using sequencing
PCA	Principal Component Analysis
KO	Knock-Out
TF	Transcription Factor
IACUC	the Institutional Animal Care Use Committee

DMEM	Dulbecco's Modification of Eagle's Medium
OVA	Ovalbumin
TNFα	tumor necrosis factor-alpha
IFNγ	interferon-gamma
DEGs	Differentially Expressed Genes
GSEA	Gene Set Enrichment Analysis

TABLE OF CONTENTS

Page

LIST OF FIGURES

Page

LIST OF TABLES

Page

CHAPTER I

INTRODUCTION

Immune therapy – Current Progress

Immunotherapy is one of the most rapidly growing fields in cancer research. Given its high promise to eradicate cancers, immunotherapy joined the mainstay treatments to become a new pillar of cancer treatment over the past years. It is now well known that tumor cells express distinctive antigens, which are recognized explicitly by adaptive immune system, such and T and B cells. This is called tumor-specific adaptive immunity.

The adaptive immune system plays a critical role in the antigen-specific immune response against cancer. $CD8^+$ cytotoxic T lymphocytes (CTLs) are combatants in the adaptive immunity force that attacks cancer. During cancer progression, as well as in chronic infections, CTLs may switch from a naïve state to an exhausted state. To maximize their capacity for fighting against cancer, $CD8^+$ T cells must be appropriately primed and maintained in the activated state, rather than being driven to the exhausted state and being clearing out.

T cell exhaustion is a dysfunctional state of T cell that occurs during many chronic infections and cancer[1, 2]. T cell exhaustion generally is defined by poor effector function, continuous expression of inhibitory receptors, and a distinctive transcriptional state, when compared with functional effector T cells[2]. Exhaustion prevents optimal control of infection and tumors. A crucial and unique feature of exhausted T cells is

sustained upregulation of cell surface inhibitory receptors (IRs) that include programmed cell death 1 (PD-1), cytotoxic T lymphocyte antigen-4 (CTLA-4), Lag-3, and Tim-3.

When IRs are engaged by their ligands, the ensuing signaling events will block the effector functions of activated T cells[3]. IRs discovered in exhausted T cells constitute the molecular basis of immune checkpoints that regulate the T cell effector function, which can be exploited for developing new therapeutic options[4]. Antibodies targeting those inhibitory pathways mainly block PD-1 and CTLA-4, leading to paradigm-shifting advances in cancer treatment by changing the focus from cancer cells to the manipulation of the immune system.

In the past decade, hundreds of clinical trials have shown that blocking the PD-1 pathway dramatically enhances immune cell functions by reversing exhausted T cells and reducing tumor burden in different types of cancer, including hematological malignancies, melanoma, renal cell carcinoma (RCC), and non-small cell lung carcinoma (NSCLC)[5]. However, a majority of patients still do not experience effective responses to anti-PD-1 treatment. Improved therapeutic strategies can be established by elucidating the molecular mechanisms underlying PD-1 mediated T cell exhaustion.

Although the PD-1 involved T cell exhaustion pathways remain to be fully defined, researchers have reported some critical factors related to this process. Intrinsically, T cells can be dysfunctional upon excessive or suboptimal antigen stimulation, followed by the continuous expression of IRs. Overexpressed PD-1 inhibits the activity of Akt, a crucial regulator of glucose metabolism of T cells, by preventing CD28-mediated activation of phosphatidylinositol 3-kinase (PI3K)[6]. This finding raises

the possibility that glucose metabolism may affect T cell exhaustion[7] and could explain, in part, how PD-1 inhibition reverses T cell dysfunction and exhaustion in cancer.

Different transcriptional states of IR-expressing T cells also affect the degree of exhaustion. In this connection, the transcription factor AP-1 binding site is found in the promoter regions of Pdcd-1 (mouse PD-1). Its subunit c-Fos induces PD-1 expression in tumor-infiltrating lymphocytes (TILs) by binding to the AP-1 binding site[8], suggesting that AP-1 directly regulates T cell exhaustion specifically in cancer cells. Also, in melanoma patients and tumor-bearing mouse models, PD-1 and other IRs-expressing cells produce smaller amounts of IFN-γ, TNF-α and IL-2, resulting in impaired T cell functions[3, 9]. The expression levels of PD-L1, a tumor side inhibitory ligand, are correlated inversely with the numbers of TILs in tumor tissues, suggesting that the advanced stage of exhausted T cells is the physical deletion of T cells from the lesion[1, 10].

Extrinsically, tumor microenvironment (TME) is the most important factor for regulating T cell exhaustion in cancer. TME consists of various cell types, such as cancer cells, inflammatory cells, basal stromal cells, and soluble factors like cytokines. All those components form a complex immunosuppressive network in cancer. Among them, regulatory T (Treg) cells, myeloid-derived suppressor cells (MDSCs), and suppressive cytokines, such as IL-10 and TGF-β, etc. are relatively well-defined for their roles in regulating tumor growth. Treg is an inhibitory subset of $CD4^+$ T cells that is closely related to peripheral tolerance maintenance and autoimmune disease prevention. Treg cells accumulate in tumor tissues and contribute to the immune evasion of cancer

cells. Treg cells usually express a high level of CD25 on their surface, resulting in excessive consumption of IL-2 and T cell dysfunction[11].

Similarly, the accumulation of myeloid-derived suppressor cells (MDSCs) also is known as a primary mechanism of tumor progression. MDSCs exhibit a high level of PD-L1 expression to cause T cell dysfunction via the PD-1 signaling pathway[12]. Immunosuppressive cytokines also play critical roles during the whole process of carcinogenesis, mainly by inhibiting key cytokines expression and inducing Treg cells[13]. Taken together, PD-1/PD-L1 blockade strategy possibly bars the pathways, as mentioned earlier, to achieve its therapeutic efficacy in cancer immunotherapy.

Although there are numerous achievements in the field of cancer immunotherapy, challenges remain. One of the major challenges is demonstrating the different regulation roles of various IRs. The current focus of the checkpoint blockade strategy is mostly on the PD-1 and CTLA-4 blockade. However, there are many IRs on exhausted T cells, such as LAG-3, Tim-3, TIGIT, and different populations of IRs combinations show distinctive phenotypes[14, 15].

The other aspect we need to consider is disturbing the immune balance. Reversing exhausted T cells in cancer may induce excessive cytotoxicity caused by over-activated T cells. For example, over boost of the immune system could result in tumor growth, as re-activated immune cells likely produce excessive pro-tumor factors that can provide the benefit to residual cancer cells[16].

To overcome the current limitations of cancer immunotherapy, researchers suggest various combination therapies. For example, there is widespread examination of

blocking additional IRs using monoclonal antibodies together with the PD-1 blockade. Other options are combination therapies with (1) inhibitors of soluble mediators, such as IL10, TGF-β; (2) agonists for targeting activated receptors on T cells; (3) adoptive CAR-T cell transfers; (4) anti-CCR4 monoclonal antibody to modulating Treg activity (Treg depletion)[17], combined with checkpoint blockade strategy. However, further studies are required to find factors closely related to these processes and detailed underlying molecular mechanisms in the checkpoint blockade strategy.

Epigenetic regulation and T cell development

Epigenetic modification is defined as heritable and stable alterations in gene expression and cellular function, not due to changes in a DNA sequence[18]. These processes alter accessibilities and structures of DNA and chromatin by regulating patterns of gene expression, rather than DNA sequence alteration.

DNA methylation, primarily catalyzed by DNA methyltransferases (DNMTs), is one of the crucial epigenetic modifications of the genome that is involved in regulating many cellular processes. These include embryonic development, transcription, chromatin structure, X chromosome inactivation, genomic imprinting, chromosome stability, and hematopoietic stem cell (HSC) development and differentiation[19-21]. Among them, hematopoiesis is regarded as a well-defined model for studying epigenetic modifications during cell fate determination. Evidence suggests that DNA methylation plays a crucial role in controlling not only HSC self-renewal, but also a commitment to myeloid and lymphoid fates[22, 23]. Notably, there is an urgent need to understand the epigenetic

modification of proper and effective differentiation of cytotoxic $CD8^+$ T cells, a major player in fighting cancer.

Appropriate adaptive immune functions are achieved by the successful generation of distinctive $CD8^+$ T cell subsets, functionally as well as phenotypically. Therefore, it is essential to understand how these different subsets of T cells are formed to control the immune system with maximized therapeutic effects.

The adaptive immune system shows remarkable plasticity during the immune response. When viral infection or cancer progression has occurred, antigen (either pathogen or tumor)-specific T cells undergo massive proliferation. This is followed by the acquisition of effector functions and migration into the site of infection or cancer. During this course of T cell activation, activated T cells provoke a wide range of alterations in gene expression, protein expression, cell cycle, and metabolism to generate various cells with distinctive cellular phenotype. All the cells in a living organism are genotypically identical; therefore, epigenetic regulation significantly contributes to the generation of diverse subsets of immune cells, using restricted genetic information.

Current evidence indicates that multiple signals, including T-cell receptor (TCR), inflammation, and co-stimulation metabolic pathways, are involved in controlling $CD8^+$ T cell fate determination[24, 25]. It is important to understand the key transcription factors that are known to regulate T cell fate decisions, as the aforementioned signals received by individual T cells set off diversified transcriptional programs. In addition, it is critical to understand the epigenetic regulation of these transcriptional changes. That is because epigenetic mechanisms allow signal transduction cascades, derived from common

transcription factors, to promote cell type-specific responses. Also, they provide a mechanism for heritable maintenance of cell type specific gene expression, when primary instigating signals are depleted[26].

DNA methylation is one of the extensively studied epigenetic mechanisms. Most DNA methylation analyses focus on CpG islands, CG dinucleotide dense regions in which the transcription start sites (TSSs) are located. In general, DNA methylation is correlated with transcriptional repression. This phenomenon is valid during the $CD8^+$ T cell differentiation process. Genome-wide DNA methylation status profiles show that DNA methylation is reduced at the promoter regions of actively transcribed genes during differentiation, and increased at the promoters of genes that are silenced or show decreased expression levels[27, 28].

It should be noted that DNA methylation can occur throughout the genome, which contains intergenic region as well as gene bodies[29]. As a result, the genome-wide level of methylation analysis should be performed, rather than regional locus specific analysis, in order to decipher the comprehensive meaning of DNA methylation in terms of T cell differentiation.

The epigenetic patterns in specific stages during differentiation of T cells from naïve to memory and effector T cells show distinctive traits (Figure 1-1). For example, DNA methylation is reprogrammed globally during effector $CD8^+$ T cell differentiation. The number of effector-gene-associated transcription factors, such as EOMES and effector genes, including GZMA/B and IFNG, exhibited increased gene expression and decreased promoter DNA methylation level[27]. Interestingly, memory-cell-associated

factors and specific gene sets, such as TNFA and CCR7, that are highly expressed in memory subsets, indicated decreased expression level in effector $CD8^+$ T cells[30].

The overall understanding of DNA methylation on gene expression has linked methylation of CpG sites at the promoter regions with a decrease in gene expression. However, recent evidence indicates that there is a substantial amount of positive association between DNA methylation either, within promoter regions, or gene body regions and gene expression. This conflicts with a commonly recognized negative correlation. What remains is to define further the mutual relation between DNA methylation and T cell differentiation.

Evidence has shown that 5-methylcytosine (5mC), a major player of DNA methylation and also widely observed 5-hydroxymethylcytosine (5hmC), a first intermediate component of active DNA demethylation mediated by Ten-eleven translocation (TET) family enzymes, are found in both intergenic regions and gene bodies. They have critical functions in transcriptional activities during T cell fate decision[29, 31].

Both DNA methylation and demethylation can affect transcriptional activity through direct and indirect mechanisms. Methylated DNA can change the binding affinity with transcription factors (direct)[32]. It interacts with methyl-CpG-binding protein (MBP1) to recruit histone modifying enzymes that show repressive effect (indirect)[33]. The first step in manipulating the immune system for maximizing therapeutic efficiency is understanding the epigenetic regulation of cell fate decisions and appropriate immune cell population formation (Figure 1-1). Consequently, it is a rapidly growing field with

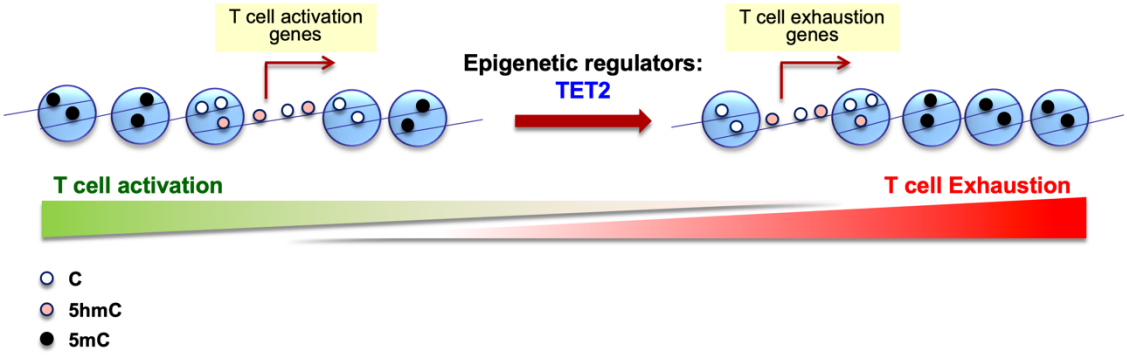

Figure 1-1. Schematic cartoon for the epigenetic regulation of cell fate decisions. TET2 is suggested as one of the possible candidates of epigenetic regulators to determine the state of immune cells.

the connection of recent cancer immunotherapy. But detailed mechanisms are still largely unknown.

TET2 – a methyl cytosine dioxygenase

DNA methylation is a crucial epigenetic modification of the genome that is involved in regulating many cellular processes. These include embryonic development, transcription, chromatin structure, X chromosome inactivation, genomic imprinting, and chromosome stability[19]. Consistent with these important roles, researchers have found a growing number of human diseases, like cancer, to be associated with aberrant DNA methylation.

The major player of DNA methylation is 5-methylcytosine (5mC). DNA methylation mostly refers to the addition of a methyl (CH3) group to the carbon-5 position of a cytosine ring. This conversion is catalyzed by DNA methyltransferases (DNMTs). These modified cytosine residues usually lie next to a guanine base to form

the CpG islands. Although methylated cytosine is stable chemically[34] and genetically[35], 5mC still can be converted back to the unmodified state.

Ten-eleven translocation (TET1, TET2, and TET3)-family of Fe(II)-dependent and 2-oxoglutarate-dependent dioxygenases make up a new class of enzymes that successively oxidizes 5-methylcytosine (5mC) to 5-hydroxymethylcytosine (5hmC), 5-formylcytosine (5fC), and 5-carboxylcytosine (5caC) in the mammalian genome (Figure 1-2). These 5mC oxidation products are not only intermediates in the DNA

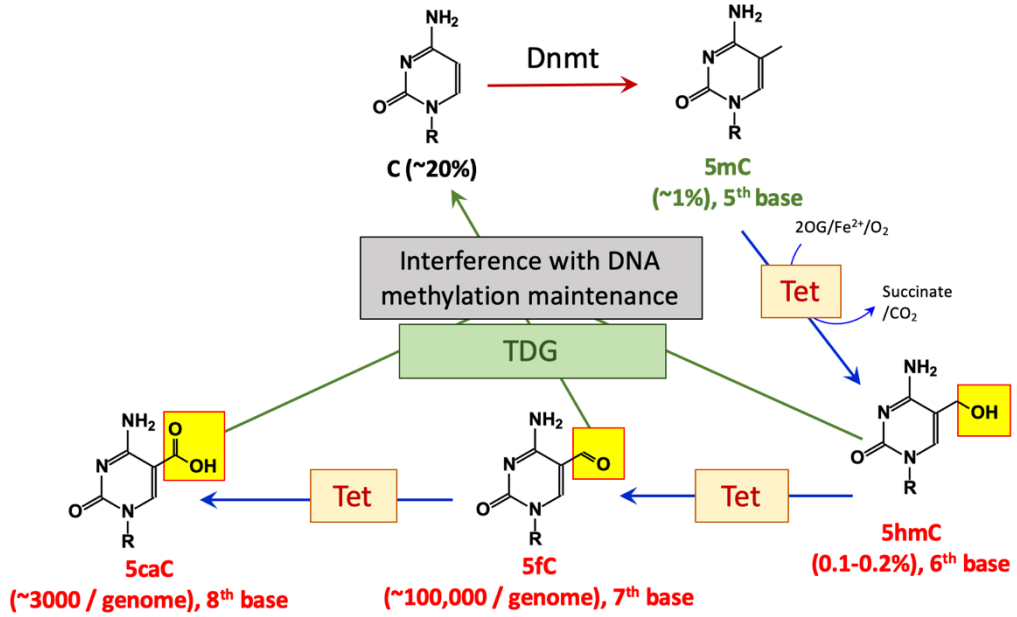

Figure 1-2. The DNA methylation-demethylation cycle in mammalian cells. DNA methyltransferases (DMNTs) methylate cytosine (C) to yield 5-methylcytosine (5mC); TET enzymes successively oxidize 5mC to "oxi-mC" species, including 5-hydroxymethylcytosine (5hmC), 5-formylcytosine (5fC) and 5-carboxylcytosine (5caC). 5fC and 5caC can be converted to C in multiple pathways of DNA demethylation: First, all 3 oxidized bases interfere with maintenance DNA methylation mediated by DNMT1/ UHRF1, resulting in passive DNA demethylation; second, thymine DNA glycosylase (TDG) can excise 5fC and5caC, which can be replaced by C through base excision repair. Disruption of this cycle due to abnormal activities of TET and/or DNMT proteins is often associated with the onset and progression of blood cancers.

methylation/demethylation cycle but, also function as novel epigenetic marks[36, 37]. TET-mediated oxidation of 5mC leads to replication-dependent dilution or thymine DNA glycosylase (TDG)-dependent base excision repair process to convert 5mC to unmodified cytosine.

Similar to DNA methylation, DNA demethylation, mediated by TET proteins, also have crucial biological functions. TET proteins and 5mC derivatives are essential in development, as well as in other disease states. Based on its dominant distribution, each TET protein has distinctive roles. Tet1 is a major TET protein found in embryonic stem cells and involved in germinal layer differentiation. TET2 is highly correlated with hematopoietic cell lineage and myeloid cancer. TET3 is the only TET protein that is found in a gamete. Active DNA demethylation of the paternal chromosomes is an important part of the early development of the fertilized zygote[38-42]. However, there is still the need to elucidate the relative importance of each member of TET within a specific cell type. Moreover, while they have varying expression levels and recruitment mechanisms, in some cases, the deletion of one or multiple TET enzymes can be compensated by others[43].

The past decade has seen the rapid development of whole-genome based DNA modification profiling techniques with high resolution[44-46]. Those technological advances in mapping and tracing the 5hmC have been used successfully to profile hydroxymethylome in various systems, including mouse embryonic stem cells (mESCs) and hematopoietic stem cells (HSCs)[47, 48]. Research revealed that 5hmC is enriched in gene bodies, promoters, transcription start sites (TSSs), and enhancer elements of active

genes in ESCs[48]. Furthermore, TET protein-mediated DNA hydroxymethylation is crucial for the regulation of chromatin accessibility[49]. TET proteins also interact with histone modification enzymes, such as HDAC2[50], to modulate gene expression. In addition to regulating DNA methylation, TET proteins modulate RNA cytosine methylation during gene transcription[51, 52]. Advanced sequencing technology makes it possible to appreciate more novel functions of the TET protein family.

Although TET family proteins share catalytic activity, each TET protein is functionally nonredundant. It has been reported that combined TET activity is crucial for appropriate embryonic development[43]. However, in the hematopoietic system, each TET has distinctive roles[53-55]. TET2 is the most highly expressed TET protein in the hematopoietic system and is indispensable for normal hematopoiesis[17-19]. Genetic TET2 deficiency in mice gives rise to increased self-renewal of hematopoietic stem cells HSCs and biased differentiation of HSCs toward the myeloid lineage, which indicates HSCs are uniquely sensitive to changes in TET2 activity. Somatic alterations in TET2 are frequently observed in patients with lymphoid or myeloid malignancies[56, 57]. TET2 mutations are the most common genetic disorder found in myelodysplastic syndrome (MDS), chronic myelomonocytic leukemia (CMML), and adult acute myeloid leukemia (AML)[58, 59]. Also, TET2 loss-of-function (LOF) is often found in B-cell and T-cell lymphoma, as well as peripheral T-cell lymphoma with relatively less frequency. Therefore, TET2 deficiencies are involved in various hematopoietic disease processes rather than limited to a specific disease subtype, and it suggests TET2 is an important tumor suppressor within the hematopoietic system. Besides, in the murine system, Tet2

ablation in murine $CD4^+$ T cells has been reported to result in imbalanced $CD4^+$ T cell polarization and to impair cytokine production[60], and Tet2 deletion in $CD8^+$ T cells also results in abnormal memory $CD8^+$ T cells during chronic infection[61], suggesting that TET2 has crucial roles for properly controlling competent immune cell function.

However, there are now several lines of evidence that imply an anti-tumor activity of TET2 deficiency. Tet2 loss in murine myeloid cells suppressed melanoma growth in vivo and suggesting the tumor-promoting function of TET2. Another compelling evidence is that Tet2 deficiency promotes $CD8^+$ T cell memory differentiation without disturbing cell expansion or effector function, and those established Tet2 loss memory T cells exhibit remarkable pathogen control, demonstrating that TET2 is an important regulator of $CD8^+$ T cell fate decisions that can be used therapeutically.[61] In addition, in the clinical setting, TET2-disrupted chimeric antigen receptor (CAR) T-cells s were found to exhibit potent therapeutic efficacy in the blood cancer patient[62]. Conclusively, those impressive results suggest a tumor-promoting function of TET2, and TET2 disruption can benefit anti-tumor immunotherapy. These contradictory experimental results imply that TET2 acts as a "double-edged sword." TET2 maintains normal hematopoiesis, and LOF of TET2 in humans tends to increase the susceptibility of blood cells toward malignant transformation[36, 37, 63]. On the other hand, TET2 disruption benefits the cancer immunotherapy by enhancing the activity of cells of the immune system against tumor[62, 64]. Therefore, precise control of TET2 activity is important to maximize its benefit in cancer immunotherapy.

CHAPTER II

DEVELOPING EPIGENOME EDITING AND PROFILING TECHNIQUES TO DISSECT THE EIGENOME REMODELLING FUNCTION OF TET2*

Introduction

DNA methylation is a biological process that can change gene expression without changing the sequence. DNA methylation mainly occurs at cytosine base. Briefly, a methyl group is added to the carbon 5 position of cytosine by DNA methyltransferases (DNMTs) to form 5-methylcytosine (5mC) This process is one of the heritable epigenetic marks and closely related with other epigenetic modification, such as histone code, nucleosome positioning, polycomb complexes, noncoding RNA, and chromatin remodeling proteins, as a component of the chromatin structure. Researchers generally believe that a substantial number of human diseases, including cancer, are associated with aberrant DNA methylation[36]. The Ten-eleven translocation (TET) family of 5mC dioxygenases catalyzes the conversion of 5mC into 5-hydroxymethylcytosine (5hmC) and further oxidized species to promote active DNA demethylation[37].

The discovery of TETs have sparked intense interest in the epigenetic field to unveil the biological functions of TET proteins and their major catalytic product 5hmC.

---

* Part of this chapter is reprinted with permission from "Engineered Split-TET2 Enzyme for Inducible Epigenetic Remodeling." By Lee, M., Li, J., Liang, Y., Ma, G., Zhang, J., He, L., Liu, Y., Li, Q., Li, M., Sun, D., Zhou, Y., Huang, Y., 2017. *J Am Chem Soc*, 139(13):4659-4662, Copyright [2017] by Minjung Lee and Yun Huang.

5hmC is regarded to serves as an intermediate during TET-mediated active DNA demethylation[65-67], as well as a stable epigenetic mark[68-71]. It has been observed widely that DNA hydroxymethylation is highly correlated with gene expression and some human disorders[36, 56, 72]. However, is challenging to establish the causal relations between epigenetic modifications on DNA and the phenotypes, largely owing to the lack of reliable tools to accurately add or remove DNA modifications in the genome at defined temporal and spatial resolution.

In addition, there has been contradictory evidence about the role of TET2 in some cancer types. Among the TET family enzymes, TET2 is highly correlated with hematopoietic cell lineage, as well as malignancies. Researchers report that Tet2 mutation in HSC confers enhanced self-renewal and clonal expansion during hematopoiesis, and that Tet2 mutations and hematological malignancies are highly correlated[57, 73, 74]. Therefore, TET2 is thought to be an important tumor suppressor within the hematopoietic system. However, accumulating evidence suggests an anti-tumor activity of TET2 deficiency in both human and mouse models[61, 62, 64]. In order to utilize the beneficial effects of Tet2 in cancer treatment, it is important to control Tet2 activity precisely.

It is now known whether TET proteins generating 5hmC act as a base that presents in mammalian genomes at significant levels. 5hmC has multiple biological features, as distinct from 5mC. Expression levels of 5hmC in the genome in different tissues are quite varied. They are related closely to several normal developmental processes, such as in mouse embryonic stem cells (mESCs)[37]. Moreover, 5hmC levels

are significantly lower in different types of cancers, including myeloid malignancies, and some solid types of tumors, such as breast and colon cancers, implying the possibility that the level of 5hmC is linked to cancer progression.

To understand biological functions of 5hmC in detail, it is necessary to delineate 5hmC distribution genome widely. Currently used anti-CMS-IP seq method, developed by the Rao group[46], has several limitations, especially in that it requires a relatively large amount of starting materials. Therefore, there is an urgent need to develop an improved method to profile 5hmC with a low amount of DNA in order to handle properly a limited quantity of precious patient and in vivo samples.

Materials and Methods

Design and construction of CiDER

The mammalian expression vector pCMVTnT was purchased from Promega. TET2 catalytic domain (TET2CD) was amplified from TET2 cDNA by using a KOD hot start DNA polymerase (EMD Millipore, Billerica, MA, USA) inserted between XhoI-KpnI restriction sites in the backbone of pCMVTnT. The researcher added a Myc-tag (EQKLISEEDL), a nuclear localization signal from SV40 (KRPAATKKAGQAK), and a linker (GGSASGGS) to the N-terminus of TET2CD. There was a subsequent insertion of mCherry tot he C-terminus between KpnI-NotI sites. Two versions of (Δ1482-1839, Δ1463-1839) truncated TET2CD constructs were made with standard PCR procedures. Additionally, cDNAs encoding the chemical dimerization module FKBP-2A-FRB were purchased as a gBlocks Gene Fragments (Integrated DNA Technologies). These were inserted individually into the 6 selected split sites within TET2CD (positions 1258, 1390, 1430, 1462, 1482, and 1839; primers listed in Table1) within the AscI-XmaI restriction sites.

Cell culture and plasmid transfection

HeLa and human embryonic kidney HEK293T cell lines from the American Type Culture Collection (ATCC) were cultured in Dulbecco's modified Eagle's medium (DMEM, Sigma-Aldrich), supplemented with 10% heat-inactivated fetal bovine serum, 100 U/ml penicillin/ streptomycin at 37 °C with 5% CO2. Transfection was performed by using lipofectamine 3000 (Life Technologies), following the manufacturer’s

recommended protocol. We used 200-500 ng DNA for each well of a 24-well plate. Then 200nM rapamycin or AP1903 (Sigma-Aldrich) was applied to the cells. The culture media were replaced every 24 hours with fresh media containing 200 nM rapamycin or AP-1903.

Table 1. Primer list

L 1258	Forward	Cttctt GGCGCGCC CTCACCAAT CGCCGGTGTGCC
	Reverse	Cttctt CCCGGG CGTGCCGTATTTCCTCAGCGTC
N 1390	Forward	Cttctt GGCGCGCC AAT GGCAGCACATTGGTA TGCAC
	Reverse	Cttctt CCCGGG CTGCATGTTGTGCAAGTCTCTGTG
G 1430	Forward	Cttctt GGCGCGCC GGGAGTGTGGAAGCTCAGGAG
	Reverse	Cttctt CCCGGG AAACTCATCCACGTCAGAGACTTTG
T 1463	Forward	Cttctt GGCGCGCC ACTTGCCGA CAAAGGAAACTAGAA G
	Reverse	Cttctt CCCGGG CTTGACTGGCTCTGCTAACATCC
L 1482	Forward	Cttctt GGCGCGCC CTGGAGAACAGCTCAAATAAAAATG
	Reverse	Cttctt CCCGGG GGAGGAAAGCTTTTCAGCTGCAGC
6G 1839	Forward	Cttctt GGCGCGCC GGTGCAGAGGACAACGATGAG
	Reverse	Cttctt CCCGGG AGAAGCCACACCCTGGACTAGTG

5hmC immunofluorescence staining and imaging

HeLa cells (4 x 10^5) were plated on sterile coverslips in 24-well plates. After 24-48 h rapamycin treatment, cells were fixed at 4% paraformaldehyde in PBS for 15 minutes and permeabilized with 0.2% Triton X-100 in PBS for 30 minutes at room temperature. Next, DNAs were denatured with 3N HCl at room temperature for 15 minutes and neutralized with 100 mM Tris-HCl buffer (pH 8.0) for 10 minutes. After extensive washing with PBS, cells were blocked with 1% BSA for 30 minutes, and then incubated with rabbit anti-5-hmC polyclonal antibody (diluted at 1:500, Active Motif) for 2 hours at room temperature.

After washing with PBS (3 times; 15 minutes each), FITC-conjugated anti-rabbit IgG (Sigma-Aldrich) was added to cells for 1 hour. After thoroughly washing with PBS, 250 ng/ml of 4', 6-diamidino-2-phenylindole (DAPI) was added to the fixed cells and then the slides were mounted for confocal imaging. The fluorescent images were acquired by using a Nikon A1R+ confocal imaging system, equipped with multiple laser sources (405/488/561/640 nm). The 488 nm laser (green) was used to obtain 5hmC staining signals, as was 561-nm laser to excite mCherry for detecting protein expression. The NIS-Elements software was used for image analysis. The averaged FITC intensity in the nuclei of mCherry-positive cells were collected and analyzed. The data were plotted using the Prism 5 software.

Flow cytometry

Cells were re-suspended in FACS buffer (PBS with 1% BSA, 2 mM EDTA) and incubated with Fc blocker for 10 minutes on ice. After washing with FACS buffer, cells were fixed and permeabilized using the Cell Fixation/permeabilization kit (BD Biosciences). DNA were denatured using 2N HCl and neutralized by 10 mM Tris-HCl (pH 8.0) for 20 minutes. Next, anti-5hmC antibody (diluted at 1:200, Active Motif) and FITC conjugated goat anti-rabbit secondary antibody (at a dilution of 1:200; Thermo Fisher Scientific) were used for 5hmC staining. Flow cytometry analysis was performed using LSRII (BD Biosciences). Data were analyzed by using the FlowJo software.

A dot-blot assay to quantify genomic 5hmC and 5mC

Dot blot assays were performed, as described previously[56]. Briefly, purified genomic DNA was denatured in 0.4 M NaOH, 10 mM EDTA at 95 °C for 10 minutes, followed by neutralization with ice-cold 2 M ammonium acetate (pH 7.0). Two-fold serial dilutions of the denatured DNA samples were spotted on a nitrocellulose membrane in an assembled Bio-Dot apparatus (Bio-Rad), according to the manufacturer's instructions. A synthetic oligonucleotide with a known amount of 5hmC was used as standard[56, 75].

The membrane was washed with 2xSSC buffer, air-dried, and vacuum-baked at 80°C for 2 hours. The dried membrane was blocked with 5% non-fat milk for 1 hour and incubated with an anti-5hmC antibody (dilution of 1:5000, Active Motif) for 1 hour at 4°C, followed by incubation with horseradish peroxidase-conjugated anti-rabbit IgG

secondary antibody (diluted at 1:10,000; Sigma). The membrane was visualized by West-Q Pico Dura ECL Solution (GenDEPOT). To ensure equal loading of total DNA on the membrane, the same blot was stained with 0.02% methylene blue in 0.3 M sodium acetate (pH 5.2) to visualize the total amounts of loaded DNA samples.

Pull-down experiments and functional reconstitution in vitro

Myc-CiDER-mCherry, encoding the split CiDER (N-terminal half tagged with Myc and C-terminal half fused with mCherry), was transfected into HEK293T cells by using Lipofectamine 3000 (Life Technologies). At 48 hours post-transfection, $1X10^7$ cells were lysed in a RIPA lysis buffer (150 mM NaCl, 50 mM Tris-HCl, pH 8.0, 1% Triton X-100, 0.1% sodium deoxycholate and 0.05% SDS), supplemented with protease inhibitor cocktail (GenDEPOT), and incubated on ice for 20 minutes. Cell debris was removed by centrifuging at 20,000x g for 10 minutes at 4°C. Cell lysates were incubated with anti-Myc antibody (ab1253, Abcam) and/or a rabbit polyclonal anti-mCherry antibody (ab167453, Abcam) for 4 hours at 4°C, followed by incubation with precleared protein A/G beads (30 ul) overnight at 4°C. Protein/beads mixtures were washed 5 times with 50 mM HEPES (pH 8.0) containing 50 mM NaCl.

Then the immunoprecipitated TET2CD, N-half, or both CiDER fragments with substrate (a double-stranded 5mC containing DNA oligos that were used in an earlier study[75]) were mixed in a reaction buffer (50 mM HEPES (pH 8.0), 50 mM NaCl, 1 mM α-ketoglutarate, 3.7 μM ammonium iron (II) sulfate hexahydrate, 0.1 mg ml^{-1} BSA, 1 mM ATP) at 37°C for 30 minutes. Following this, EDTA (11 mM)

added to quench the reaction. DNA and protein mixtures were eluted with 50 mM HEPES (pH 8.0) containing 200 mM NaCl, 0.2% SDS with incubation at 95°C for 10 minutes. DNA fragments were further purified by MicroElute Cycle-Pure Kit (Omega). The 5hmC level were measured by the dot-blot assay as described above.

CMS-IP sequencing library preparation

Cytosine 5-methylenesulphonate (CMS)-IP seq were performed as described previously[39, 46]. Genomic DNA was isolated using a DNeasy blood and tissue kit (Qiagen). Purified genomic DNA was sonicated into ~300 bp using Covaris focused ultrasonicator. Sheared DNA was ligated with methylated adaptors using a TruSeq DNA library preparation kit (Illumina) followed by sodium bisulfite treatment (Methylcode bisulfite conversion kit, Life Technologies) to convert 5hmC to CMS.

CMS fragments were enriched using anti-CMS antibody that binds to protein A/G dynabeads. Enriched fragments were cleaned using the phenol/chloroform/isoamyl-alcohol method and then amplified using KAPA HiFi Uracil+ (Kapa Biosystems) polymerase with 8 PCR cycles. Amplified libraries were sequenced using Illumina NextSeq instrument (75 cycles, single-ended).

ATAC-seq sequencing library preparation

The researcher conducted an assay for Transposase-Accessible Chromatin, using sequencing (ATAC-seq) library preparation, as previously described[76]. Briefly, nuclei were isolated in lysis buffer (10 mM Tris-HCl, pH 7.4, 10 mM NaCl, 3 mM MgCl2,

0.1% IGEPAL CA-630), followed by centrifugation at 500 ×g for 10 minutes at 4 °C. Next, the transposition reaction was carried out by using Illumia Nextera DNA library preparation kit (37°C for 30 minutes). Tagmented DNAs were purified using the MiniElute kit (Qiagen). Purified DNAs were amplified with the KAPA real-time library amplification kit (Kapa Biosystems), followed by library purification using AmpuXP beads. The quality of purified DNA libraries was checked by Agilent TapeStation and then subjected to high throughput sequencing on an Illuminutesa NextSeq instrument (150 cycle, pair-ended).

Bioinformatic analysis for CiDER

For 5hmC peak identification, reads were mapped to hg19 assembly of the human genome, using bsmap2 software with default parameters. We kept uniquely mapped reads for the following analysis. A sliding window method was used to split the human whole genome to 300 bp size windows, and count the numbers of reads mapped in each window with 100 bp spacing. By comparing with the reads from input samples (without antibody enrichment), regions with more than 2-fold enrichment were identified as a peak. For heatmap generation, Mplot (unpublished software) was used to plot control (0 h) and 48 h ATAC/CMS signals on ATAC/CMS control peaks regions (normalized to 400 bp). For the ATAC-seq analysis, reads were aligned to the hg19 assembly of the human genome, using bowtie2 with the "-very-sensitive" parameter. The duplicate reads were discarded, and only properly paired mapped reads, with mapping quality ≥, were kept for downstream analysis.

The ATAC peak calling was done by MACS2 with "-nomodel" and "extsize 147" parameters. For the differential ATAC/CMS peaks analysis, the ATAC/CMS peaks in all groups were merged to form a merged peak set (ATAC merged peaks set: 107545 peaks; CMS merged peaks set: 231705 peaks). Next, we counted the reads in each group falling in the peaks. DESeq2 was used to call significantly differential ATAC/CMS peaks, which were identified as fold change ≥4 and q-value ≤0.05.

Highly-sensitive CMS-IP sequencing (sCMS-IP-seq)

The sCMS-IP-seq was performed as described previously[46], with some modifications. Briefly, genomic DNA was combined with unmethylated λ-bacteriophage DNA (NEB) for bisulfite conversion efficiency check, and then sheared into median 300-bp size range using a Covaris M220 Focused-ultrasonicator (Covaris). Sheared DNA was bisulfite converted using a EZ DNA methylation-lightning kit (Zymo Research), with suggested protocols, to convert 5-hydroxymethylcytosin (5hmC) to cytosine-5-methylenesulfonate (CMS). CMS-containing DNA fragments then were immunoprecipitated using CMS-specific antiserum pre-conjugated with protein A/G dynabeads. Precipitated DNA fragments were purified by the conventional phenol/chloroform/isomyl-alcohol method.

Purified enriched fragments were amplified with random primers, followed by adaptor ligation. Final amplification was performed with illumina TruSeq indices using a Pico Methyl-Seq Library Prep Kit (Zymo Research), with manufacturer's protocols. Constructed library size distribution was determined by a Bioanalyzer with an Agilent

High Sensitivity DNA Kit (Agilent). Library concentration was measured by a Qubit 4 Fluorometer using a Qubit dsDNA high sensitivity assay kit (Thermo Fisher Scientific). Pooled DNA libraries were sequenced on NextSeq 500 (Illumina) with a NextSeq 500/550 High Output Kit v2 (75 Cycles, single-ended), following protocols suggested by the manufacturer (Illumina).

sCMS-IP-seq data analysis

Raw fastq data for sCMS-IP were aligned to hg19 using BSMAP [46]. After discarding PCR duplicated reads, the uniquely mapped reads were kept for downstream analyses. MACS2[77] with default parameters was used to call CMS-IP peaks. A count table, including the raw counts for each peak across all the samples, was generated using an in-house script. DESeq2[78] was used to normalize the reads count for each sample and to identify the differentially hydroxymethylation (CMS-IP) peaks (DHMRs; FDR <= 0.05, when compared with health donor samples).

To facilitate the visualization of hydroxymethylation (5hmC) signals, we generated bigWig files for read coverage from the aligned BAM files and visualization in the UCSC genome browser. Functional annotations of DHMRs were performed using the GREAT analysis with default settings[79]. The R package ggplot2 was used for violin plots and boxplots. We generated heatmap with hierarchical using the R package heatmap3 (https://www.rdocumentation.org/packages/heatmap3/versions/1.1.6/ 329 topics/heatmap3). Following this, t-Distributed Stochastic Neighbor Embedding (t-SNE)

analysis was performed using the R package Rtsne (https://github.com/jkrijthe/Rtsne). The smoothed scatterplots were plotted using the R package: geneplotter.

Results

Design chemical-inducible epigenome remodeling tool (CiDER) using TET2 and its functional analysis

To overcome the hurdle facing studies of causal relationships between DNA hydroxymethylation and gene transcription, I designed a chemical-inducible epigenome remodeling tool (CiDER; Figure 2-1). There are several reasons for choosing TET2, rather than TET1 or TET3, as the target for engineering a split epigenomic modifier.

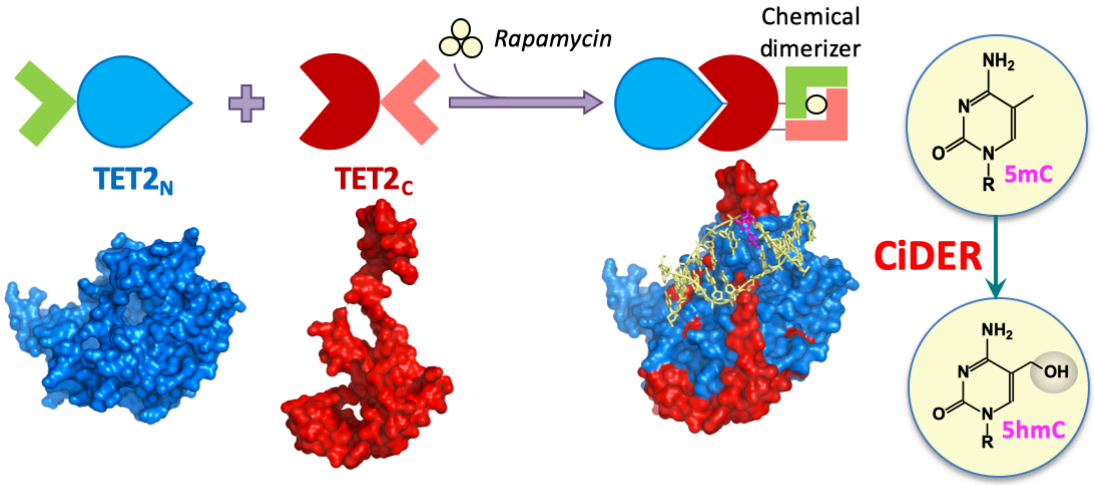

Figure 2-1. Design of a chemical-inducible epigenome remodeling (CiDER tool based on a split TET2 enzyme. FKBP12/FRB heterodimerization or FKBP-F36V homodimerization modules are fused with two inactive fragments of a split TET2CD. Upon the addition of rapamycin, split TET2CD fragments reassemble into a functional methylcytosine dioxygenase to catalyze the conversion of 5mC into 5hmC and further oxidized species, thus promoting DNA demethylation to remodel the epigenetic landscapes in mammalian cells.

TET2 is among the most frequently mutated genes in hematological malignancies[36]. Exome sequencing in cancer patients has revealed a large panel of disease-associated mutations[57, 80], thereby providing abundant information with regard to sensitive spots to be avoided during our selection of split sites. The determination of crystal structures of the catalytic domain of TET2 (TET2CD) in complex with 5mC or 5hmC[81, 82] enabled us to prioritize the selection and validation of split sites in a more rationalized manner.

Importantly, the low complexity region (residues 1481-1843) of TET2CD can be replaced by a flexible GS linker without significantly compromising its catalytic activity[82]. This clearly speaks for the structural malleability of TET2 and the high flexibility to accommodate the insertion of foreign polypeptide sequences. Omitting this large fragment of low complexity region (~1.2 kb) further allows generating constructs with minimized sizes. Based on those major consideration, we tested the idea that TET2CD can be split into two inactive fragments and its enzymatic function can be restored by taking a chemically-inducible dimerization approach.

To develop a split-TET2CD system, we selected six sites in TET2CD (Figure 2-

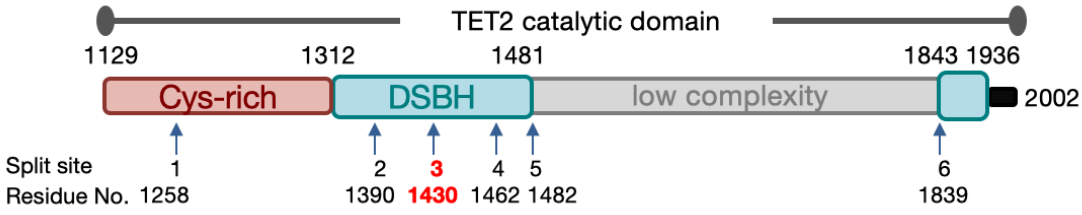

Figure 2-2. Domain architecture of the catalytic domain of TET2 (TET2CD; residues 1129-2002) and positions of split sites. A chemical (rapamycin) inducible module, composed of FKBP12 and FRB, was inserted individually into six selected split sites. DSBH, double stranded beta helix.

2), composed of a Cys-rich region and a double-stranded beta-helix (DSBH) fold, on the basis of a crystal structure of TET2-DNA complex that lacks a low complexity region[82]. A synthetic gene encoding FK506 binding protein 12 (FKBP12) and FKBP rapamycin binding domain (FRB) of the mammalian target of rapamycin[83, 84], separated in the middle by a self-cleaving T2A polypeptide sequence[85, 86], was inserted individually into the selected split sites within TET2CD or TET2CD lacking low complexity region (Figure 2-3). Then mCherry-tagged construct was transfected into human embryonic kidney 293T

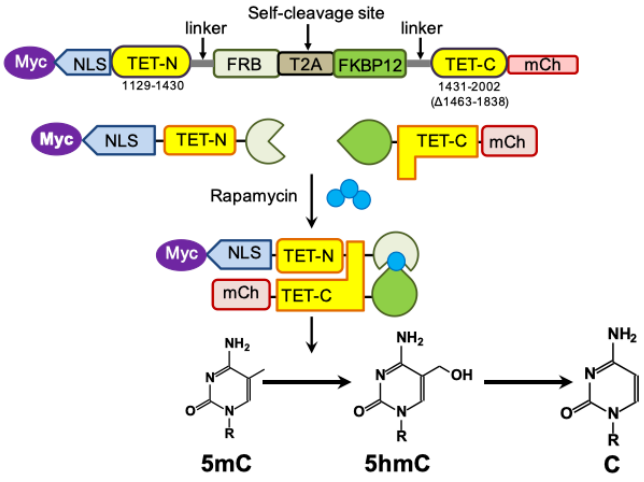

Figure 2-3. Design of CiDER as a split-TET2 enzyme for inducible 5mC oxidation. Diagram of CiDER. The chemical-inducible dimerization modules FRB and FKBP12, along with a self-cleaving peptide T2A, were inserted into the catalytic domain of TET2. The N-terminal region of TET2CD (TETN) is tagged with an Myc tag and a nuclear localization signal (NLS); whereas the C-terminal region of TET2CD (TET-C) is fused with mCherry to aid the detection of protein expression. Following the expression of CiDER in mammalian cells, the fusion protein was cleaved into two inactive TET2CD fragments. Upon addition of rapamycin, the chemically-inducible heterodimerizaiton of FRB and FKBP12 brings the two complementary fragments of TET2CD into close proximity to restore its enzymatic function, thereby catalyzing 5mC oxidation to produce 5hmC.

(HEK293T) or HeLa cells, both with very low basal 5hmC levels. Once expressed in HEK293T cells, the fusion protein was self-cleaved into two fragments (Figure 2-3) to reconstitute a functional enzyme *in vitro*, as reflected by inducible production of 5hmC after incubating the enriched fragments with a synthetic 5mC-containing dsDNA oligo in the presence of rapamycin (Figure 2-4).

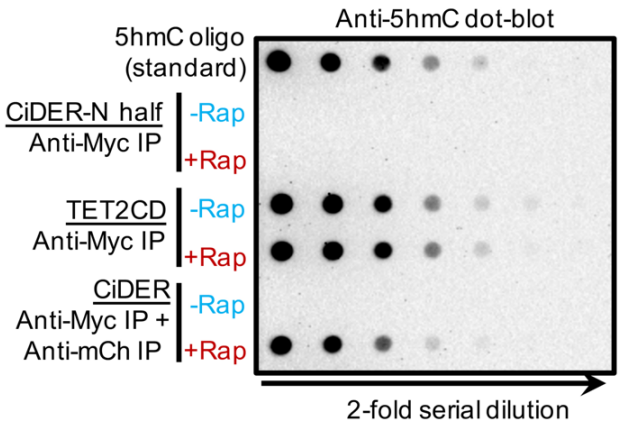

Figure 2-4. A dot-blot assay to quantify in vitro 5mC-to-5hmC conversion in reaction mixtures containing the following combinations: i) N-half of CiDER (negative control; enriched by an anti-Myc antibody) + 5mC dsDNA oligo (with all C replaced by 5mC); ii) Myc-TET2CD-mCherry (positive control; enriched by an anti-Myc antibody) + 5mC dsDNA oligo; or iii). both enriched fragments (enriched by antibodies against Myc and mCherry) + 5mC dsDNA oligo. The reactions were carried out in the absence (blue) or presence (red) of 1 μM rapamycin.

By using an antibody that specifically recognizes 5hmC, we compared the global 5hmC levels in transfected cells, before and after rapamycin treatment, by flow cytometry (Figure 2-5A). After screening over 15 constructs, we identified a split-TET2CD variant (designated as CiDER for chemical-inducible epigenome remodeling tool; see Supporting Information for the sequences) that exhibited rapamycin-inducible restoration of enzymatic activity (data not shown). We detected almost no background

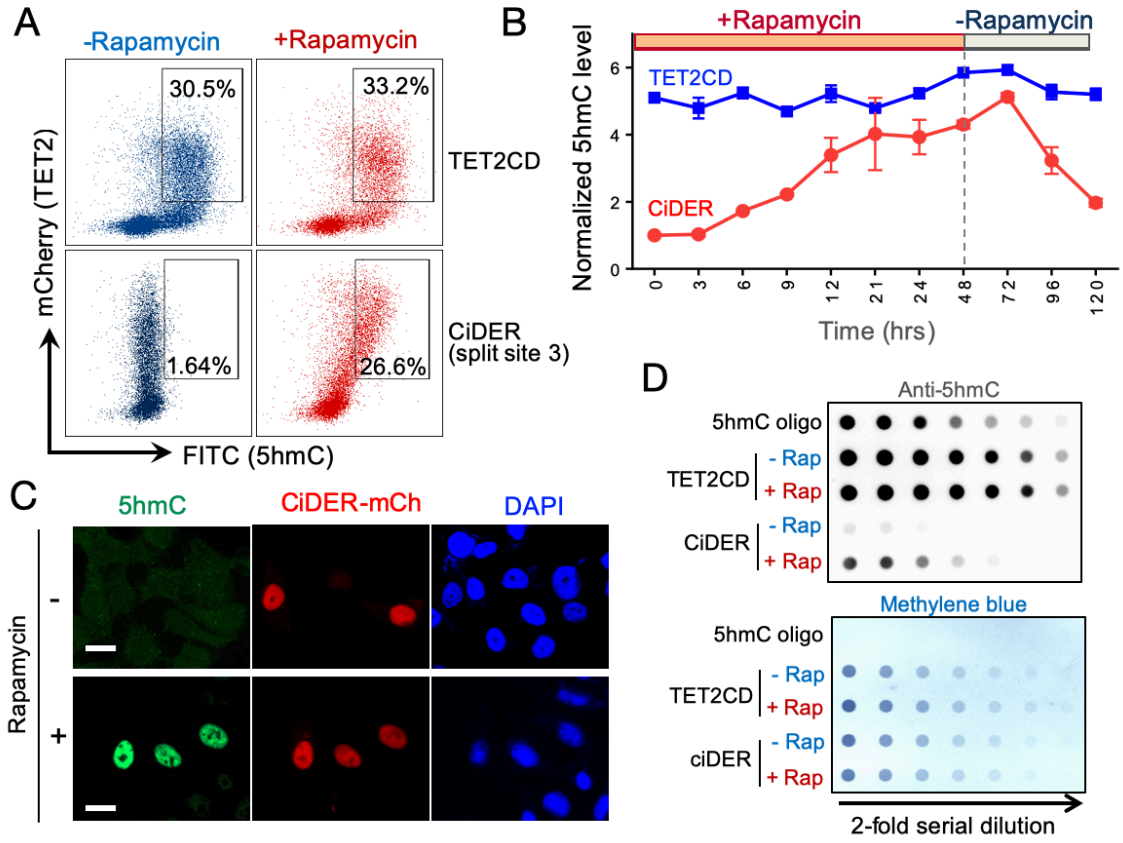

Figure 2-5. An engineered split-TET2 enzyme for inducible DNA hydroxymethylation in mammalian cells. **A.** Quantification of CiDER-mediated 5hmC production by flow cytometry. HEK293T cells transfected with mCherry (mCh)-tagged CiDER or mCh-TET2CD (positive control) were immunostained with an anti-5hmC primary antibody and an FITC-labelled secondary antibody. **B**. Time course of rapamycin (200 nM)-induced production of 5hmC in HEK293T of 5hmC in HEK293T cells expressing CiDER or TET2CD (as positive control). Rapamycin was washed away 48 h after incubation with cells. **C.** Representative fluorescent images of 5hmC (green), CiDER-mCh (red), and nuclear staining with DAPI (blue) in HEK293T cells before and after rapamycin (200 nM) treatment. **D.** Dot-blot assay to quantify rapamycin (200 nM)-induced changes of 5hmC levels in genomic DNA purified from HEK293T cells expressing CiDER or TET2CD. A synthetic oligonucleotide with a known amount of 5hmC was used as a positive control. The loading control is shown in the bottom panel by methylene blue staining of total amounts of input DNA. See Supporting Information (Figures S1-2) for more results and sequences. n=5. Scale bar=10 μm.

activity of CiDER prior to the addition of rapamycin. Following the addition of rapamycin, the total 5hmC amount was restored to a level comparable to cells expressing intact TET2CD proteins (split site 3; Figure 2-5A).

Chemical-induced 5hmC production at different time points was further monitored. We noticed that the functional restoration reached a maximum approximately 48 hours after rapamycin treatment. Notably, approximately 3 days after withdrawal of rapamycin, the 5hmC level returned to its basal level, presumably owing to the constant dilution of 5hmC after multiple rounds of cell division (Figure 2-5B). By contrast, the 5hmC level in the control group expressing an intact TET2CD remained largely unaltered under the same experimental conditions.

Next, rapamycin-inducible generation of 5hmC was confirmed by two additional methods: immunostaining with an antibody against 5hmC in individual cells (Figure 2-5C) and a more quantitative dot-blot assay that measures the total amounts of 5hmC in the whole cell population (Figure 2-5D). Both assays clearly demonstrated that rapamycin elicited robust production of 5hmC in CiDER-expressing HEK293T cells with negligible background activity.

Chromatin accessibility changes associated with CiDER-mediated chemical inducible epigenetic states remodeling

To systematically examine the CiDER-mediated changes in the epigenetic landscapes between untreated and rapamycin-treated mammalian cells, genome-wide

5hmC mapping was performed in HEK293T cells by immunoprecipitation (IP) of bisulfite-treated DNA with a highly specific home-made antibody against cytosine-5-methylenesulphonate (CMS)[39, 46]. Compared with the untreated control group (0 h), we observed a large number (n = 13,125) of differentially hydroxymethylated genomic regions (DHMRs) in cells treated with rapamycin (48 h), with the majority (n = 11,808) showing significant gain of 5hmC (Figure 2-6A and B left).

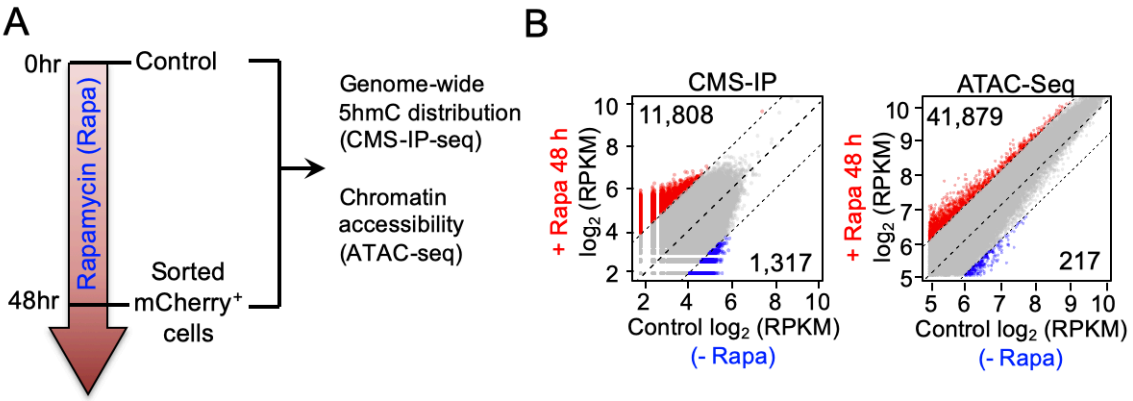

Figure 2-6. CiDER-mediated chemical inducible remodeling of epigenetic states to increase chromatin accessibility in mammalian cells. A. Schematic of the experimental setup. 0 or 48 h after 200 nM rapamycin treatment, genomic DNA samples from HEK293T cells were subjected to genome-wide 5hmC profiling and ATAC-seq to monitor chromatin accessible regions in the genome. **B.** Scatter plots of differential 5hmC peaks (left) and ATAC peaks (right) between 0 hand 48 h treatment groups. Red and blue dots represent significantly up- or down-regulated ATAC/5hmC peaks at 48 h, respectively. The grey dots represent peaks without significant changes at 48.

Very recently, researchers have shown that TET loss-of-function with the resultant reduction of genomic 5hmC is correlated with reduced numbers of chromatin

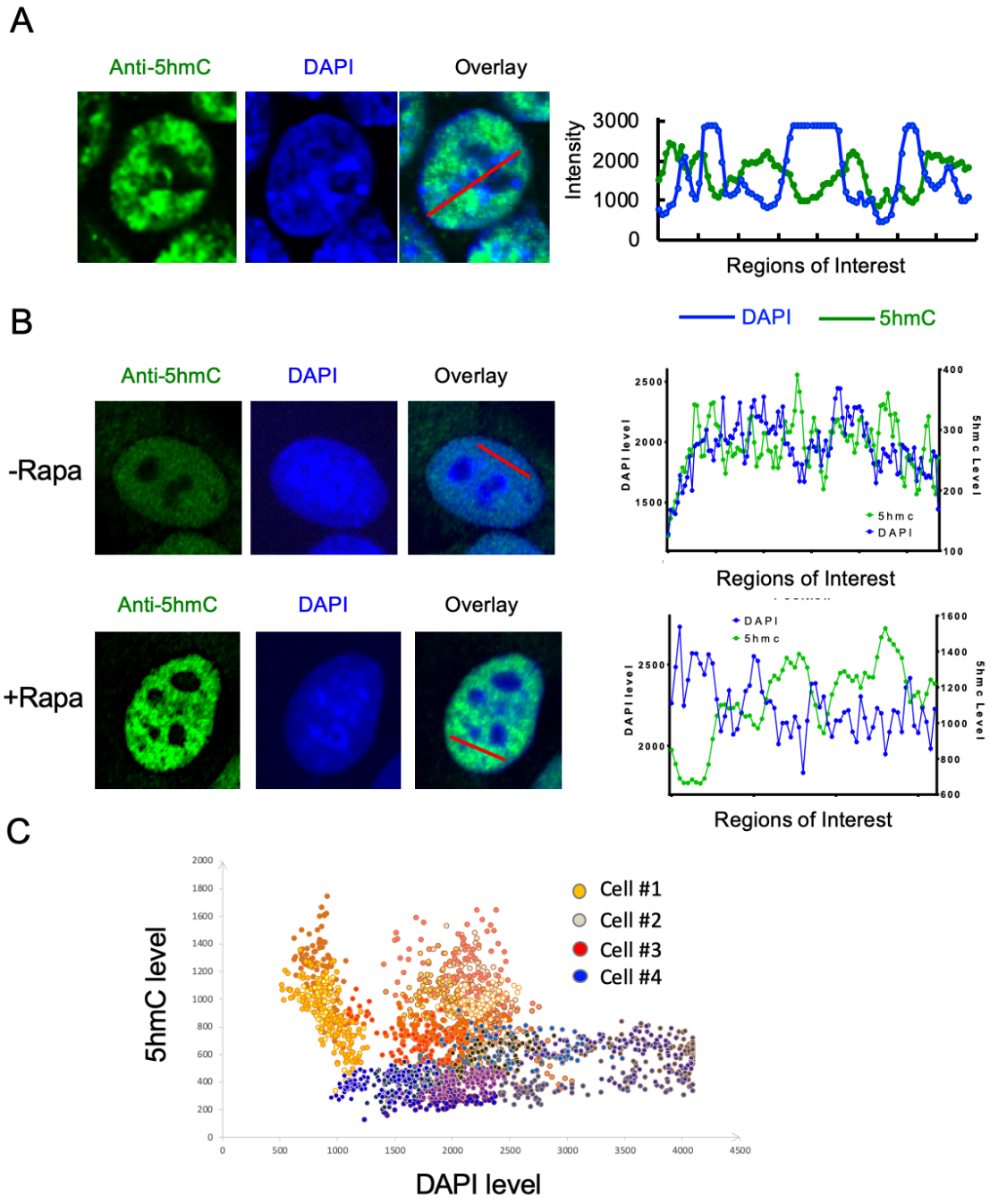

Figure 2-7. 5hmC and DAPI staining in the nuclei of mouse embryonic stem cells and CiDER expressing HEK293T cells (before and after rapamycin treatment). A. Mouse embryonic stem cells were immunostained with an anti-5hmC antibody (green). The nuclei were stained by DAPI (blue). The fluorescent signals across the red line were plotted on the right. **B.** Anti-5hmC (green) and DAPI (blue) staining in HEK293T cells expressing CiDER. Transfected HEK293T cells were cultured in the absence (0 h) or

presence of (48 h) 200 nM rapamycin prior to immunostaining. The fluorescent signals across the red lines were plotted on the right. **C**. Scatter plot of 5hmC vs DAPI staining in four representative CiDER-expressing HEK293T cells after incubation with rapamycine for 48 h. In general, higher 5hmC staining was correlated with lower DAPI staining in the same cell, and *vice versa*.

accessible regions. This suggests a potential role of TET and/or 5hmC in the maintenance of chromatin accessibility in mammals[69, 87], and the possibility that 5hmC-enriched regions might mark more accessible chromatin regions.

Since increased chromatin accessibility often is indirectly indicated by a lower DAPI staining of the nuclear euchromatin[88], we examined if the intensity of 5hmC staining is correlated with DAPI staining levels in two types of cells, the mouse embryonic stem cells that are rich in 5hmC (Figure 2-7A) and rapamycin-treated HEK293T cells that expressed chemical-inducible TET2CD (Figure 2-7B and C). In each individual cell, high 5-hmC areas in the same nucleus were correlated generally with pronouncedly decreased nuclear staining by DAPI, and *vice versa.* In both cell types, we observed a general inverse relationship between intensities of 5hmC and DAPI staining (Figure 2-7), a clear indication of the involvement of 5hmC in the regulation of chromatin accessibility.

The causal relationship between 5hmC and chromatin accessibility remains unresolved, primarily owing to the lack of tools to temporally control the hydroxymethylation of 5mC in living cells. To clarify this, we tested CiDER-mediated chemical-inducible deposition of 5hmC in the genome to determine whether it would cause changes in the chromatin architecture. The genome-wide chromatin accessibility

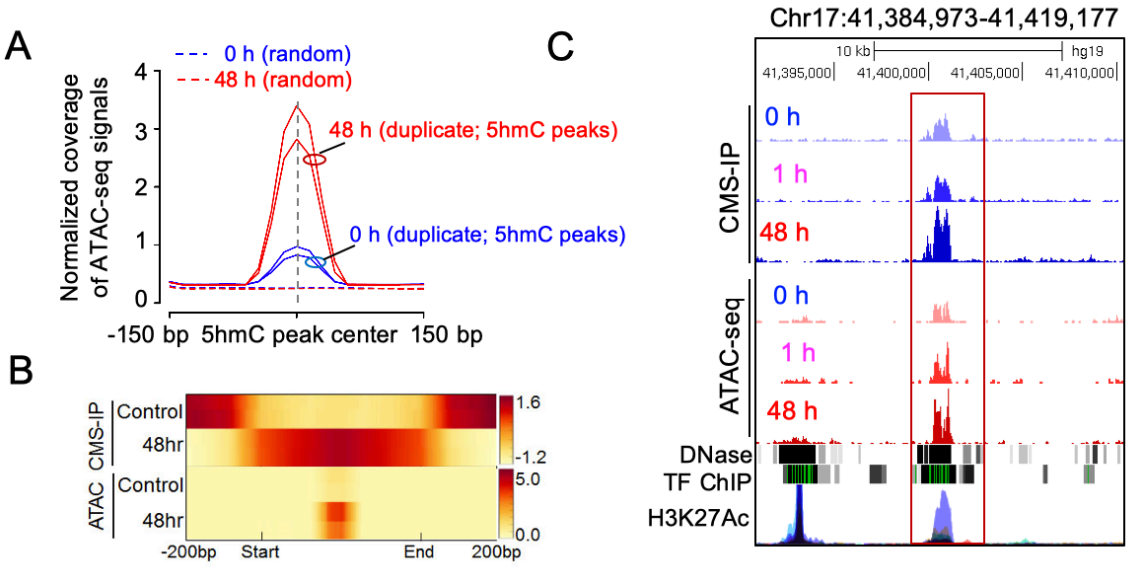

Figure 2-8. CiDER-mediated 5hmC deposition positively correlates with increased chromatin accessibility in mammalian cells. A. Normalized coverage of ATAC-seq signals (0 h and 48h; with biological duplicates). These were plotted 150 bp up- and down-stream of the centers of 5hmC-peaks at 0 h (control). **B.** Distribution of averaged 5hmC enrichment (2 upper panels) and (2 upper panels) and ATAC-seq peak enrichment (2 lower panels) at control ATAC/5hmC peaks regions in CiDER-expressing HEK293T cells at time 0 (control) or 48 h following rapamycin treatment. **C.** Representative genome browser view of one HMDR in the LINC00854 locus on chromosome 17. This showed rapamycin-induced gain of 5hmC and ATAC-seq peaks, which was overlaid with traces representing DNase I hypersensitive sites, transcriptional factor binding (TF ChIP) and H3K27Ac enrichment.

was profiled by ATAC-seq (assay for transposase-accessible chromatin using sequencing[76]) before and after rapamycin treatment in the same batch of cells (Figure 6A and B right).

Sequencing analysis shows that 41,879 regions were more accessible in rapamycin-treated cells compared to untreated cells (Figure 2-6B right). When taking a genome-wide approach to compare the 5hmC enrichment and ATAC-Seq peaks, we

observed a substantial enrichment of ATAC-seq peaks within the 5hmC enriched regions (Figure 2-8A and B).

In parallel, the Principal Component Analysis (PCA) of ATAC-seq and 5hmC enriched regions displayed similar distribution patterns on the plots before (0 h) and after (48 h) rapamycin treatment (Figure. 2-9), clearly indicating that CiDER-mediated chemical inducible generation of 5hmC was strongly correlated with the increase of chromatin accessible regions.

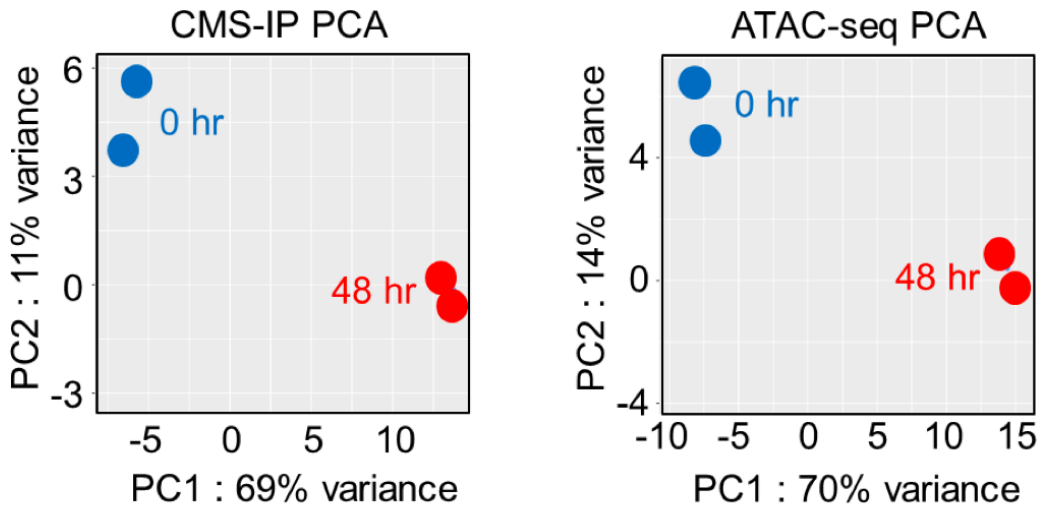

Figure 2-9. The principle component analysis (PCA). PCA plots of CMS-IP (left) and ATAC-seq (right) results for HEK293T cells expressing CiDER (before rapamycin treatment (0 h, blue; two biological replicates), or treated for 48 h, red. Two biological replicates).

The observed overlapping enrichment of 5hmC in chromatin accessible regions (Figure 2-8A and 8B) further imply that CiDER, with its enzymatic function restored by rapamycin, could actively mark these chromatin regions with 5hmC to maintain their

accessibility in mammalian cells. Figure 2-8C shows a genome browser view of one DHMR located in the LINC00854 locus. The distal region of LINC00854 contains moderate levels of both 5hmC and chromatin accessible regions prior to the addition of rapamycin (0 h), and showed a substantial gain of 5hmC and ATAC-Seq peaks after rapamycin-induced restoration of TET2 enzymatic activity (48 h). This region might also function as distal-regulatory regions (e.g., enhancers), as it is enriched with an enhancer mark (Histone H3 lysine 27 acetylation, H3K37Ac) as well as DNase I hypersensitivity regions identified from the ENCODE database.

Taken together, by controlling the formation of 5hmC at real time in living cells, we demonstrated that TET-mediated 5mC oxidation constitutes one important epigenetic regulatory mechanism to modulate chromatin accessibility without altering the genetic code. This suggests that CiDER-mediated epigenome remodeling can be applied diverse system to answer fundamental biological questions.

Develop high-sensitive CMS-IP seq (sCMS-IP) for low amount of input DNA

TET family enzymes and their derivatives have diverse biological functions in different organs, including normal developmental processes, as well as various disease phenotypes[36, 37]. To understand biological roles of TET proteins and 5hmC, a major product of the enzymatic reaction of TETs, comprehensively, researchers must map 5hmC onto the genome with high precision and better resolution. By doing that with various types of tissues, 5hmC enriched regions are able to correlate with diverse genomic events, such as gene expression and chromatin architecture.

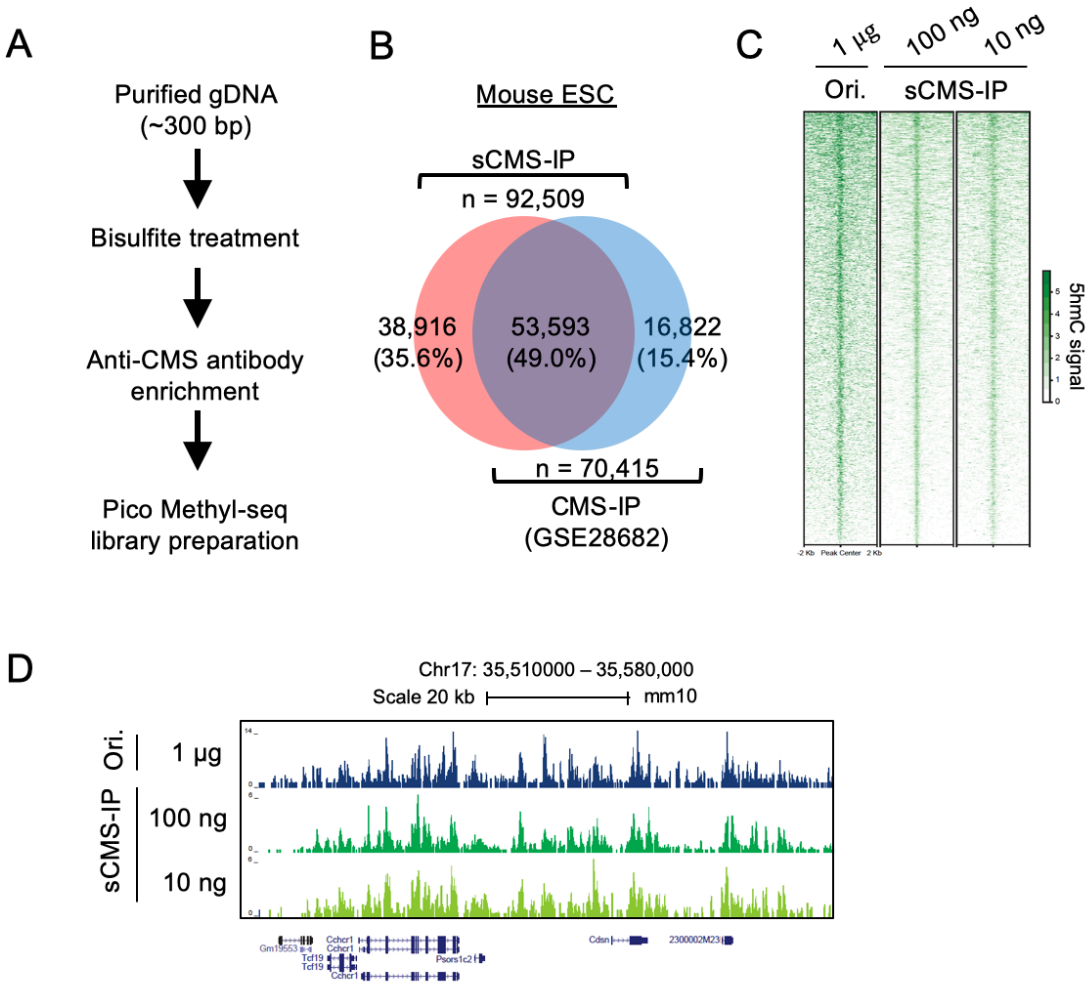

Figure 2-10. A high-sensitive CMS-IP sequencing (sCMS-IP-seq) method to profile genome-wide 5hmC landscapes using low-input DNA. A. The work-flow of sCMS-IP-seq. **B.** Venn diagram showing the overlapping 5hmC peaks in mouse embryonic stem cells (mESC). 5hmC peaks were mapped either using the previously published conventional CMS-IP-seq method (1µg input), or the sCMS-IP-seq (10 ng input) described in this study. **C.** Heatmap representation of 5-hmC profiling results using the regular CMS-IP-seq method and sCMS-IP-seq method (100 ng and 10 ng input). The gDNA input amounts for CMS-IP are indicated on the top of the heatmap. The up- and down- 2kb of the center of 5hmC peaks, identified in regular CMS-IP-seq, were used to plot heatmaps. **D.** Genome-browser views of DNA hydroxymethylation distribution in a genomic locus identified using the regular CMS-IP-seq method or the sCMS-IP-seq method (100 ng and 10 ng input).

Previously reported CMS-IP seq method[46] is a powerful tool to profile 5hmC genome-widely, using a highly immunogenic by-product of sodium bisulfite treatment with 5hmC, called cytosine 5-methylenesulphonate (CMS). Although it is an effective method, the major caveat of this technique is that a relatively large amount of starting materials are required to get high quality mapping results. A high-sensitive CMS-IP (sCMS-IP) seq method was developed to achieve genome-wide 5hmC profiling using limited DNA, as low as 10 ng, purified from tumor infiltrate lymphocytes (TILs), (Figure 2-10A). Briefly, when compared with traditional CMS-IP seq, this method applied multiple amplification steps, including random priming using pico-methylseq library prep kit developed by Zymo Research. To validate the reliability of this technique, we compared in parallel 5hmC profiles in mouse embryonic stem cells (mESCs) using sCMS-IP method with 10 ng and 100 ng of genomic DNA (gDNA) and previously published regular CMS-IP method with 1 μg of gDNA. The results indicate substantial overlapping of 5hmC peaks in mESCs between sCMS-IP and traditional CMS-IP (Figure 2-10B). We observed consistent 5hmC peaks intensity (Figure 2-10C) and distribution (Figure 2-10D). This showed that we successfully employed our sCMS-IP method without sacrificing the overall accuracy and sensitivity.

Discussion

DNA methylation and demethylation are the chemical modifications of DNA bases that play a crucial role in epigenetic gene regulation. During those processes, 5mC and 5hmC perform as epigenetic marks to control diverse biological processes from normal development to cancer progression. Although much attention has been focused on 5mC, the role of 5hmC is relatively limited. Hydroxymethylated cytosine levels are generally around 0.1% in mammalian tissues. TET family enzymes generate 5hmC from existing 5mC. Therefore, the proportion of 5hmC is much less than 5mC in different types of tissues (less than 20-fold in mESCs[67]), indicating the necessity of highly sensitive tools to examine the function of 5hmC in the genome. Several methods were already developed to reliably map 5hmC genome-widely[46, 89]. However, those techniques require high concentration of genomic DNA (1-10 μg) as a starting material to properly generate sequencing libraries. This suggests that there is an urgent need to develop a highly sensitive sequencing library preparation method to utilize low-amount of DNA.

In this chapter, we introduced a high-sensitive CMS-IP (sCMS-IP) seq that is able to capture 5hmC information, using as low as 10 ng, and tested the method in mESCs and myelodysplastic syndromes (MDS) patient samples (data not shown). We demonstrated that our sCMS-IP technique can yield high quality epigenomic data with data coverage, peak intensity, and distribution patterns comparable to the conventional profiling approaches that often require 10-100-fold more genomic DNA as input.

The study of epigenetic modification of DNA currently is in an exponential phase of growth with development of massive sequencing techniques. The aim is to find novel biomarkers, including diagnosis and prognosis of certain diseases, as well as target specific factors for personalized therapy. We also proposed an advanced and sensitive technique to map 5hmC genome-widely in this chapter.

Challenges remain in verifying how those epigenetic modifications on DNA, by marking with 5hmC and further oxidative products, directly change the gene expression and derived phenotypes. To overcome this hurdle, we engineered a split-TET2 enzyme to enable temporal control of 5mC oxidation and subsequent remodeling of epigenetic states in mammalian cells. We further demonstrated the use of this chemically-inducible system to dissect the correlation between DNA hydroxymethylation and chromatin accessibility in the mammalian genome. This chemical-inducible epigenome remodeling (CiDER) tool will find broad use in interrogating cellular systems, without altering the genetic code, as well as in probing the epigenotype-phenotype relations in various biological systems.

In general, TET2 is thought to be a strong tumor suppressor in hematopoietic malignancy. TET2 loss-of-function can cause myeloid or lymphoid transformations. Moreover, various types of TET2 mutations have been found to be associated with MDS, acute myelocytic leukemia (AML), acute lymphocytic leukemia (ALL), and other hematologic malignancies[57, 80]. On the other hand, previous research suggest tumor promoting functions of TET2 in different settings, including CAR-T cells[62] and murine myeloid lineage cells [64]. Our own results of the immunotherapy model will be described

in Chapter III also indicate that Tet2 depletion in $CD8^+$ cytotoxic T cells reduces tumor burden, suggesting immunosuppressive function of TET2 in an *in vivo* system. Certainly, TET2 deficiency increases clonal hematopoiesis, and it may result in promoting certain types of tumorigenesis. Along with our own data, there is growing evidence that Tet2 deletion increases anti-tumor efficacy. Therefore, TET2 expression should be controlled precisely in order to potentiate the benefit to cancer immunotherapy. We anticipate that our drug-inducible epigenome remodeling tool, CiDER, can be applied to our immunotherapy model to maximize tumor killing effect of $CD8^+$ T Cells by controlling TET2 activity.

To confer spatial control over the CiDER system, one of our immediate future plans is to fuse CiDER with a catalytically-inactive Cas9, or its orthologues. This should enable loci-specific targeting and precise control of 5mC oxidation in the genome. Ideally, epigenome remodeling is a powerful strategy for interrogating, perturbing and engineering cellular systems without altering the genetic code. It could thus serve as a high entry point for reprogramming cell fate and disease intervention.

CHAPTER III

DEVELOPING A MOUSE MODEL OF MELANOMA TO EVALUATE IMMUNOTHERAPY

Introduction

Accumulated studies reported dynamic epigenetic landscape changes during the course of T cell development, and tumor infiltrating lymphocytes (TILs) during tumor progression. This suggests that epigenetic changes make up one of the important factors controlling proper T cell development. They regulate the key genes and define the status of TILs during tumor development.

A number of studies showed that DNA methylation plays an essential role in regulating immune response of $CD8^+$ T cell during chromic infection and tumorigenesis. Both effector and inhibitory genes are tightly controlled by DNA methylation during $CD8^+$ expansion, activation, and exhaustion. For example, the demethylation of Gzmb, Infg, and Pdcd-1 loci are essential for active gene expression of these genes in $CD8^+$ T effector cells during acute infection[3, 26]. Also, researchers report that blockage of de novo DNA methylation by DNA methyltransferases 3a (Dnmt3a) deletion resulted in prolonged $CD8^+$ T cell immunity during persistent immune response[90]. Indeed, impaired DNA methylation in T cells directly affects the outcomes of immune-related therapies including checkpoint treatment[91]. Therefore, it is highly likely that modulation of DNA methylation in T cells might benefit cancer immunotherapy.

In addition to Dnmts mediated DNA methylation, TET protein family mediated DNA methylation oxidation is one of critical regulatory mechanisms for DNA demethylation process. Deletion of TET proteins resulted in impaired chromatin accessibility[92] and transcription factor binding in different immune cells, including B cells, T cells, and macrophages[93]. Among three TET proteins, TET2 is highly expressed in the hematopoietic system[56, 94, 95], and frequently mutated in the hematopoietic and immune system. Maintaining normal hematopoiesis and loss-of-function (LOF) of TET2 in humans, TET2 tends to increase the blood cells' susceptibility to malignant transformation[36, 37, 63]. Genetic deletion of Tet2 in mice resulted in the expansion of hematopoietic stem progenitor cells (HSPCs) and caused a myeloid bias during hematopoiesis[54].

TET2 mutations frequently are observed in individuals with clonal hematopoiesis, who are at a higher risk to develop hematological malignancies. Indeed, TET2 mutations also are detected in patients with hematological malignancies, both myeloid and lymphoid lineages[54, 96]. Researchers report that Tet2 ablation in murine $CD4^+$ T cells result in imbalanced $CD4^+$ T cell polarization and impair cytokine production[60]. Tet2 knock-out (KO) in $CD8^+$ T cells also result in abnormal memory $CD8^+$ T cells during chronic infection[61].

Several recent papers indicated that Tet2 deficient hematopoietic stem cells and immune cells, including T cells and macrophages, exhibited distinct immune activities in responding to external stimulations. For example, Tet2 deficiency in $CD8^+$ T cells promotes memory differentiation and enhanced pathogen control[61]. In addition,

disruption of TET2 improves immunotherapy efficiency in both chimeric antigen receptors (CARs) T cells and tumor-infiltrating myeloid cells[62], suggesting the beneficial effects of TET2 LOF during anti-tumor immunotherapy. Tet2 LOF also enhances the anti-tumor efficiency of tumor-infiltrating myeloid cells[64].

TET2 seems to act as a "double-edged sword" in immune system. At the molecular level, our group and others have shown that Tet protein mediated DNA methylation oxidation regulates gene expression by controlling chromatin accessibility and transcription factor binding (TF) during embryonic development. However, the role of Tet2 in TILs in anti-tumor immunity is unclear.

One of the most popular and versatile models of murine melanoma is created by inoculating B16 cells in the syngeneic C57BL/6J mouse strain. Upon inoculation, B16 cells will form a detectable tumor around 5 days after injection and grow gradually. The B16-OVA cell line is modified mouse melanoma cells that are specifically engineered to express ovalbumin (OVA) peptide. To enhance the likelihood that B16-OVA cells will interact with $CD8^+$ T cells, the transgenic T cell receptor was designed to recognize OVA peptide, called OT-1. The $CD8^+$ T cells isolated from *OT-1* mice primarily recognize OVA when they are presented by the MHC1 molecule.

In this chapter, we report the creation of a mouse model of melanoma using a melanoma cell line and Tert2 deficient OT-I mouse to delineate how Tet2 depletion in cytotoxic $CD8^+$ T cells affects tumor growth. We also investigate the function of Tet2 in TILs.

Materials and Methods

Mice

C57BL/6J mice (The Jackson Laboratory) and *Tet2*$^{-/-}$ mice (The Jackson Laboratory) were crossed with OT-1^{+} mice (*C57BL/6-Tg(TcraTcrb)1100Mjb/J*, The Jackson Laboratory) with transgenic T cell receptocan recognize ovalbumin ($OVA_{257-264}$) in the context of CD8 co-receptor interaction with MHC class I. Crossed mice \6-20 weeks in age were used for CD8^{+} T cell isolation and I vivo experiments. CD45.1^{+} mice (B6.SJL-Ptprca Pepcb/BoyJ, The Jackson Laboratory, or a kind gift from Dr. Goodell, BCM), age between 6-12 weeks, were challenged with B16-OVA mouse melanoma tumor cells then used as recipients for adoptive T cell transfer. All mice were maintained in the animal facility at the Institute of Biosciences and Technology, Texas A&M University. All animal studies were approved by the Institutional Animal Care Use Committee (IACUC) of the Institute of Biosciences and Technology, Texas A&M University.

Mouse T cell isolation and in vitro culture

CD8^{+} T cells were isolated using a mouse CD8a^{+} T Cell Isolation Kit (Miltenyi Biotec). Briefly, harvested spleens and lymph nodes from WT-*OT1*$^{+}$ and *Tet2*$^{-/-}$ *OT1*$^{+}$ mice were ground and filtered with 70-μm cell strainers (Falcon) to remove debris. The suspended cells were treated with ACK lysis buffer (Fisher Scientific) to lyse red blood cells, and residual cells were purified for total CD8^{+} T cell isolation, using the T cell isolation kit according to the manufacturers' protocol. Purified CD8^{+} T cells were

activated by anti-CD3 (clone 17A2, InVivoMAb), anti-CD28 (clone 37.51, InVivoMAb) and high dose of mouse IL-2 (100 units/ml, eBioscience). Then they were placed on pre-coated plate with Goat anti-Hamster IgG (H+L, Invitrogen). After 2 days of culture, T cells were removed from original coated plate and recultured with low dose of mouse IL-2 (20 units/ml, eBioscience). Activated T cells were used for adoptive T cell transfer experiment.

B16-OVA tumor model[97] and adoptive T cell transfer

B16-OVA mouse melanoma cells (a kind gift from Dr. Anjana Rao, La Jolla institute for Immunology, CA) were cultured in complete Dulbecco's Modification of Eagle's Medium (DMEM) and passaged at least two times before injection. CulturedB16-OVA cells were trypsinized and washed with 1X PBS and diluted at 6 million cells/ml. Prepared B16-OVA cells were injected intradermally into the lower back of $CD45.1^+$ mice. Tumor sizes were measured and recorded each day. In 10-12 days after B16-OVA inoculation, *in vitro* cultured and activated WT-$OT1^+$ and $Tet2^{-/-}$ $OT1^+$ $CD8^+$ T cells were retroorbitally injected on tumor bearing $CD45.1^+$ mice. The injected T cell number is fixed (2 million cells, diluted at 10 million cells/ml in PBS then injected 200 ul). Mice were killed on day 3 and day 8 after adoptive T cell transfer.

Harvesting materials including tumor infiltrating lymphocytes (TILs)

Spleens, peripheral blood, and tumor mass were dissected at specific time points after adoptive T cell transfer. Spleens and peripheral blood undergo red blood cell lysis

step with ACK lysis buffer and were used for downstream flow cytometry analysis. Dissected tumors were cut in pieces, using ultra fine scissors and tweezer, then incubated in RPMI media with Liberase TL (100 μg/mL, Roche) for 15 min at 37 °C.

After that, we added the same amount of Liberase onto the sample and incubated for additional 10 min at 37 °C. Suspended tissues were passed through 70-μm cell strainers (Falcon), then washed with PBS several times. Cell suspensions then were labeled with mouse anti-CD63-biotin (Miltenyi Biotec), followed by anti-biotin microbeads (Miltenyi Biotec), and passed through magnetic column to specifically remove B16-OVA cells. Roughly purified TILs were stained immediately with different cell surface markers for sorting for single cell (sc) RNA-seq and flow cytometry analysis. For scRNA-seq sample preparation, samples from different mice in the same group were pooled together to increase cell yield. All antibodies are listed below.

In vitro re-stimulation for cytokine staining

In vitro activated $CD8^+$ T cells (before injection, Day 0 control) and purified TILs with anti-CD63 antibody were plated in 48-well plate with enough density (at least 0.25 million cells/well). Then we added T cell media containing 10 nM of PMA (Sigma-Aldrich), 500 nM of ionomycin (Thermofisher), and 1 μg/ml of brefeldin (BioLegend). The plate was Incubated for 4 hours at 37 °C. After incubation, the cells were stained with appropriate cell surface antibodies (CD45.1, CD45.2 and CD8). Then the cells were fixed and permeabilized with BD Cytofix/Cytoperm™ Fixation/Permeabilization

Solution Kit (BD biosciences). Fixed and permeabilized cells were stained with cytokines antibody (IFNG and TNFA) and advanced to flow cytometry analysis.

In vitro cytotoxicity assay

We prepared $CD8^+$ T cells from WT-*OT1*$^+$ and *Tet2*$^{-/-}$ *OT1*$^+$ mice, as described in Mouse T cell isolation and *in vitro* culture, that were at least 2-day activated. B16-OVA cells were labeled with Cell Proliferation Dye with APC (eBioscience), then plated 250,000 B16-OVA cells on 24-well plate and incubate for 1 hour at 37 °C. After an hour, media were removed and we added 4X amount of activated T cells with complete T cell media onto pre-plated, labeled B16-OVA cells. These were incubated for 4 and 8 hours at 37 °C. Co-cultured cells were then washed twice with 1X PBS and stained dead cells with CellEvent™ Caspase-3/7 Green Detection Reagent (Invitrogen), according to the manufacturers' instructions. Double stained populations were examined by flow cytometry. Plating cell numbers and effector and target cell ratio were optimized previously.

Anti-PD-L1 treatment

Anti–PD-L1 Ab (clone no. 10F.9G2, BioXCell), or control anti-KLH rat IgG2b (BioXCell) were treated in certain groups of animals. Two different inoculations were performed on Day 3 and Day 6 after adoptive T cell transfer into tumor-bearing mice. Antibodies were injected intraperitoneally (IP) with 200 μg per mouse at each time.

Single-cell RNA-seq (scRNA-seq) library preparation and sequencing analysis

Dissected tumors were digested twice with 100 μg/mL of Liberase TL (Roche), and suspended tissues were passed through 70-μm cell strainers (Falcon). Then cell suspension was stained with anti-mouse CD45.2 and anti-mouse CD8 antibodies that conjugated with fluorescence dye for flow cytometry. The CD45.2+CD8+ population was sorted out by FACSFusion Cell sorter (BD Biosciences). Wes generated ingle-cell RNA-seq libraries using the Chromium Single-Cell 3′ Reagent V2 Kit (10× Genomics), according to the manufacturer's protocol. Briefly, barcoded single cell Gel Bead-in-Emulsion (GEMs) was generated in a Chromium Controller (10× Genomics). Then RNA transcripts, isolated from single cells. were reverse transcribed, amplified, and fragmented.

Last, adapter and indices were incorporated into the fragmented cDNA. Concentration. Size distribution of pre-amplified cDNA and generated libraries were measured by Bioanalyzer with Agilent High Sensitivty DNA Kit (Agilent). Libraries were normalized in certain concentrations and pooled in an equimolar ratio, then sequenced on NextSeq 500 (Illumina) with NextSeq 500/550 High Output Kit v2.5 (single-end reads, 75 Cycles), with a customized paired-end, dual indexing (26/8/0/58-bp) format, as recommended by 10 x Genomics.

The illumina bcl2fastq (version, 2.20.0.422) was firstly used to demultiplex the raw sequencing data into fastq files. Cellranger (version, 3.0.2) was used to align raw fastq files to mm10 reference genome and perform barcode and UMI counting. The count matrix for each gene of each cell was taken as input file for R package Seruat

(version, 2.3). Reads with the same UMI were combined and then annotated to ensemble genes (mm10). To ensure the data quality, the genes detected in less than 10 cells and the cells with less than 20 genes were filtered out firstly from each dataset. We used the first 8 principle components to perform cell cluster and t-Distributed Stochastic Neighbor Embedding (t-SNE) with resolution = 0.4. To identify the marker genes, differential expression analysis was performed by FindAllMarkers function with Wilcoxon rank sum test. Violin plots were generated using Seurat Vlnplot function. The raw reads of different CD8+ tumor-infiltrating lymphocytes (TILs) cells (bulk RNA-seq dataset) were downloaded from GSE122969, and the data analysis was similar to RNA-seq data of this study. The heatmap of scaled gene expression level across top 20 significant marker genes for each cluster was plotted by R package ComplexHeatmap.

RNA-seq library preparation and sequencing analysis

First, isolated total RNA from *in vitro* activated $CD8^+$ T cells, purified TILs with anti-CD63 antibody from Day 3 and Day 8 collected tumors, were used to select mRNA using NEBNext Poly(A) mRNA Magnetic Isolation Module (NEB) by incubating with oligo-dT beads magnetic beads. Then we used mRNA to generate RNA-seq library with NEBNext Ultra™ II Directional RNA Library Prep Kit for Illumina (NEB), based on manufacturers' protocols. Briefly, selected mRNA was converted into cDNA through two rounds of cDNA synthesis. Then adaptor for illumine sequencing system was ligated into cDNA, followed by final library amplification with illumine TruSeq single indices (NEB). Constructed libraries were purified with AmpureXP beads.

Constructed library size was determined by Bioanalyzer with Agilent High Sensitivity DNA Kit (Agilent). Library concentration was measured by Qubit 4 Fluorometer with Qubit dsDNA high sensitivity assay kit (Thermofisher). Normalized libraries were pooled in an equimolar ratio and sequenced on NextSeq 500 (Illumina) with NextSeq 500/550 High Output Kit v2.5 (single-end reads, 75 Cycles), following the manufacturers' protocols.

To process the sequencing data, low quality bases and adaptor were trimmed using TrimGalore v.0.5.0 with default parameters (https://github.com/FelixKrueger/TrimGalore). Clean reads of RNA-seq data were aligned to mm10 reference genome using Hisat2 (version, 2.1.0) with default parameters and only uniquely mapped reads were used for downstream analysis. Count matrix for each gene were generated using htseq-count (HTSeq package). DESeq2 was used to identify significantly differentially expressed genes (DEGs) in TET2 knockout and wild-type samples between different time points (fold change ≥ 2; FDR < 0.05). In-house R scripts were used to plot the volcano and scatter plots for DEGs. The 'ClusterProfilter' package in R was performed for the functional enrichment analysis of DEGs in KEGG pathways. Hierarchical cluster analysis of the union DEGs was used to determine group-specific signature genes.

ATAC-seq library preparation and sequencing

ATAC-seq library preparation was performed, as previously described[2]. In brief, nuclei were isolated from 50,000 cells (freshly prepared) in lysis buffer (10 mM Tris-HCl,

pH 7.4, 10 mM NaCl, 3 mM MgCl2, 0.1% IGEPAL CA-630), then transposition reaction was performed using Illumina Nextera DNA library preparation kit at 37 °C for 30 minutes. Tagmented DNA fragments were purified using the MinElute PCR purification kit (Qiagen), and purified DNA were amplified with KAPA real-time library amplification kit (Roche), with careful monitoring to prevent overamplified library generation. Amplified libraries were than purified with AmpureXP beads. Size and concentration measurements of constructed libraries and pooling normalized libraries were performed as described in the RNA-seq library preparation section. Equimolarly combined libraries were sequenced on NextSeq 500 (Illumina) with NextSeq 500/550 High Output Kit v2.5 (paired-end reads, 150 Cycles), following the manufacturers' protocols.

Adaptor trimming of raw reads were performed by TrimGalore v0.5.0 with default parameters, and high-quality ($Q \geq 20$) reads were uniquely aligned to mm10 reference genome using Bowtie2 with '--very-sensitive' option. Only uniquely mapped reads were finally extracted for downstream analysis. The resulting alignment of each sample (with two biological replicates) were analyzed by Genrich v.0.5 (https://github.com/jsh58/Genrich) with ATAC-seq mode (option: -j, -q 0.05, -d 150) and the options to remove PCR duplicates (-r) and to discard alignments to chrM (-e chrM) to call ATAC peaks. Bedtools merge was used to count the reads fall into non-overlapped peak regions, and the significantly Differential Accessible Regions (DARs) were detected using DESeq2 with normalized peak signals (fold change ≥ 2; FDR $<$ 0.05). Venn diagram was plotted using R package ggplot2 to find group-specific chromatin changed regions. Motif annotation of DARs was performed using HOMER

software. GREAT analysis with single-nearest genes option was used to perform the functional annotation of DARs.

Results

Generating WT/Tet2KO-OT1^{+} mice

To establish a mouse model of melanoma, we used a B16-OVA melanoma cell line (a kind gift of Dr. Rao lab, La Jolla Institute for Immunology, La Jolla, CA), modified to express the exogenous antigen chicken ovalbumin (OVA)[97, 98]. OT-I mice donated OT-I^{+} CD8^{+} T cells that have the transgenic T cell receptor designed for recognizing ovalbumin peptide in the context of CD8 co-receptor. WT-OT-I^{+} mice (C57BL/6-Tg(TcraTcrb)1100Mjb/J) were crossed with Tet2$^{-/-}$ mouse, generating the

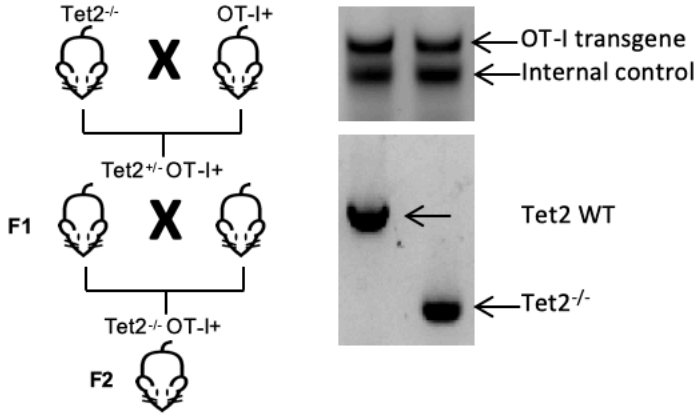

Figure 3-1. Genetic scheme for generating Tet2$^{-/-}$ OT-I+ mouse and OT-I+ transgene confirmation. To generated OT-I transgene expressed Tet2$^{-/-}$ mice, Tet2$^{-/-}$ mice was mated with OT-I^{+} mice (the Jackson Laboratory). In F1 generation, Tet2$^{+/-}$ containing OT-I transgene mice were selected and crossed. Tet2$^{-/-}$-OT-I^{+} mice were generated by the Mendelian laws of inheritance in F2 generation. OT-I transgene and Tet2 knockout were confirmed by PCR.

desired model that bears OT-I transgene in a Tet2$^{-/-}$ background (Figure 3-1). We observed that the *Tet2*$^{-/-}$*-OT-I*$^{+}$ male is less fertile than Tet2 heterogenous. Hence, the *Tet2*$^{+/-}$*-OT-I*$^{+}$ pair was used for breeding.

Next, we generated a mouse immunotherapy model. To distinguish between the endogenous and adoptively transferred CD8^{+} T cells, CD45.1^{+} (B6.SJL-Ptpr Pepcb/BoyJ) mice (a kind gift from Dr. M. A. Goodell, Baylor College of Medicine, Houston, TX) were used as a recipient.

First, 300,000 of B16-OVA cells were injected intradermally into CD45.1^{+} WT mice[97] (Figure 3-2). In this widely established model, we tried to control the aggressive

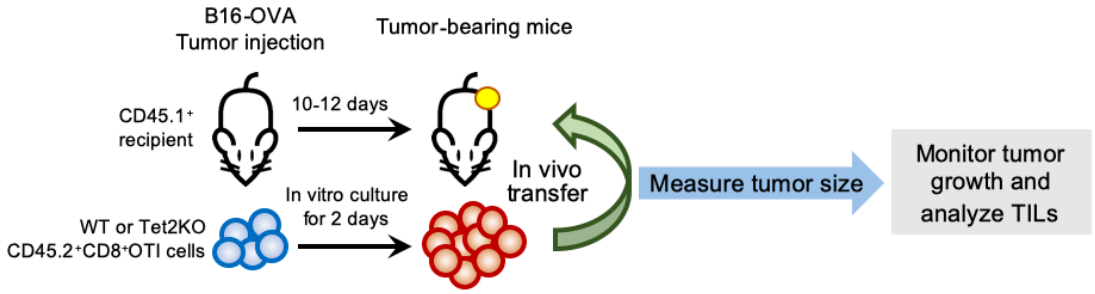

Figure 3-2. Flowchart of experiment: generating mouse melanoma models and adoptive T cell transfer. The B16-OVA mouse melanoma cell line expressing the ovalbumin protein was cultured in Dulbecco modified eagle medium (DMEM) with 10% FBS and passaged several times before inoculation. At the time of injection, cells were trypsinized and resuspended in DPBS. *B6.SJL-Ptprca Pepcb/BoyJ CD45*.1 female mice (12–16 weeks old) were injected intradermally with B16-OVA cells (50 µL per injection). Tumor measurements were recorded manually each day, and the tumor area was calculated in centimeters squared (length × width). After 10-12 days of tumor cell injection, we collected WT and *Tet2*$^{-/-}$ *OT-I*$^{+}$ CD8^{+} T cells, activated *in vitro*, were washed and resuspended in PBS, then injected into the retroorbital vein in anesthetized mice bearing B16-OVA tumors. Mice were killed on day 8 after adoptive T-cell transfer, then TILs were isolated.

growth of the B16-OVA tumor by adoptive T cell transfer. After 10-12 days of tumor injection, each genotype (WT and *Tet2*$^{-/-}$-*OT-I*$^{+}$) of 2 million of CD8^{+} T cells was adoptively transferred retroorbitally. Injected CD8^{+} T cells were isolated from OT-I expressing WT and *Tet2*$^{-/-}$ mice and activated in vitro with appropriated cytokines for 2-3 days. Tumor size was measured and recorded in each day, and mice were sacrificed on day 3 and day 8 after adoptive T cell transfer.

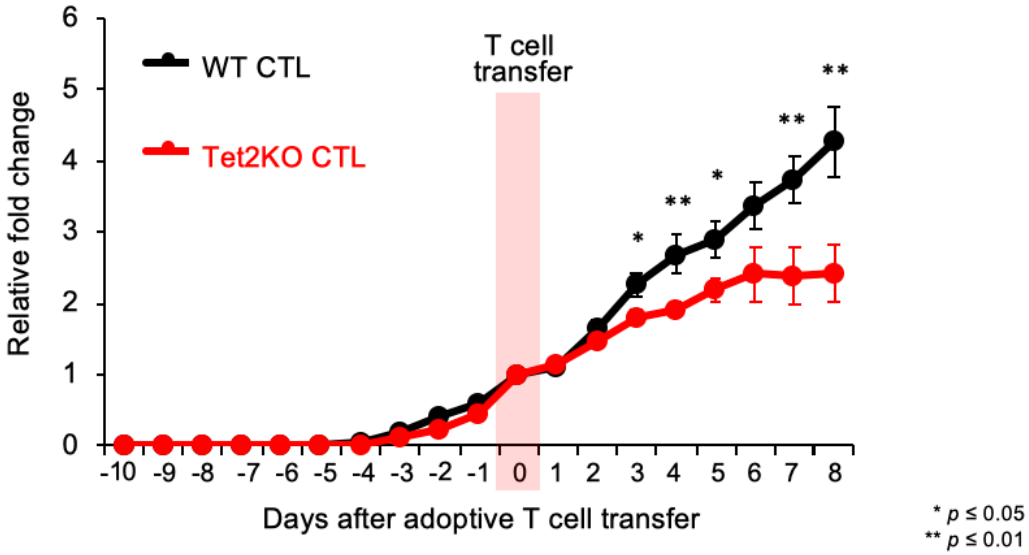

Figure 3-3. Growth curves of injected B16-OVA tumor. Growth profiles of B16-OVA tumors inoculated intradermally into B6.SJL-Ptprca Pepcb/BoyJ CD45.1^{+} recipient mice. On day 11 after tumor inoculation (red box), OT-I^{+} CD8^{+} T cells were adoptively transferred into tumor-bearing mice retroorbitally. Tumor size was measured and recorded each day. The graph shows the relative value of tumor progression upon tumor injections; n = 20 mice per group. The average ±SE is shown. Mice transferred with Tet2KO CD8^{+} T cells shows dramatic reduction of tumor growth and reduced tumor progression. * p<0.05; ** p<0.005

Compared to control tumor-bearing mice adoptively transferred with WT-OT-I^{+} CD8^{+} T cells, tumor-bearing mice adoptively transferred with Tet2$^{-/-}$ OT-I^{+} CD8^{+} T cells showed a strong delay of tumor progression and up to 80% reduction of the tumor size (Figure 3-3). Tumor size differences were detected as early as 3 days after adoptive T cell transfer. We performed at least 3 independent sets of experiments and observed the same trend every time. This finding suggests that Tet2 ablation in CD8^{+} T cells could reduce the tumor burden.

Comparison of Wild type and Tet2-deficient Cytotoxic T Cells Within the Tumor Microenvironment.

To obtain the molecular insight into this phenotype, we first checked the percentage of injected CD8^{+} tumor infiltrating T cells (TILs) in tumor by using flow cytometry. The absolute number of each cells varies greatly among individual mice

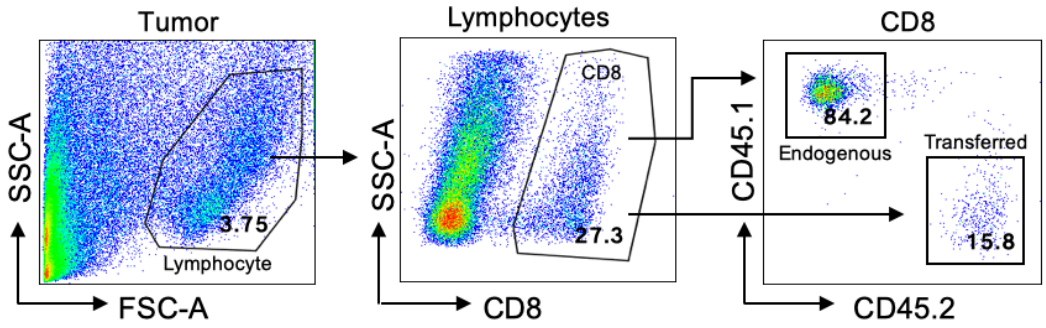

Figure 3-4. Gating strategies to identifying CD8^{+} CD45.1^{+} endogenous and CD8^{+}CD45.2^{+} injected TILs. Representative flow cytometry. A flow cytometry plot showing (left) lymphocyte population gating in tumor mass, (middle) CD8^{+} T cell population in lymphocytes and (right) distinct CD45.1^{+} and CD45.2^{+} population within CD8^{+} cells.

based on collected tumor size. We recorded and analyzed the percentage of each $CD45.1^+$ and $CD45.2^+$ population within total tumor mass. The gating strategy of flow cytometry plot is presented in Figure 3-4. Flow cytometry data analysis indicated that injected $CD45.2^+$ $Tet2^{-/-}$ TILs are substantially increased in tumors isolated from our immune therapy model at 8 days after adoptive T cell transfer (Figure 3-5A).

To verify the exact timing of the growth advantage in the Tet2 deficiency condition, we checked the percentage of $CD45.2^+$ TILs in tumor at different time points. Tumor-bearing, adoptive T cell transferred mice were sacrificed at 3 days and 5 days after adoptive T cell transfer, then TILs were isolated for flow cytometry analysis. Interestingly, augment TILs expansion in disrupted Tet2 condition was observed only at the Day 8 time point (Figure 3-5B), suggesting that Tet2 deletion in $CD8^+$ T cells

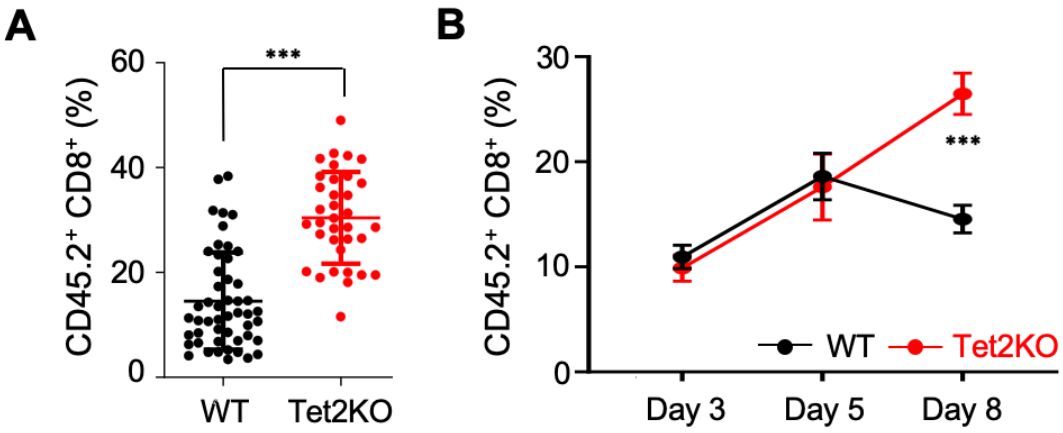

Figure 3-5. Tet2-deficient confers growth advantage to $CD8^+$ T cells. A. Tet2KO tumor infiltrating $CD8^+$ T cells show dramatic increase of cell numbers in a tumor isolated from a melanoma injected mouse after 8 days of adoptive T cell transfer. **B.** Tet2KO derived growth advantage is exhibited only on the Day 8 condition.

confers growth advantage, but also enhances cytolytic activity, as notable tumor regression in the Tet2$^{-/-}$-OT-I^{+} CD8^{+} T cells transferred group was noted in 3 days after adoptive T cell transfer.

The percentage of injected WT-OT-I^{+}CD8^{+} and Tet2$^{-/-}$-OT-I^{+} CD8^{+} T cells data in the day 8 condition was collected in three different sites (total tumor mass, spleen, and peripheral blood). Then we normalized the percentage into WT-OT-I^{+}CD8^{+} T cells in order to see whether the observed growth advantage on tumor foci was local or global. Tet2$^{-/-}$-OT-I^{+} CD8^{+} T cells exhibited a notable growth advantage when compared with

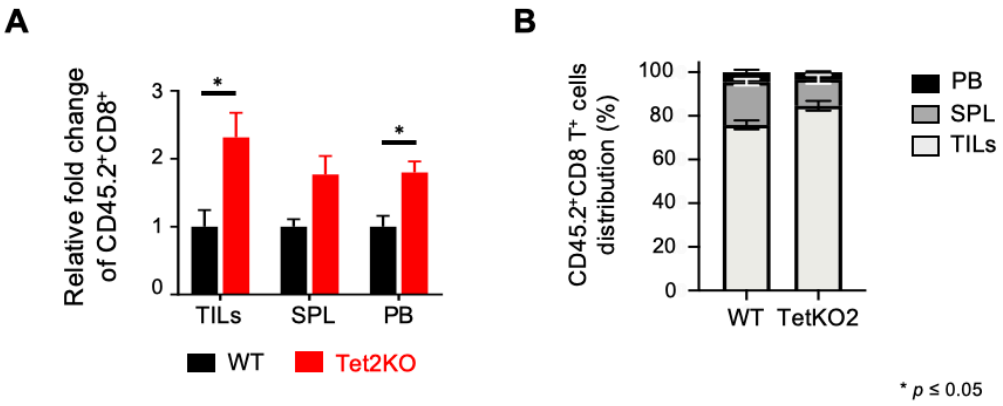

Figure 3-6. Tet2 alters CD8^{+} T cell behaviors in B16-OVA tumor bearing mice. **A.** Quantification of relative fold change of CD45.2^{+}CD8^{+}WT and Tet2KO T cells in tumor (TILs), spleen (SPL) and peripheral blood (PB). CD45.2^{+}CD8^{+} Tet2KO condition exhibited a notable growth advantage over the corresponding WT group in all three organs. The percentage of injected CD8^{+} T cells was measured and normalized by WT in each organ. **B.** Quantification of the percentage of WT and Tet2KO CD45.2^{+}CD8^{+}T cells (among all the analyzed CD8^{+}T cells) within tumor, spleen and peripheral blood. Tet2KO CD8^{+} T cells tend to have high enrichment at tumor foci, compared with the WT condition, by tracking the distribution on CD45.2^{+}cells in different organs. Bars show values with multiple data points for independent experiments.

the control group in all three sites (Figure 3-6A). However, endogenous $CD8^+$ T cells did not show the increased cell numbers in spleen and peripheral blood (data not shown).

Next, we examined the distribution of injected WT and $Tet2^{-/-}$-$OT\text{-}1^+CD8^+$ T cells by calculating the percentage of those cells in tumor foci, spleen, and peripheral

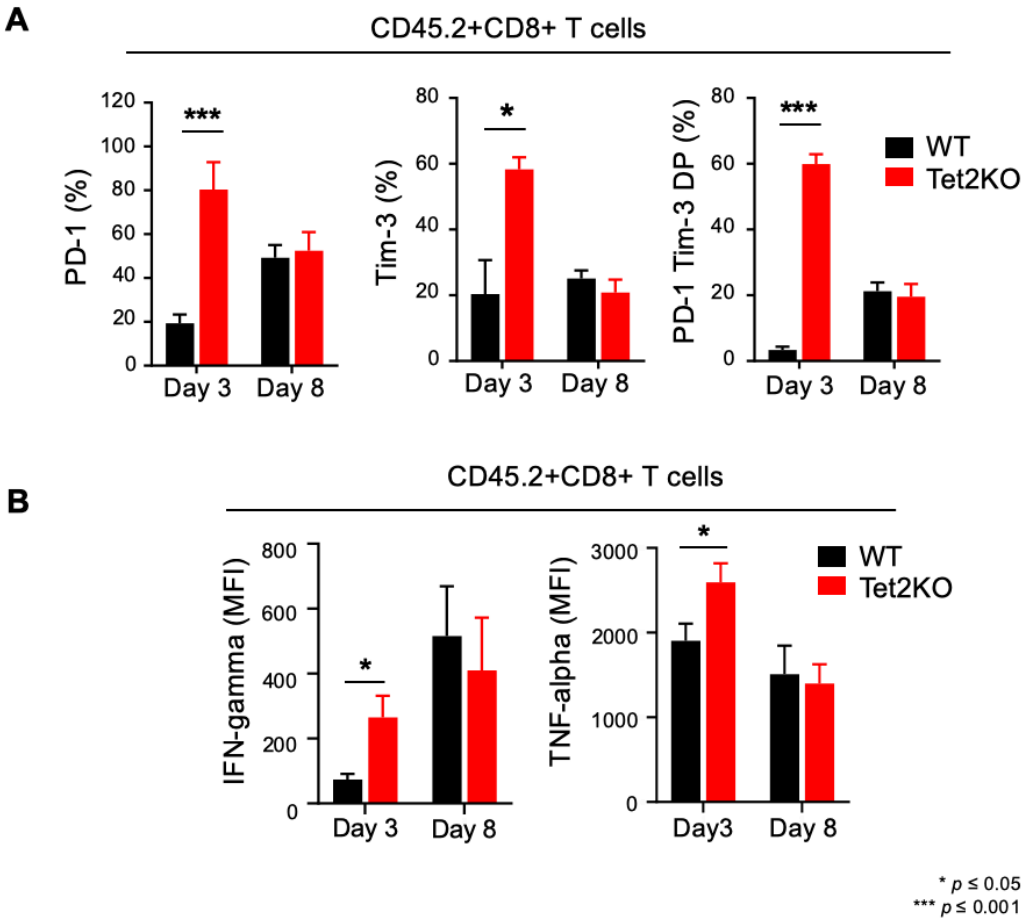

Figure 3-7. Injected Tet2KO $CD8^+$ $OT1^+$ TILs exhibit activated T cell phenotypes in day 3 condition. A. Quantification of PD-1, Tim-3 single positive and double positive population in WT and TET2KO $CD45.2^+$ $CD8^+$ TILs isolated at different time points. **B.** Quantification of cytokine production after re-stimulation with PMA and ionomycin in WT and Tet2KO $CD45.2^+$ $CD8^+$ TILs isolated in different time points. Bars show values with multiple data points for independent operations.

blood. The result showed that Tet2$^{-/-}$-OT-1^{+}CD8^{+} T cells tend to have high enrichment at tumor foci, compared with WT condition (Figure 3-6B). Interestingly, endogenous CD8^{+} T cells (CD45.1^{+}; all the cells are wild-type) also showed higher enrichment at the tumor site, indicating possibility of interaction between injected and endogenous CD8^{+} T cells.

To understand why Tet2 disrupted CD8^{+} TILs exhibit considerable tumor reduction, we examined expression levels of specific cell surface markers in isolated TILs. We examined T cell activation markers, CD44 and ICOS, and exhaustion markers, PD-1 and Tim-3, by flow cytometry, following the strategy mentioned above (Figure 3-4).

Interestingly, both activation and exhaustion markers, including single positive and double positive, indicated substantial increase only in Day 3 samples (data not shown and Figure 3-7A). We noted that rapidly activated T cells also express exhaustion markers. Also, we found that expression levels of tumor necrosis factor-alpha (TNFα) and interferon-gamma (IFNγ) significantly increased in Tet2$^{-/-}$-OT-1^{+}CD8^{+} T cells in the day 3 condition.

TNFα and IFNγ are major cytokines that are critical for both innate and adoptive immune responses. TNFα is a multifunctional molecule involved in the regulation of a wide spectrum of biological processes, including cell proliferation, differentiation, and apoptosis. IFNγ is well known for its immunostimulatory and immunomodulatory functions, produced predominantly by CD8^{+} cytotoxic T lymphocytes after developing antigen-specific immunity[99]. Therefore, increased expression of those cytokines generally is considered as a sign of activated state of immune cells.

To confirm whether activated Tet2 deleted TILs show increased ability to fight cancer, we performed an *in vitro* cytotoxicity assay, using co-cultured B16-OVA cells with either WT or Tet2 disrupted OT-I^{+} CD8^{+} T cells. Each CD8^{+} T cell was isolated from WT and *Tet2*$^{-/-}$*-OT-I*$^{+}$ mice, and activated with CD3, CD28, and an appropriate

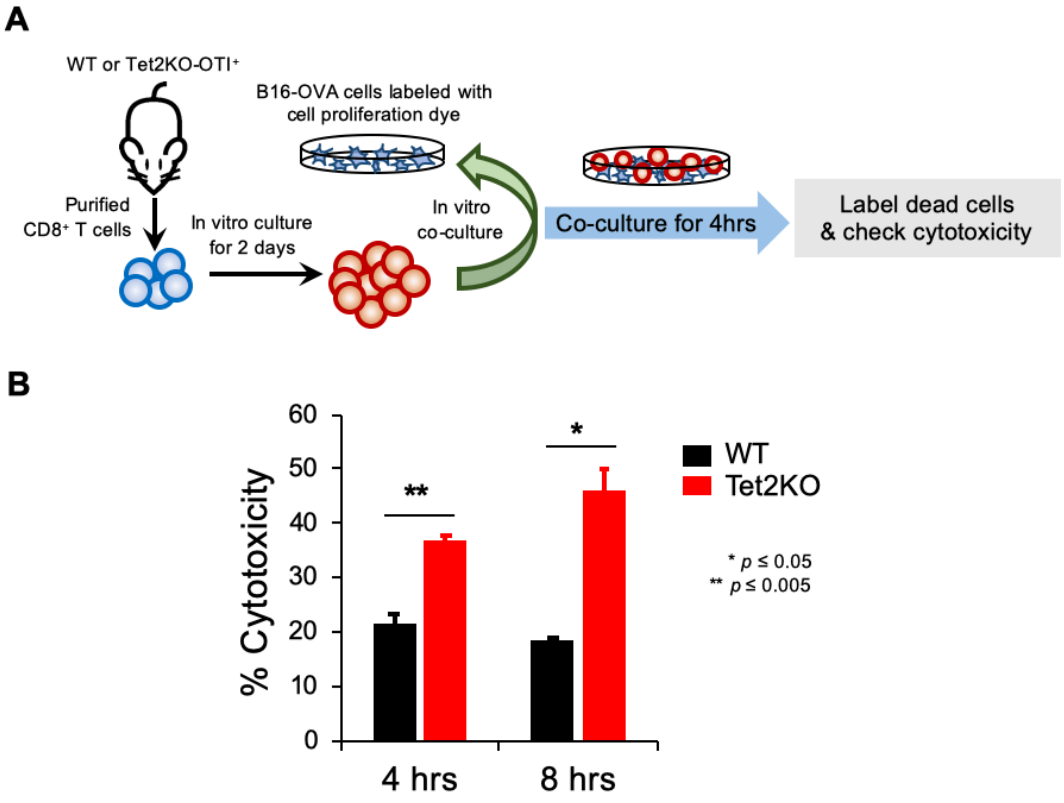

Figure 3-8. In vitro cytotoxicity test using co-cultured B16-OVA cells with WT and Tet2KO CD8^{+} T cells. A. Flowchart of experiment. CD8^{+} T cells were isolated from WT and Tet2KO OT1+ mice and activated *in vitro* with cytokines for 2 days. B16-OVA cells were labeled with cell proliferation dye to recognize them after co-culture. Pre-stained B16-OVA cells were plated on cell culture plate. Then 4X number of each T cell were plated on top of the B16-OVA. Cells were co-cultured with T cell specific medium for 4 and 8 h, followed by dead cell staining with FITC-conjugated caspase. **B.** Quantification of cytotoxicity of B16-OVA cells. Caspase positive population is considered as dead cells. Both 4 and 8 hours of co-culture condition showed a similar trend.

dose of IL-2 for 2-3 days *in vitro*. Then the optimized ratio of pre-labeled B16-OVA and OT-I$^+$ CD8$^+$ T cells (1:4) was co-cultured in T cell specific media for 4 and 8 hours.

After incubation, killed B16-OVA cells were stained with Caspase and detected by flow cytometry. Compared to WT control, depletion of Tet2 confers increased cytotoxicity on TILs (Figure 3-8), as we expected. Conclusively, disrupted Tet2 in CD8$^+$ T cells has increased antitumor efficacy by promoting proliferation and cytotoxicity of CD8$^+$ T cells.

Effect of anti-PD-L1 treatment on tumor progression

PD-1 is a surface receptor that negatively regulates TCR responses[100]. Immunotherapy targeting the PD-1/PD-L1 axis (check point blockade) has shown remarkable results in certain types of cancer, including melanoma[101, 102]. Although it is clinically proven and accepted for therapy, few patients receive a favorable prognosis. More detailed mechanism and cofactors should be examined to maximize its therapeutic potential.

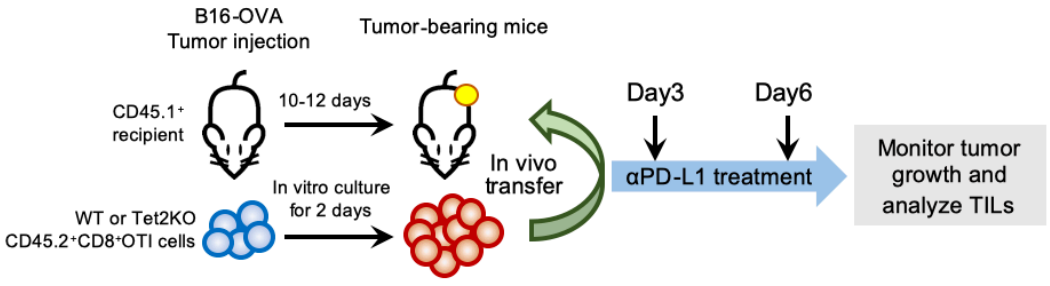

Figure 3-9. Flowchart of experiment: generating mouse melanoma models and adoptive T cell transfer with PD-L1 antibody treatment. The same experimental procedure was used as described in Figure 2. Anti PD-L1 antibody was treated twice on Day 3 and Day 6 after adoptive T cells transfer.

Continuing the research process, we observed augmented PD-1 expression in Tet2 deleted TILs. To examine whether the blocking PD-1 signaling pathway in our immunotherapy model induced change in tumor progression, we generated immunotherapy with the same method described previously in this chapter. Then we injected 200 μg of anti-PD-L1 antibody per mouse (Figure 3-9). For the control group, anti-rat IgG2b was used with same amount.

Anti-PD-L1 treatment showed dramatic regression of tumor growth in the WT-OT-I^{+}CD8^{+} T cell injected group. However, it did not show statistically significant change in Tet2$^{-/-}$-OT-I^{+}CD8^{+} T cell injected group (Figure 3-10), indicating Tet2

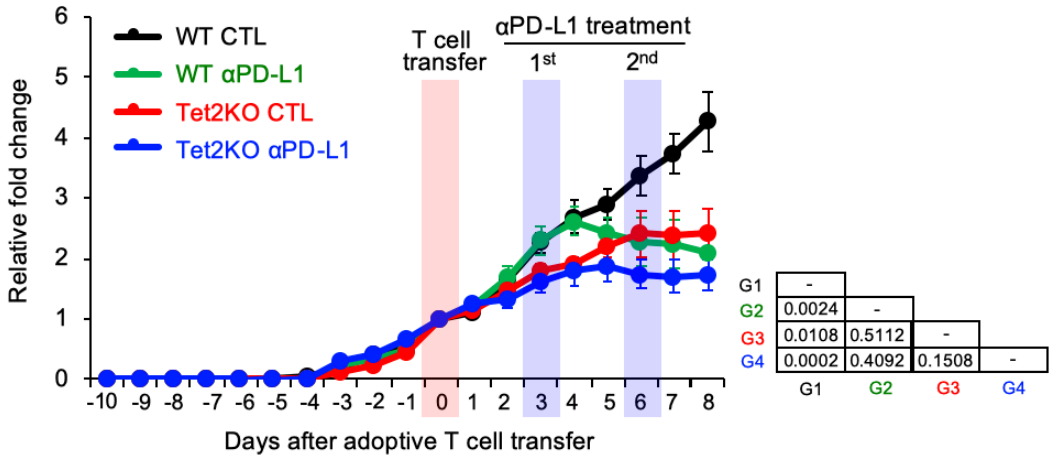

Figure 10. Growth curves of injected B16-OVA tumor with anti-PD-L1 treatment. Growth profiles of B16-OVA tumors inoculated intradermally into *B6.SJL-Ptprca Pepcb/BoyJ CD45.1*$^{+}$ recipient mice. On day 11 after tumor inoculation (red box), OT-I^{+} CD8^{+} T cells were transferred adoptively into tumor-bearing mice retroorbitally. Tumor size was measured and recorded each day. The graph shows the relative value of tumor progression upon tumor injections; n = 20 mice per group. Theaverage ±SE is shown. Mice transferred with Tet2KO CD8^{+} T cells show a dramatic reduction of tumor growth and reduced tumor progression. Anti-PD-L1 treatment exhibited a notable decrease of tumor volume in WT, but not in the Tet2KO condition.

deficiency in TILs have at least a similar effect with anti-PD-L1 treatment. Results also show that increased PD-1 expression in Tet2 deleted TILs is certainly a marker for an activated state of $CD8^+$ T cells, rather than an exhausted state.

Single-cell RNA-seq (scRNA-seq) revealed enhanced activation of Tet2KO TILs

To further identify the cell populations contributing to anti-tumor immunity, we performed scRNA-seq analysis in $CD45.2^+CD8^+$ TILs in four experimental groups (WT, Tet2KO, WT + anti-PD-L1, and Tet2KO + anti-PD-L1) on 8 days after adoptive T cell

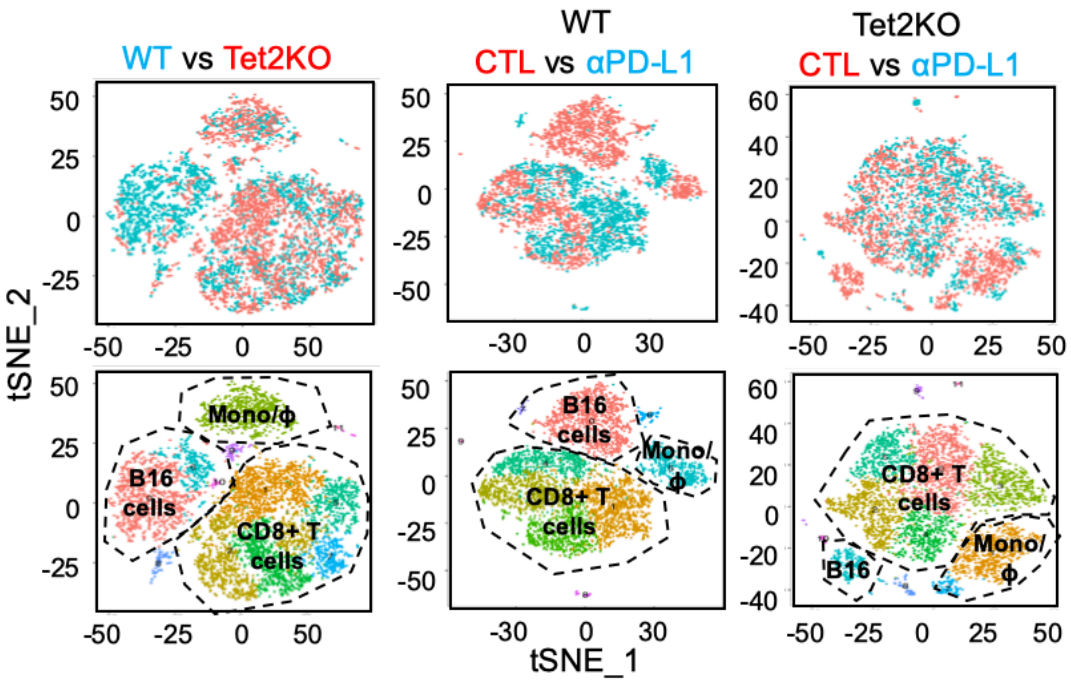

Figure 3-11. Dissection and clustering of Tumor infiltrating lymphocytes in isolated tumor mass. The t-SNE (t-distributed stochastic neighbor embedding) projection of scRNA-seq data obtained from wild-type (WT) (cyan) and Tet2KO (red) (left), WT with control (red) and WT with PD-L1 antibody treated (cyan) (middle) and Tet2KO with control (red) and Tet2KO with PD-L1 antibody (cyan) (right) treated tumor infiltrating lymphocytes.

transfer (Figure 3-11). We observed three major groups of cells from our analysis: TILs ($CD8^+$), monocytes ($F4/80^+$), and B16-OVA tumor cells ($CD63^+$) (Figure 3-11 and 12). We performed cross-comparison analysis between WT and Tet2KO without anti- PD-L1 treatment, WT with and without anti-PD-L1 treatment, and Tet2KO with and without anti-PD-L1 treatment. From these analyses, we observed that the Tet2KO group exhibited significant reduction of B16-OVA tumor cells, compared with the WT group (Figure 3-11 left). Similarly, in the WT group, anti-PD-L1 treatment also displayed

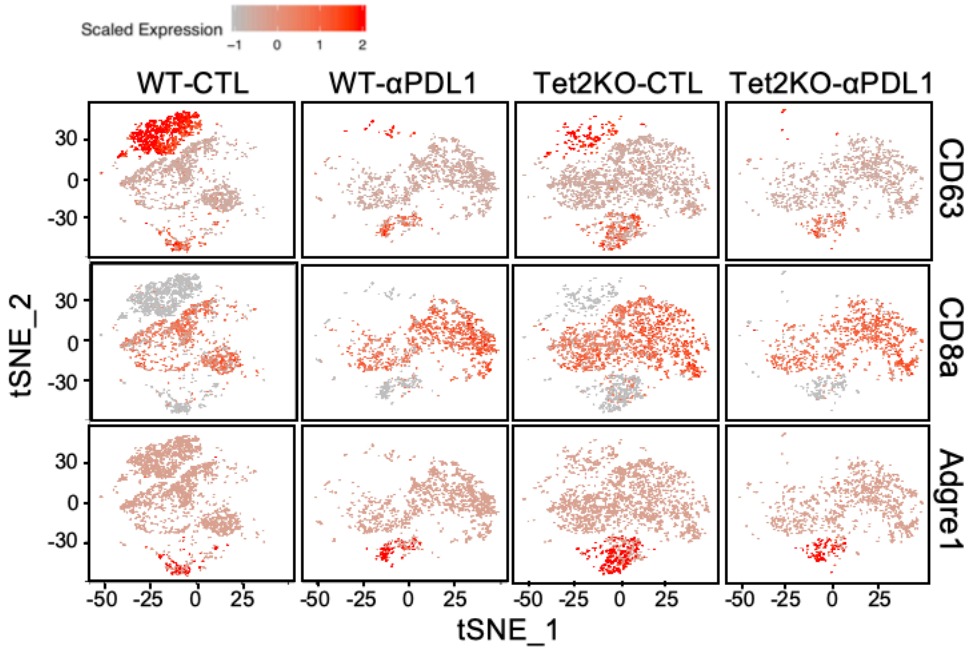

Figure 3-12. Subtype analysis based on scRNA-seq gene expression. t-SNE plot of scRNA-seq data collected from WT with or without PD-L1 antibody treated and Tet2KO with or without PD-L1 antibody treated tumor infiltrating lymphocytes. WT treated with PD-L1 antibody and all Tet2KO groups showed significant reduction of tumor cell population and increased $CD8^+$ population when compared with WT control antibody treated condition.

notable decreased B16-OVA tumor cells, compared with untreated group (Figure 3-11 middle). The anti-PD-L1 treatment has minor effects within Tet2KO group compared with untreated group (Figure 3-11, right).

These results are highly consistent with our experimental results shown in Figure10. Since our analysis is focused on $CD8^+$ TILs, we then selected $CD8^+$ T cells among four experimental groups, and performed cluster analysis. We identified 5 major clusters in selected $CD8^+$ TILs. Our analysis showed that the distribution of cells from four experimental groups varies within 5 clusters (Figure 3-13A). Cluster 0 showed similar cellular distribution among four groups, while anti-PD-L1 treatment resulted in significantly decreased cell number in cluster 1 and 2. Tet2KO led to increased cell numbers in cluster 3 and 4; while anti-PD-L1 treatment promotes the cell number only in WT group in cluster 3 and 4, but not in Tet2KO group (Figure 3-13A).

To further characterize the cell types within clusters, we downloaded publicly available RNA-seq data from the purified subsets of $CD8^+$ T cells, including naïve, effector, memory $CD8^+$ T cell (GEO database, GSE122969), $PD1^+Tim3^+$ double positive $CD8^+$ TILs, with and without anti-PD1 treatment (GEO database, GSE122969). Then we selected the top 20 differentially expressed genes among these groups and checked the expression level of these genes within identified 5 clusters.

Based on the gene expression pattern, the cluster 0, 1 and 2 are an exhausted-like cell. On the other hand, cluster 3 and 4 exhibited activated $CD8^+$-like feature (Figure 3-13B). This analysis further confirmed that Tet2 deletion has minor effects on $CD8^+$ T cell exhaustion, but significantly contributed to $CD8^+$ T cell activation during anti-tumor

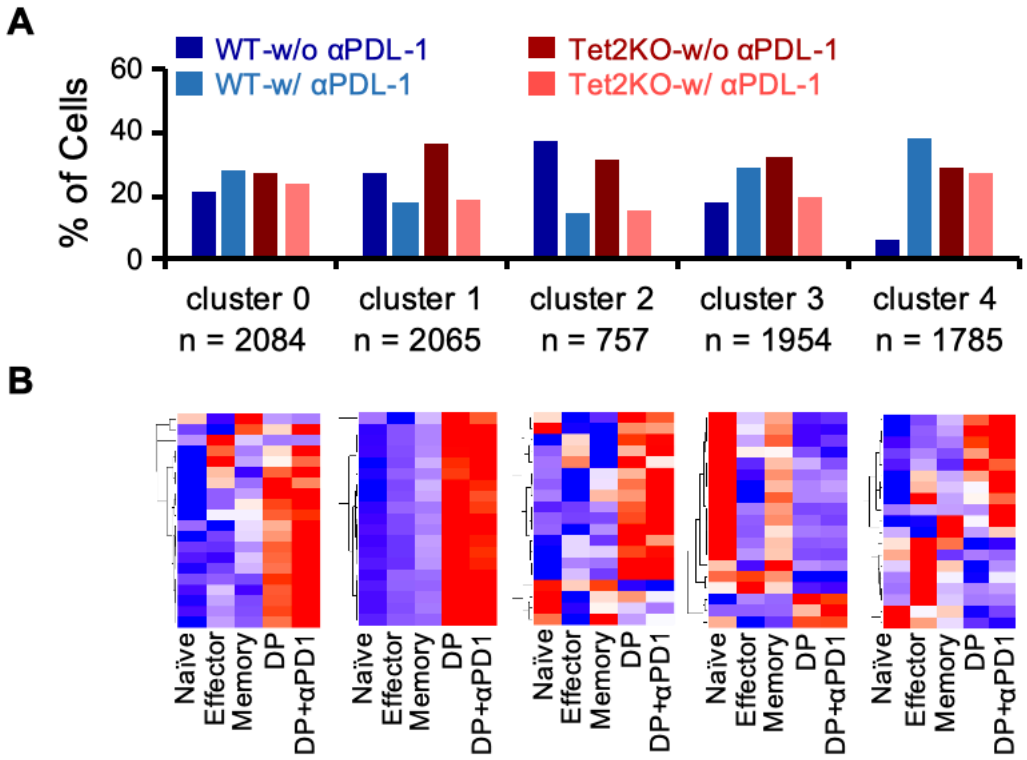

Figure 3-13. Cluster analysis based on scRNA-seq gene expression. A. Quantification of cell number in each group. **B.** Heat map presentation of expression data of T cell differentiation-associated differentially expressed genes (DEGs) in each cluster. DP: PD-1^{+}Tim3^{+} double positive, DP+αPD1: PD-1^{+}Tim3^{+} double positive with anti-PD-1 treatment. RNA-seq data were obtained from Gene Expression Omnibus (GEO database).

immunity. However, the anti-PD-L1 treatment significantly reduced the exhausted TILs during anti-tumor immunotherapy.

Tet2 deletion enhances the transcription of anti-tumor related gene

From scRNA-seq analysis, we observed that CD45.2^{+}CD8^{+} selection contains B16-OVA tumor cells and monocytes, which both highly express CD63. To further

investigate how Tet2 regulates $CD8^+$ TILs during anti-tumor immunity, we then purified $CD63^-CD45.2^+CD8^+$ T cells from tumor tissue and performed RNA-seq (transcriptome) and ATAC-seq (chromatin accessibility) analysis at days 0, 3, and 8

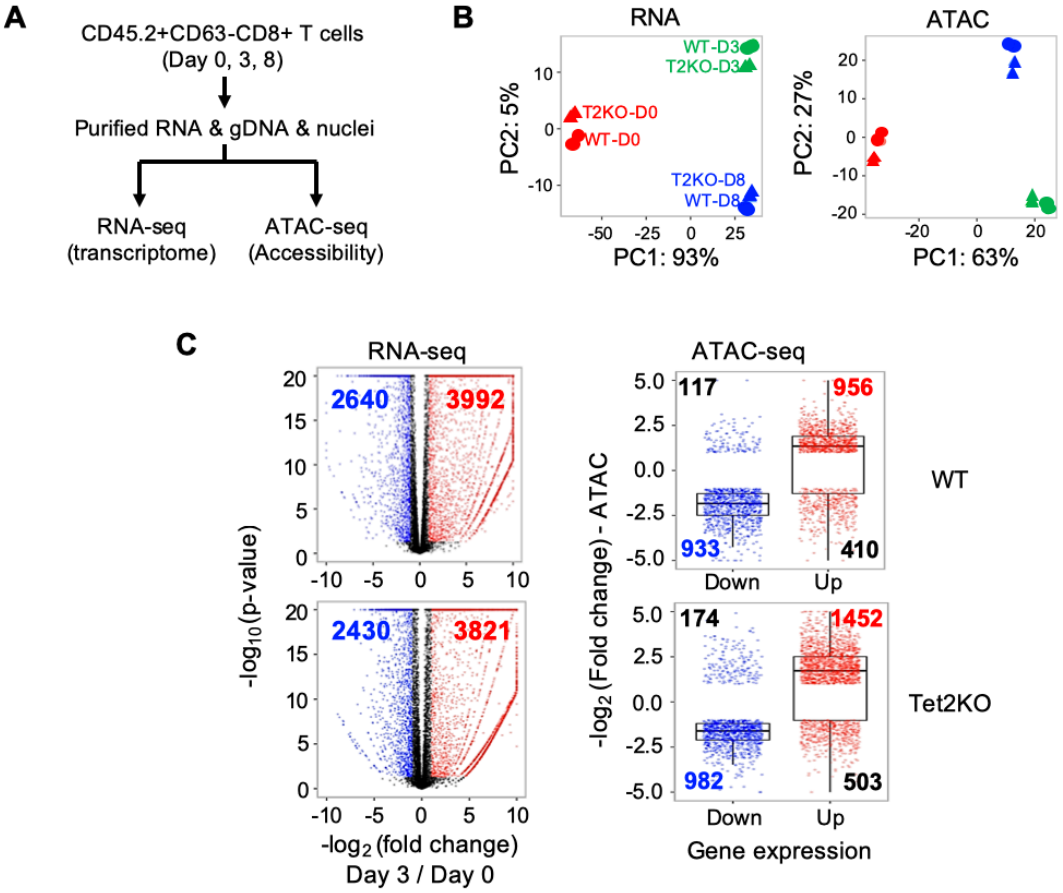

Figure 3-14. **Analysis on RNA-seq and ATAC-seq data obtained from WT and Tet2KO TILs at different time points A.** Flowchart of experiment. $CD63^-CD45.2^+CD8^+$ T cells were isolated from tumor in each group of mice, then mRNA and 50,000 of nuclei were prepared for downstream analysis. **B.** PCA plot of RNA-seq (left) and ATAC-seq data. **C.** Volcano plot illustrating the differentially expressed genes (DEGs) between Day 0 and Day 3 groups in both WT and Tet2KO TILs (p value <= 0.05 and |log2 fold change|>1). D. Dot plots depicting the number (Day 3 over Day 0) of ATAC signals (Y-axis) at WT (up), or Tet2KO ITLs (down) of DEGs which are downregulated (blue), or upregulated (red) in Day 3 compared to Day 0.

after adoptive transfer (Figure 3-14A). We observed dramatic changes of gene expression, and chromatin accessibility at different days after adoptive transfer (Figure 3-14B and C) during anti-tumor process.

By comparing the RNA-seq and ATAC-seq data, we observed dramatic transcriptome and epigenetic remodeling events in both WT and Tet2KO TILs (Figure 3-14C). Consistent with previous research, we observed a strong positive association between transcription changes and chromatin accessibility in analyzed TILs (Figure 3-14C), suggesting that epigenetic remodeling is one of key regulators contributing to transcription output during anti-tumor immunity.

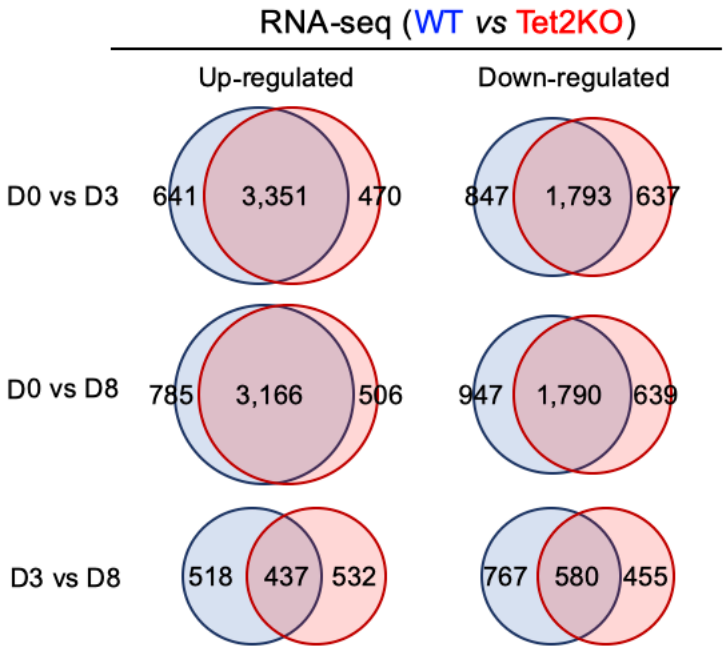

Figure 3-15. Venn diagram showing the degree of overlaps between WT and Tet2KO. Differentially expressed genes (DEGs) in Day 0 vs Day 3, Day 0 vs Day 8, and Day 3 vs Day 8, within WT and Tet2KO, were categorized first. This revealed the overlap between WT and Tet2KO DEGS.

To further examine the function of Tet2 during this process, we first compared differentially expressed genes (DEGs) between WT and Tet2KO groups to identify WT- or Tet2KO-specific DEGs during anti-tumor immunity at different days (Figure 3-15). In total, we identified 12 groups of WT- or Tet2KO-specific DEGs by comparing gene expression at different days after adoptive transfer (D0 vs 3, D0 vs 8, and D3 vs 8) (Figure 3-15, 3-16A and B). The Gene Set Enrichment Analysis (GSEA) showed that the genes that are specific up-regulated in Tet2KO TILs are enriched with cytokine production and immune signaling pathways (e.g., Interferon-gamma responding genes) (Figure 17); while genes that are specific down-regulated in Tet2KO TILs are associated

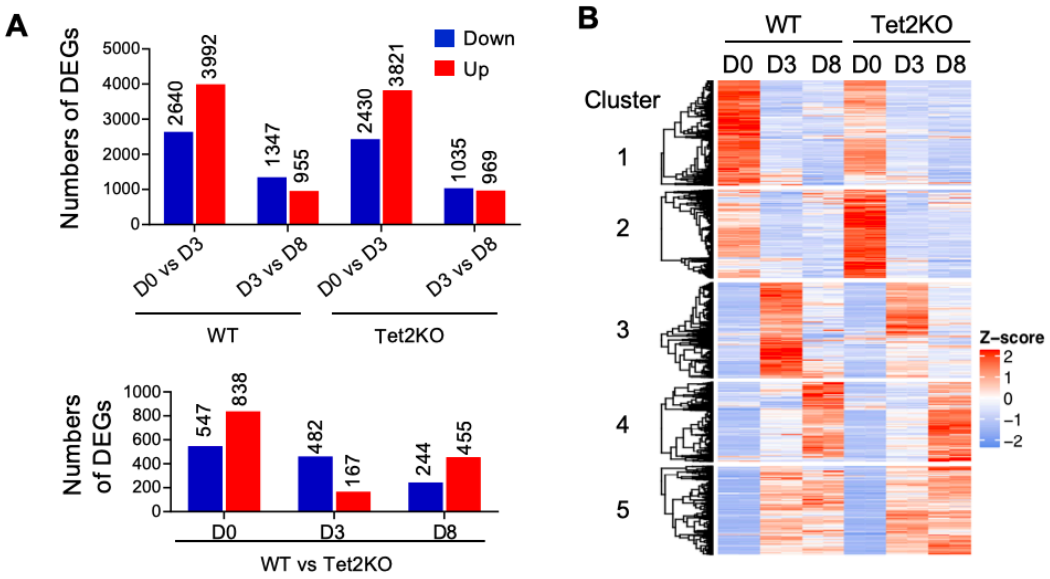

Figure 3-16. **Dynamic changed in gene expression in WT and Tet2KO TILs at different time points**. A. Visualization of differentially expressed genes (DEGs) in each group. DEGs in Day 0 vs Day 3, and Day 3 vs Day 8, within WT and Tet2KO each were categorized and compared (up), or DEGs in WT and Tet2KO were compared on Day 0, Day 3, and Day 8 (down). **B.** Heat map presentation of DEGs WT and Tet2KO in different time points in each cluster.

with cell cycle and proliferation (e.g., Cdk1, Aurka, centromere proteins) (Figure 3-17).

One the other hand, the genes that are specific up- or down-regulated in WT TILs

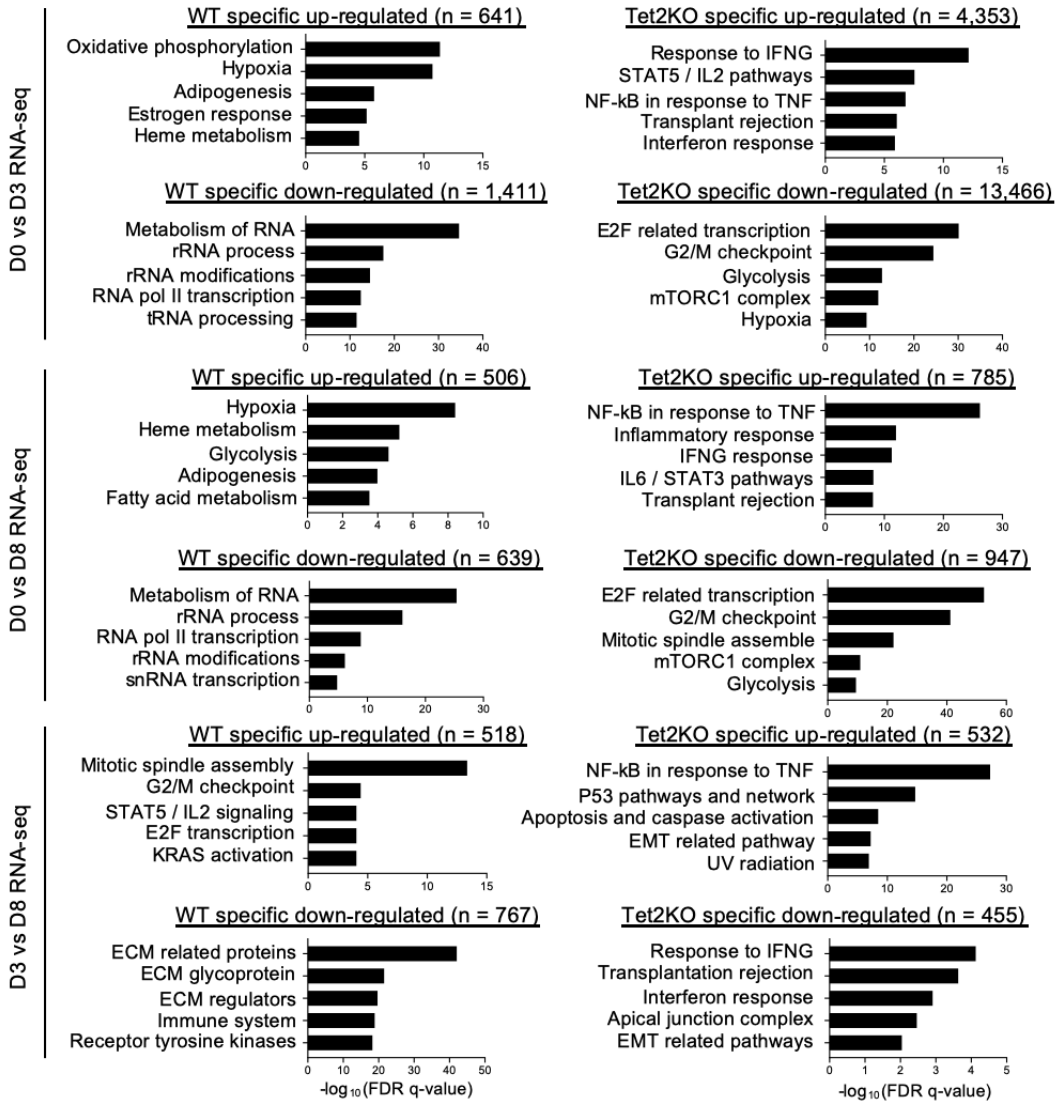

Figure 3-17. Gene set enrichment analysis (GSEA). Left, WT-specific up or down regulated DEGs analyzed in different time points of data set (Day 0 vs Day 3, Day 0 vs Day 8, and Day 3 vs Day 8, respectively), Right, Tet2KO-specific up or down regulated DEGs analyzed in different time points of data set (same with WT condition).

are associated with certain house-keeping functions, such as metabolism (e.g., cytochrome c oxidase family members), RNA processing (e.g., WD repeat domains), and extracellular matrix function (e.g., laminin subunits) (Figure 3-17). These data suggested that Tet2 deficient TILs exhibited enhanced anti-tumor immunity by increasing the transcription of cytokines and innate immune related genes.

Tet2 deficiency reshapes the chromatin accessibility in TILs

Next, we performed a similar comparison analysis using ATAC-seq analysis (Figure 3-18A and B). We first identified the differential enriched region between Day 0 and 3, Day 0 and 8, and Day 3 and 8 within WT or Tet2KO TILs. From this analysis, we

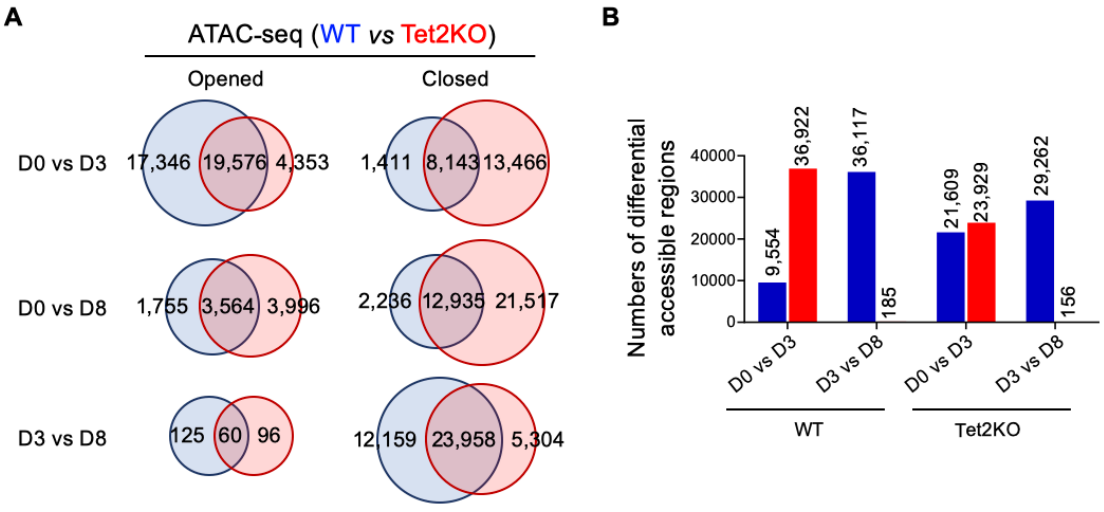

Figure 3-18. **Comparison of opened and closed regions of chromatin in WT and Tet2KO TILs at different time points. A.** Venn diagram showing the degree of overlaps between WT and Tet2KO. Different ATAC peaks in Day 0 vs Day 3, Day 0 vs Day 8, and Day 3 vs Day 8, within WT and Tet2KO. Each was categorized first, then the overlap between WT and Tet2KO ATAC peaks was displayed. **B.** Visualization of ATAC peaks in each group. ATAC peaks in Day 0 vs Day3, and Day 3 vs Day 8, within WT and Tet2KO. Each was categorized and compared.

observed dramatic increased chromatin accessibility from day 0 to day 3, and pronounced closed chromatin from day 3 to day 8 during this anti-tumor process in WT TILs (Figure 3-18A and B). To further investigate how Tet2 regulates the function of

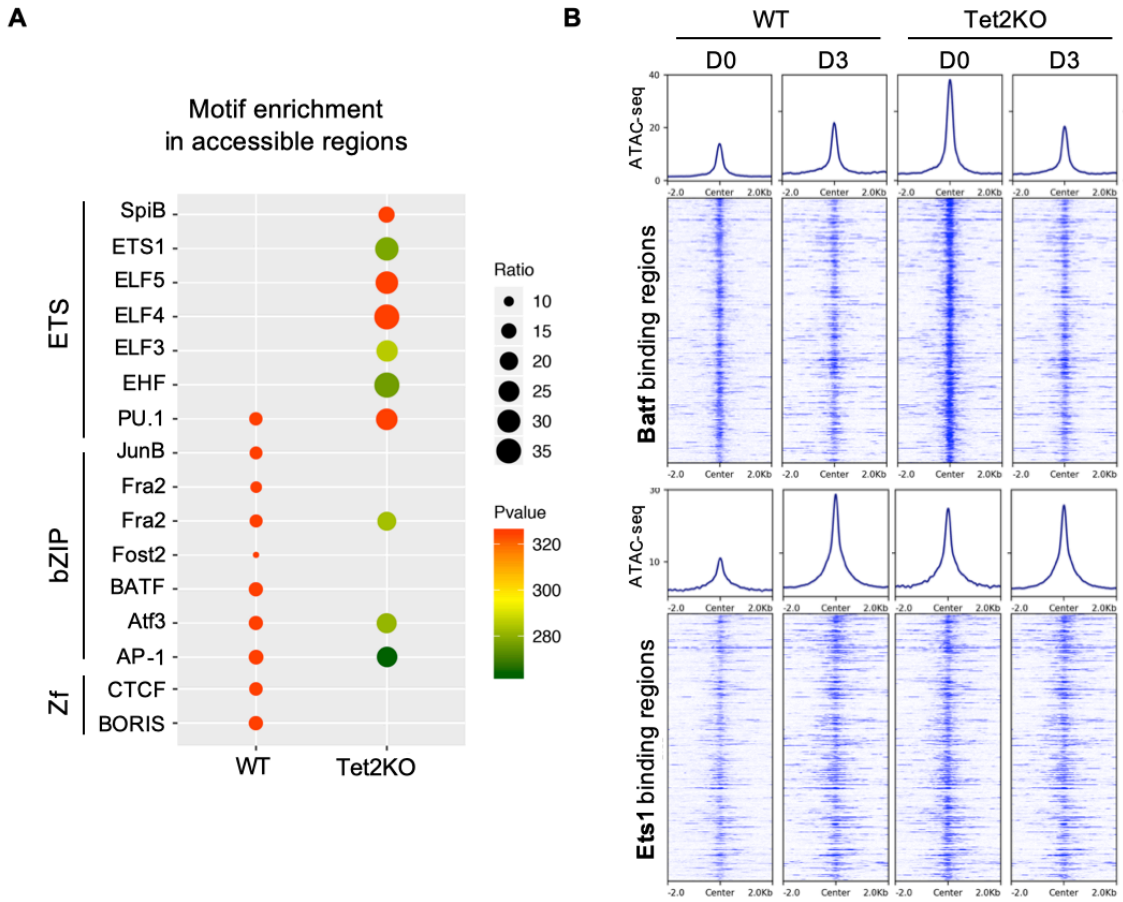

Figure 19. **Motif heatmap & ATAC-seq peaks.** A. Enrichment of motif in WT (left) and Tet2KO (right) specific opened chromatin regions between Day 0 and Day 3. The color scale represents –log10 (P-value), and the circle size represents the fraction of peaks with each motif. B. Normalized ATAC signals plot (top) and heatmap (bottom) representations of BATF and ETS1 binding loci (±5 kb) in Day 0 and 8 of WT and Tet2KO TILs. The color scale in each heatmap, from blue to white, represents high to low normalized signal.

TILs during this process, we identified WT- or Tet2KO-specifically changed chromatin accessible regions (Figure 3-18A and B). Accumulated studies report that chromatin accessible regions are critical for transcription factor (TF) binding.

We then analyzed the enrichment of TF motifs within identified WT- or Tet2-specifically regulated chromatin accessible regions (Figure 3-19A). Interestingly, we observed enrichment of bZIP and Ets motifs within WT- and Tet2-specific regulated regions, respectively (Figure 3-19B). To validate this observation, we compared ATAC-seq data collected from this study with published Batf (bZIP family) and Ets1 (Ets family) ChIP-seq data. Indeed, we observed differential enrichment of Batf and Ets1 in WT and Tet2KO TILs at Day 0 and Day 3. At Day 0, the chromatin accessibility of Batf and Ets1 in Tet2KO $CD8^+$ T cells is significantly higher than the WT group, suggesting high activity of Tet2KO $CD8^+$ T cells. At day 3, the chromatin accessibility of Batf decreases in Tet2KO groups, but not in the WT group; while the chromatin accessibility of Ets1 is increased in WT, but not in Tet2KO groups. These results are consistent with the motif enrichment analysis, suggesting that Tet2 deletion reshapes the chromatin accessibility of bZIP and Ets TF families in TILs.

Discussion

In this chapter, I generated an immune therapy model using a B16-OVA mouse melanoma cell line to examine how the Tet2 deficiency in immune cell type affects tumor progression. I first compared tumor progression in tumor bearing mice with transfer of WT or Tet2KO-OT1$^+$ CD8$^+$ T cells. Interestingly, theTet2KO- OT1$^+$ CD8$^+$ T cells transferred group showed significant reduction of tumor size as early as 3 days after adaptive T cell transfer. This result suggested that Tet2 has a tumor promoting functions, contradicting previous studies which found that Tet2 is an important tumor suppressor.

Although TET2 functions, especially in hematopoietic system, are well established as a tumor suppressor, it is unclear how Tet2 deletion affects different immune cell types and whether Tet2 activity within various hematopoietic cells influences other cell types and tumor microenvironment. To answer the question, I first established an immune therapy model using B16-OVA mouse melanoma cells and OT-I$^+$ CD8$^+$ T cells that specifically recognize ovalbumin peptide. For a mouse model system, we used immune competent mouse and Tet2 deleted CD8$^+$ T cells because of the contradictory function of TET2. We used Tet2 disrupted CD8$^+$ T cells into tumor bearing wild type mice, which have endogenous CD8$^+$ T cells and all the other immune cells. As a result, we (1) reduced the risk that may be caused by total Tet2 knock out, and (2) successfully demonstrated that depletion of Tet2 in cytotoxic T cells can benefit anti-tumor efficiency by enhancing CD8$^+$ T cell differentiation toward activated T cell state.

We expect that this model system will open up new opportunities to study the dynamic interaction between cytolytic T cells with tumor microenvironments, including various immune cells and connective tissues. Still to be investigated is how Tet2 might be regulated by tumor environment, or *vice versa*, and whether Tet2 affects gene expression and, thereby, the function of $CD8^+$ T cells. To address those issues more carefully, we need to perform tumor injection onto the total Tet2 deficiency mouse and record the tumor progression. Then we must compare the result with our previous model system for sorting out the $CD8^+$ T cell specific effect of Tet2.

We found that Tet2 knock out $CD8^+$ T cells display dramatic increase of T cell activation markers (data not shown), as well as exhaustion markers. Since Tet2 disrupted $CD8^+$ T cells exhibit augmented expression of TNF-alpha and interferon-gamma as certain phenotypic traits of activation, increased expression of PD-1 and Tim-3 should be considered as a sign of rapid activation, rather than of exhaustion. However, the long-term effect of Tet2 depletion in $CD8^+$ T cell should be tested because we only tested tumor progression in a relatively short period of time (8 days after adoptive T cell transfer), and rapid activation of T cell could be a sign of early exhaustion.

Certainly, controlling Tet2 activity is the way to maximize its benefit for cancer immunotherapy. In an *in vitro* co-culture setting with B16-OVA cells and Tet2 deleted $CD8^+$ T cells showed increased cytotoxicity. To get more detailed molecular insights into this phenomenon, we should examine proliferation rate, cell death rate, and cell cycle or DNA replication frequency in co-cultured WT and Tet2KO $CD8^+$ T cells.

PD-1 is a surface receptor and type I membrane protein[103] that first was found as a gene that involved in apoptosis. Later, it was shown that PD-1 knock down mice were prone to autoimmune disease[104], suggesting a negative regulator of immune reaction. Currently, it is being used widely in clinical check point inhibitor therapy, and has shown remarkable results in multiple categories of cancer. However, only a limited number of patients respond accordingly after either PD-1 or PD-L1 antibody treat and this non-responsiveness remains a major challenge for its success. Therefore, there is an urgent need to find more effective and novel approaches for cancer immunotherapy related with checkpoint blockade.

Based on our preliminary data, we found that expression levels of PD-1 and other T cell exhaustion markers are substantially changed in *Tet2* total knock out mice. In this connection, we applied PD-L1 antibody treatment in our immunotherapy model, and discovered that PD-1 pathway inhibition only dramatically affects in WT-OT-1^+ $CD8^+$ T cells transferred condition. The antibody treatment on Tet2KO-OT-1^+ $CD8^+$ T cells injected condition showed subtle changes, but none of them was statistically significant. Interestingly, besides tumor growth curve, scRNA-seq data also indicated that Tet2 deficiency in $CD8^+$ T cells seemed to resemble PD-1 blockade in WT condition, suggesting disrupted Tet2-mediated $CD8^+$ T cell activation mechanisms somehow overlapped with the effect of PD-L1 inhibition.

Cluster analysis further indicated that depleted Tet2 in TILs exhibit activated $CD8^+$-like T cells features. Interestingly, anti-PD-L1 treatment showed reduced properties of exhausted TILs in both WT and Tet2KO TILs, but only WT TILs showed

increased gene expression that related with activated T cell features after PD-L1 treatment. On the other hand, disrupted Tet2 exhibited minor effects on expression of an exhaustion-related gene set, but substantially contributed to $CD8^+$ T cells activation processes during tumorigenesis.

The data shown in this chapter identified a novel function of Tet2 deficiency in cytotoxic T cells within the context of cancer immunotherapy and its mechanism to confer benefit on antitumor efficiency. To further understand the function of Tet2 during tumor progression, we checked dynamics of transcriptome and chromatin accessibility in TILs isolated at 0, 3, and 8 days after adoptive T cell transferred tumor. We observed considerable changes of both transcriptome and epigenetic remodeling, showing a strong correlation between them. This indicated that epigenetic remodeling is crucial regulator generating specified transcription output during anti-tumor immunity.

We particularly observed that WT and Tet2KO TILs showed distinct chromatin accessibility within transcription factor (TF) binding motifs. Based on TF motif enrichment analysis, we focused on Batf and Ets1 TFs that indicated dramatic changes between the WT and Tet2KO condition. There is growing evidence that Batf and Ets play essential roles in immune system regulation, including differentiation of Th17 population and T cell exhaustion[105, 106]. It is an interesting finding that Tet2 deficiency in TILs remodels the chromatin accessibility in specific TF motifs to enhance its anti-tumor efficacy.

Certainly, there is more to be learned about the detailed mechanisms. To link these dynamic changes of transcriptomes and chromatin accessibility with Tet2 more

directly, genome-wide 5mC, as well as 5hmC profiling, should be performed and analyzed in parallel with our RNA-seq and ATAC-seq data sets to get comprehensive understanding about Tet2-mediated deposited 5hmC and chromatin dynamics, followed by altered gene expression in specific regions. In addition, it is crucial to determine how to maximize the beneficial effect of Tet2 deficiency in cancer immunotherapy.

Our data clearly showed that disrupted Tet2 in TILs exhibited anti-tumor efficiency by regulating the transcription of key genes involved in T cell activation. However, our data only focus on early stage of TILs development. It needs to determine whether Tet2 deletion is beneficial in long-term treatment. In addition, our data indicated that the expression of T cell exhaustion markers is significantly up-regulated in the Tet2 deletion condition. As this can be considered as a sign of early and rapid activation of T cells, researchers must clearly demonstrate the underlying mechanisms of the increased expressions of contradictory factors.

One possibility is that Tet2 deletion in TILs changes its chromatin state to a reprogrammable PD-1^{hi} state. Philip et al. suggested that specific chromatin states in TILs, called chromatin state 1 and 2, represent a dysfunctional state of TILs and show different plasticity[107]. Our RNA-seq data from TILs, isolated from 8 days after adoptive T cell transferred tumor, showed that Tet2 knockout TILs exhibit a substantial increase of CD5 expression. We suggest this as a prediction marker of reprogrammability of heterogeneous TILs. Although further validation is necessary, it could provide a feasible

explanation of our complexed phenotype in TILs, caused by Tet2 disruption. We expect it to reveal important the potential clinical relevance of Tet2 deletion in cancer immunotherapy.

CHAPTER IV

CONCLUSIONS

DNA modification plays a pivotal role in the epigenetic control of gene expression in an organism. Traditionally, much attention is given to 5-methylcytosine (5mC), a major form (up to 1% of the total genome) of DNA modification. The discovery of the ten-eleven translocation (TET) has prompted broad interest in the potential function of its product, 5-hydroxymethylcytosine (5hmC), in remodeling the mammalian DNA methylation landscape.

Advances in next generation high-throughput sequencing technologies, followed by progress in the epigenetics field during the past decade, have demonstrated the essential functions of TET enzymes in regulating various cellular processes, including gene expression, cell differentiation, and suppressing tumor formation in certain types of cancer. Among TET family enzymes, TET2 is one of the most frequently mutated genes in hematopoietic malignancies of both myeloid and lymphoid origin[108]. Researchers report that Tet2 deficiency leads to hematopoietic cell expansion, followed by the development of aggressive cancer in mouse models. While the role of TET2 in malignancies has been extensively reviewed, the tumor-promoting function of TET2 has been reported only recently[61, 62, 64].

Immunotherapy is an emerging field for treatment of cancers that involve the immune system. Various forms of therapy have been developed. These include infusion

of either engineered or regular T cells to fight cancer, and injection of cytokines to boost immune responses[109, 110].

Other therapies use the immune reactions of the body and contain cancer vaccines or antibody treatment to inhibit the protein expressed by cancer cells or their counterparts[111, 112]. Notably, clinicians have successfully treated different types of cancer by inhibiting immune checkpoint receptors, such as PD-1 and CTLA-4. Although this strategy has shown enormous potential as a new cancer treatment, few patients showed positive outcomes without relapse or resistances. Therefore, it is necessary to conduct further studies to find potential co-factors, or highly responsive populations, to enhance the therapeutic efficacy of checkpoint blockade treatment and to verify detailed underlying mechanisms.

Recently, several groups of researchers reported the beneficial effect of Tet2 deficiency in tumor progression. The correlation between TET2 expression in immune cells and tumor progression triggered our research team to hypothesize that Tet2 inactivation enhances the antitumor efficiency of $CD8^+$ tumor infiltrating lymphocytes (TILs) by regulating the transcription of key genes involved in T-cell activation and/or exhaustion. I show here, for the first time, that specific Tet2 knock out in cytotoxic T cells reduce melanoma progression significantly in mouse, by increasing the expression of cytokines and innate immune related genes. I further demonstrate that the Tet2-mediated change of chromatin accessibility in certain TF motifs is responsible for its anti-tumor efficacy.

The data presented in this dissertation show strong tumor regression in the Tet2 deleted $CD8^+$ T cells injected group and revealed the relationship between remodeled chromatin accessibility and altered gene expression. However, the results do not link Tet2 and chromatin dynamics directly. To validate how Tet2 activity affects chromatin landscapes, both genome-wide and locus-specific 5hmC distribution should be examined with high resolution.

In chapter II, I introduced a modified sensitive CMS-IP seq method that utilizes an ultra-low amount of DNA. Generally, the isolation efficiency of TILs from a tumor is very low. The conventional 5hmC profiling approaches require up to 10 μg of DNA as a starting material, making them unsuitable for the immunotherapy model setting. By using the sCMS-IP seq technique, researchers can manipulate only the nanogram scale of DNA to successfully map 5hmC. In addition, CiDER can be used to control the formation of 5hmC in *in vivo* to demonstrate that the Tet2-mediated 5hmC deposition is a crucial epigenetic regulatory mechanism to reshape chromatin landscapes.

Along with its drug-inducible epigenome remodeling feature, CiDER can be used for the immunotherapy model presented here to maximize the beneficial effect of Tet2 depletion in TILs. Numerous studies have reported that TET2 is a strong tumor suppressor in many different types of cancer, especially in hematopoietic malignancies (ref). Therefore, it is highly likely to knock out TET2 in hematopoietic system, both the lymphoid and myeloid lineages.

The results presented in Chapter III revealed that the most dramatic changes in Tet2 deficiency at both transcriptome and chromatin structure levels were observed in

the early stage of T cell development during tumorigenesis. Also, Tet2 knock out TILs showed a higher expression of PD-1 and Tim-3 positive population than the WT control group. This suggests that Tet2 disruption shows strong anti-tumor immunity at early time points, then may quickly transition to the exhausted state in the late stage of tumorigenesis. Therefore, temporally controllable Tet2 activity would provide the maximum anti-cancer effect, as well as new avenues of therapeutic intervention.

Overall, this research expands our understanding of a novel tumor-promoting function of Tet2 during melanoma progression in mouse model. I have demonstrated that depletion of Tet2 in $CD8^+$ T cells promotes its anti-cancer immunity by increasing the expression of certain genes that are critical for T cell activation and correlation between transcriptome and chromatin state.

This research brings to light some interesting directions for future work that will extend the scope of the dissertation. First, we can verify whether Tet2 deletion confers specific features that represent a reprogrammable dysfunctional state to T cells. It is reported that tumor-specific $CD8^+$ T cells (TSTs) have two distinctive dysfunctional states, state 1 (reversible, a plastic state) and state 2 (irreversible, a fixed state). The main features of suggested reprogrammable state 1 is increased expression of CD5 and decreased expression of CD38, CD101 and CD30L[107].

The RNA-seq data reported here showed that Tet2 deleted TILs expressed CD5 around 5-fold higher than the counterpart. Also, Tet2KO TILs showed 2-fold less expression of CD38 than WT, suggesting Tet2 deleted $CD8^+$ T cells can maintain its

functional state better than WT $CD8^+$ T cells. As $PD\text{-}1^{hi}$ is another feature of the state 1 T cell, this may explain why the Tet2 disrupted T cells showed high PD-1 expression.

Second, we can extend our immunotherapy model timeline up to 60 days to get a comprehensive understanding of the course of T cells differentiation during tumorigenesis. The data reported here suggest that dynamic changes of both transcriptome and chromatin accessibility were observed in early stage of tumor progression. However, the long-term analysis will provide valuable information about optimal time point for maximizing the therapeutic effects of cancer immunotherapy based on the state of immune cells residing within the tumor.

REFERENCES

1. Wherry, E. J.; Kurachi, M., Molecular and cellular insights into T cell exhaustion. *Nat Rev Immunol* 2015, *15* (8), 486-99.
2. Jiang, Y.; Li, Y.; Zhu, B., T-cell exhaustion in the tumor microenvironment. *Cell Death Dis* 2015, *6*, e1792.
3. Fuertes Marraco, S. A.; Neubert, N. J.; Verdeil, G.; Speiser, D. E., Inhibitory Receptors Beyond T Cell Exhaustion. *Front Immunol* 2015, *6*, 310.
4. Zhang, Z.; Liu, S.; Zhang, B.; Qiao, L.; Zhang, Y., T Cell Dysfunction and Exhaustion in Cancer. *Front Cell Dev Biol* 2020, *8*, 17.
5. Weinstock, M.; McDermott, D., Targeting PD-1/PD-L1 in the treatment of metastatic renal cell carcinoma. *Ther Adv Urol* 2015, *7* (6), 365-77.
6. Shayan, G.; Srivastava, R.; Li, J.; Schmitt, N.; Kane, L. P.; Ferris, R. L., Adaptive resistance to anti-PD1 therapy by Tim-3 upregulation is mediated by the PI3K-Akt pathway in head and neck cancer. *Oncoimmunology* 2017, *6* (1), e1261779.
7. Palmer, C. S.; Ostrowski, M.; Balderson, B.; Christian, N.; Crowe, S. M., Glucose metabolism regulates T cell activation, differentiation, and functions. *Front Immunol* 2015, *6*, 1.
8. Dong, Y.; Sun, Q.; Zhang, X., PD-1 and its ligands are important immune checkpoints in cancer. *Oncotarget* 2017, *8* (2), 2171-2186.

9. Fourcade, J.; Sun, Z.; Benallaoua, M.; Guillaume, P.; Luescher, I. F.; Sander, C.; Kirkwood, J. M.; Kuchroo, V.; Zarour, H. M., Upregulation of Tim-3 and PD-1 expression is associated with tumor antigen-specific CD8+ T cell dysfunction in melanoma patients. *J Exp Med* 2010, *207* (10), 2175-86.

10. Xia, Y.; Chen, R.; Ye, S. L.; Sun, R.; Chen, J.; Zhao, Y., Inhibition of T-cell responses by intratumoral hepatic stellate cells contribute to migration and invasion of hepatocellular carcinoma. *Clin Exp Metastasis* 2011, *28* (7), 661-74.

11. Thornton, A. M.; Shevach, E. M., CD4+CD25+ immunoregulatory T cells suppress polyclonal T cell activation in vitro by inhibiting interleukin 2 production. *J Exp Med* 1998, *188* (2), 287-96.

12. Kim, Y. J.; Park, S. J.; Broxmeyer, H. E., Phagocytosis, a potential mechanism for myeloid-derived suppressor cell regulation of CD8+ T cell function mediated through programmed cell death-1 and programmed cell death-1 ligand interaction. *J Immunol* 2011, *187* (5), 2291-301.

13. Thomas, D. A.; Massagué, J., TGF-beta directly targets cytotoxic T cell functions during tumor evasion of immune surveillance. *Cancer Cell* 2005, *8* (5), 369-80.

14. Savage, P. A.; Leventhal, D. S.; Malchow, S., Shaping the repertoire of tumor-infiltrating effector and regulatory T cells. *Immunol Rev* 2014, *259* (1), 245-58.

15. Matsuzaki, J.; Gnjatic, S.; Mhawech-Fauceglia, P.; Beck, A.; Miller, A.; Tsuji, T.; Eppolito, C.; Qian, F.; Lele, S.; Shrikant, P.; Old, L. J.; Odunsi, K., Tumor-infiltrating NY-ESO-1-specific CD8+ T cells are negatively regulated by LAG-3 and PD-1 in human ovarian cancer. *Proc Natl Acad Sci U S A* 2010, *107* (17), 7875-80.

16. Derré, L.; Rivals, J. P.; Jandus, C.; Pastor, S.; Rimoldi, D.; Romero, P.; Michielin, O.; Olive, D.; Speiser, D. E., BTLA mediates inhibition of human tumor-specific CD8+ T cells that can be partially reversed by vaccination. *J Clin Invest* 2010, *120* (1), 157-67.

17. Chang, D. K.; Peterson, E.; Sun, J.; Goudie, C.; Drapkin, R. I.; Liu, J. F.; Matulonis, U.; Zhu, Q.; Marasco, W. A., Anti-CCR4 monoclonal antibody enhances antitumor immunity by modulating tumor-infiltrating Tregs in an ovarian cancer xenograft humanized mouse model. *Oncoimmunology* 2016, *5* (3), e1090075.

18. Goll, M. G.; Bestor, T. H., Eukaryotic cytosine methyltransferases. *Annu Rev Biochem* 2005, *74*, 481-514.

19. Robertson, K. D., DNA methylation and human disease. *Nat Rev Genet* 2005, *6* (8), 597-610.

20. Tsagaratou, A.; Lio, C. J.; Yue, X.; Rao, A., TET Methylcytosine Oxidases in T Cell and B Cell Development and Function. *Front Immunol* 2017, *8*, 220.

21. Chen, Y.; Zander, R.; Khatun, A.; Schauder, D. M.; Cui, W., Transcriptional and Epigenetic Regulation of Effector and Memory CD8 T Cell Differentiation. *Front Immunol* 2018, *9*, 2826.

22. Bröske, A. M.; Vockentanz, L.; Kharazi, S.; Huska, M. R.; Mancini, E.; Scheller, M.; Kuhl, C.; Enns, A.; Prinz, M.; Jaenisch, R.; Nerlov, C.; Leutz, A.; Andrade-Navarro, M. A.; Jacobsen, S. E.; Rosenbauer, F., DNA methylation protects hematopoietic stem cell multipotency from myeloerythroid restriction. *Nat Genet* 2009, *41* (11), 1207-15.

23. Trowbridge, J. J.; Snow, J. W.; Kim, J.; Orkin, S. H., DNA methyltransferase 1 is essential for and uniquely regulates hematopoietic stem and progenitor cells. *Cell Stem Cell* 2009, *5* (4), 442-9.

24. Kaech, S. M.; Cui, W., Transcriptional control of effector and memory CD8+ T cell differentiation. *Nat Rev Immunol* 2012, *12* (11), 749-61.

25. Chang, J. T.; Wherry, E. J.; Goldrath, A. W., Molecular regulation of effector and memory T cell differentiation. *Nat Immunol* 2014, *15* (12), 1104-15.

26. Wilson, C. B.; Makar, K. W.; Pérez-Melgosa, M., Epigenetic regulation of T cell fate and function. *J Infect Dis* 2002, *185 Suppl 1*, S37-45.

27. Scharer, C. D.; Barwick, B. G.; Youngblood, B. A.; Ahmed, R.; Boss, J. M., Global DNA methylation remodeling accompanies CD8 T cell effector function. *J Immunol* 2013, *191* (6), 3419-29.

28. Abdelsamed, H. A.; Moustaki, A.; Fan, Y.; Dogra, P.; Ghoneim, H. E.; Zebley, C. C.; Triplett, B. M.; Sekaly, R. P.; Youngblood, B., Human memory CD8 T cell effector potential is epigenetically preserved during in vivo homeostasis. *J Exp Med* 2017, *214* (6), 1593-1606.

29. Ko, M.; An, J.; Rao, A., DNA methylation and hydroxymethylation in hematologic differentiation and transformation. *Curr Opin Cell Biol* 2015, *37*, 91-101.

30. Shin, M. S.; You, S.; Kang, Y.; Lee, N.; Yoo, S. A.; Park, K.; Kang, K. S.; Kim, S. H.; Mohanty, S.; Shaw, A. C.; Montgomery, R. R.; Hwang, D.; Kang, I., DNA Methylation Regulates the Differential Expression of CX3CR1 on Human IL-7Rαlow and IL-7Rαhigh Effector Memory CD8+ T Cells with Distinct Migratory Capacities to the Fractalkine. *J Immunol* 2015, *195* (6), 2861-9.

31. Branco, M. R.; Ficz, G.; Reik, W., Uncovering the role of 5-hydroxymethylcytosine in the epigenome. *Nat Rev Genet* 2011, *13* (1), 7-13.

32. Jones, P. A., Functions of DNA methylation: islands, start sites, gene bodies and beyond. *Nat Rev Genet* 2012, *13* (7), 484-92.

33. Fujita, N.; Watanabe, S.; Ichimura, T.; Tsuruzoe, S.; Shinkai, Y.; Tachibana, M.; Chiba, T.; Nakao, M., Methyl-CpG binding domain 1 (MBD1) interacts with the Suv39h1-HP1 heterochromatic complex for DNA methylation-based transcriptional repression. *J Biol Chem* 2003, *278* (26), 24132-8.

34. Okano, M.; Bell, D. W.; Haber, D. A.; Li, E., DNA methyltransferases Dnmt3a and Dnmt3b are essential for de novo methylation and mammalian development. *Cell* 1999, *99* (3), 247-57.

35. Bostick, M.; Kim, J. K.; Estève, P. O.; Clark, A.; Pradhan, S.; Jacobsen, S. E., UHRF1 plays a role in maintaining DNA methylation in mammalian cells. *Science* 2007, *317* (5845), 1760-4.

36. Huang, Y.; Rao, A., Connections between TET proteins and aberrant DNA modification in cancer. *Trends Genet* 2014, *30* (10), 464-74.

37. Pastor, W. A.; Aravind, L.; Rao, A., TETonic shift: biological roles of TET proteins in DNA demethylation and transcription. *Nat Rev Mol Cell Biol* 2013, *14* (6), 341-56.

38. Tsagaratou, A.; Äijö, T.; Lio, C. W.; Yue, X.; Huang, Y.; Jacobsen, S. E.; Lähdesmäki, H.; Rao, A., Dissecting the dynamic changes of 5-hydroxymethylcytosine in T-cell development and differentiation. *Proc Natl Acad Sci U S A* 2014, *111* (32), E3306-15.

39. Pastor, W. A.; Pape, U. J.; Huang, Y.; Henderson, H. R.; Lister, R.; Ko, M.; McLoughlin, E. M.; Brudno, Y.; Mahapatra, S.; Kapranov, P.; Tahiliani, M.; Daley, G. Q.; Liu, X. S.; Ecker, J. R.; Milos, P. M.; Agarwal, S.; Rao, A., Genome-wide mapping of 5-hydroxymethylcytosine in embryonic stem cells. *Nature* 2011, *473* (7347), 394-7.

40. Gu, T. P.; Guo, F.; Yang, H.; Wu, H. P.; Xu, G. F.; Liu, W.; Xie, Z. G.; Shi, L.; He, X.; Jin, S. G.; Iqbal, K.; Shi, Y. G.; Deng, Z.; Szabó, P. E.; Pfeifer, G. P.; Li, J.; Xu, G. L., The role of Tet3 DNA dioxygenase in epigenetic reprogramming by oocytes. *Nature* 2011, *477* (7366), 606-10.

41. Hsu, C. H.; Peng, K. L.; Kang, M. L.; Chen, Y. R.; Yang, Y. C.; Tsai, C. H.; Chu, C. S.; Jeng, Y. M.; Chen, Y. T.; Lin, F. M.; Huang, H. D.; Lu, Y. Y.; Teng, Y. C.; Lin, S. T.; Lin, R. K.; Tang, F. M.; Lee, S. B.; Hsu, H. M.; Yu, J. C.; Hsiao, P. W.; Juan, L. J., TET1 suppresses cancer invasion by activating the tissue inhibitors of metalloproteinases. *Cell Rep* 2012, *2* (3), 568-79.

42. Lian, C. G.; Xu, Y.; Ceol, C.; Wu, F.; Larson, A.; Dresser, K.; Xu, W.; Tan, L.; Hu, Y.; Zhan, Q.; Lee, C. W.; Hu, D.; Lian, B. Q.; Kleffel, S.; Yang, Y.; Neiswender, J.; Khorasani, A. J.; Fang, R.; Lezcano, C.; Duncan, L. M.; Scolyer, R. A.; Thompson, J. F.; Kakavand, H.; Houvras, Y.; Zon, L. I.; Mihm, M. C.; Kaiser, U. B.; Schatton, T.; Woda, B. A.; Murphy, G. F.; Shi, Y. G., Loss of 5-hydroxymethylcytosine is an epigenetic hallmark of melanoma. *Cell* 2012, *150* (6), 1135-46.

43. Dawlaty, M. M.; Breiling, A.; Le, T.; Raddatz, G.; Barrasa, M. I.; Cheng, A. W.; Gao, Q.; Powell, B. E.; Li, Z.; Xu, M.; Faull, K. F.; Lyko, F.; Jaenisch, R., Combined deficiency of Tet1 and Tet2 causes epigenetic abnormalities but is compatible with postnatal development. *Dev Cell* 2013, *24* (3), 310-23.

44. Wu, H.; D'Alessio, A. C.; Ito, S.; Wang, Z.; Cui, K.; Zhao, K.; Sun, Y. E.; Zhang, Y., Genome-wide analysis of 5-hydroxymethylcytosine distribution reveals its dual function in transcriptional regulation in mouse embryonic stem cells. *Genes Dev* 2011, *25* (7), 679-84.

45. Booth, M. J.; Branco, M. R.; Ficz, G.; Oxley, D.; Krueger, F.; Reik, W.; Balasubramanian, S., Quantitative sequencing of 5-methylcytosine and 5-hydroxymethylcytosine at single-base resolution. *Science* 2012, *336* (6083), 934-7.

46. Huang, Y.; Pastor, W. A.; Zepeda-Martínez, J. A.; Rao, A., The anti-CMS technique for genome-wide mapping of 5-hydroxymethylcytosine. *Nat Protoc* 2012, *7* (10), 1897-908.

47. Li, J.; Wu, X.; Zhou, Y.; Lee, M.; Guo, L.; Han, W.; Mo, W.; Cao, W. M.; Sun, D.; Xie, R.; Huang, Y., Decoding the dynamic DNA methylation and hydroxymethylation landscapes in endodermal lineage intermediates during pancreatic differentiation of hESC. *Nucleic Acids Res* 2018, *46* (6), 2883-2900.

48. Huang, Y.; Chavez, L.; Chang, X.; Wang, X.; Pastor, W. A.; Kang, J.; Zepeda-Martínez, J. A.; Pape, U. J.; Jacobsen, S. E.; Peters, B.; Rao, A., Distinct roles of the methylcytosine oxidases Tet1 and Tet2 in mouse embryonic stem cells. *Proc Natl Acad Sci U S A* 2014, *111* (4), 1361-6.

49. Lee, M.; Li, J.; Liang, Y.; Ma, G.; Zhang, J.; He, L.; Liu, Y.; Li, Q.; Li, M.; Sun, D.; Zhou, Y.; Huang, Y., Engineered Split-TET2 Enzyme for Inducible Epigenetic Remodeling. *J Am Chem Soc* 2017, *139* (13), 4659-4662.

50. Zhang, Q.; Zhao, K.; Shen, Q.; Han, Y.; Gu, Y.; Li, X.; Zhao, D.; Liu, Y.; Wang, C.; Zhang, X.; Su, X.; Liu, J.; Ge, W.; Levine, R. L.; Li, N.; Cao, X., Tet2 is required to resolve inflammation by recruiting Hdac2 to specifically repress IL-6. *Nature* 2015, *525* (7569), 389-393.

51. Fu, L.; Guerrero, C. R.; Zhong, N.; Amato, N. J.; Liu, Y.; Liu, S.; Cai, Q.; Ji, D.; Jin, S. G.; Niedernhofer, L. J.; Pfeifer, G. P.; Xu, G. L.; Wang, Y., Tet-mediated formation of 5-hydroxymethylcytosine in RNA. *J Am Chem Soc* 2014, *136* (33), 11582-5.

52. Shen, L.; Song, C. X.; He, C.; Zhang, Y., Mechanism and function of oxidative reversal of DNA and RNA methylation. *Annu Rev Biochem* 2014, *83*, 585-614.

53. Ko, M.; Bandukwala, H. S.; An, J.; Lamperti, E. D.; Thompson, E. C.; Hastie, R.; Tsangaratou, A.; Rajewsky, K.; Koralov, S. B.; Rao, A., Ten-Eleven-Translocation 2 (TET2) negatively regulates homeostasis and differentiation of hematopoietic stem cells in mice. *Proc Natl Acad Sci U S A* 2011, *108* (35), 14566-71.

54. Moran-Crusio, K.; Reavie, L.; Shih, A.; Abdel-Wahab, O.; Ndiaye-Lobry, D.; Lobry, C.; Figueroa, M. E.; Vasanthakumar, A.; Patel, J.; Zhao, X.; Perna, F.; Pandey, S.; Madzo, J.; Song, C.; Dai, Q.; He, C.; Ibrahim, S.; Beran, M.; Zavadil, J.; Nimer, S. D.; Melnick, A.; Godley, L. A.; Aifantis, I.; Levine, R. L., Tet2 loss leads to increased hematopoietic stem cell self-renewal and myeloid transformation. *Cancer Cell* 2011, *20* (1), 11-24.

55. Cimmino, L.; Dawlaty, M. M.; Ndiaye-Lobry, D.; Yap, Y. S.; Bakogianni, S.; Yu, Y.; Bhattacharyya, S.; Shaknovich, R.; Geng, H.; Lobry, C.; Mullenders, J.; King, B.; Trimarchi, T.; Aranda-Orgilles, B.; Liu, C.; Shen, S.; Verma, A. K.; Jaenisch, R.; Aifantis, I., TET1 is a tumor suppressor of hematopoietic malignancy. *Nat Immunol* 2015, *16* (6), 653-62.

56. Ko, M.; Huang, Y.; Jankowska, A. M.; Pape, U. J.; Tahiliani, M.; Bandukwala, H. S.; An, J.; Lamperti, E. D.; Koh, K. P.; Ganetzky, R.; Liu, X. S.; Aravind, L.; Agarwal, S.; Maciejewski, J. P.; Rao, A., Impaired hydroxylation of 5-methylcytosine in myeloid cancers with mutant TET2. *Nature* 2010, *468* (7325), 839-43.

57. Delhommeau, F.; Dupont, S.; Della Valle, V.; James, C.; Trannoy, S.; Massé, A.; Kosmider, O.; Le Couedic, J. P.; Robert, F.; Alberdi, A.; Lécluse, Y.; Plo, I.; Dreyfus, F. J.; Marzac, C.; Casadevall, N.; Lacombe, C.; Romana, S. P.; Dessen, P.; Soulier, J.; Viguié, F.; Fontenay, M.; Vainchenker, W.; Bernard, O. A., Mutation in TET2 in myeloid cancers. *N Engl J Med* 2009, *360* (22), 2289-301.

58. Scourzic, L.; Mouly, E.; Bernard, O. A., TET proteins and the control of cytosine demethylation in cancer. *Genome Med* 2015, *7* (1), 9.

59. Jan, M.; Snyder, T. M.; Corces-Zimmerman, M. R.; Vyas, P.; Weissman, I. L.; Quake, S. R.; Majeti, R., Clonal evolution of preleukemic hematopoietic stem cells precedes human acute myeloid leukemia. *Sci Transl Med* 2012, *4* (149), 149ra118.

60. Ichiyama, K.; Chen, T.; Wang, X.; Yan, X.; Kim, B. S.; Tanaka, S.; Ndiaye-Lobry, D.; Deng, Y.; Zou, Y.; Zheng, P.; Tian, Q.; Aifantis, I.; Wei, L.; Dong, C., The methylcytosine dioxygenase Tet2 promotes DNA demethylation and activation of cytokine gene expression in T cells. *Immunity* 2015, *42* (4), 613-26.

61. Carty, S. A.; Gohil, M.; Banks, L. B.; Cotton, R. M.; Johnson, M. E.; Stelekati, E.; Wells, A. D.; Wherry, E. J.; Koretzky, G. A.; Jordan, M. S., The Loss of TET2 Promotes CD8+ T cell Memory Differentiation. *J Immunol* 2018, *200* (1), 82-91.

62. Fraietta, J. A.; Nobles, C. L.; Sammons, M. A.; Lundh, S.; Carty, S. A.; Reich, T. J.; Cogdill, A. P.; Morrissette, J. J. D.; DeNizio, J. E.; Reddy, S.; Hwang, Y.; Gohil, M.; Kulikovskaya, I.; Nazimuddin, F.; Gupta, M.; Chen, F.; Everett, J. K.; Alexander, K. A.; Lin-Shiao, E.; Gee, M. H.; Liu, X.; Young, R. M.; Ambrose, D.; Wang, Y.; Xu, J.; Jordan, M. S.; Marcucci, K. T.; Levine, B. L.; Garcia, K. C.; Zhao, Y.; Kalos, M.; Porter, D. L.; Kohli, R. M.; Lacey, S. F.; Berger, S. L.; Bushman, F. D.; June, C. H.; Melenhorst, J. J., Disruption of TET2 promotes the therapeutic efficacy of CD19-targeted T cells. *Nature* 2018, *558* (7709), 307-312.

63. Zang, S.; Li, J.; Yang, H.; Zeng, H.; Han, W.; Zhang, J.; Lee, M.; Moczygemba, M.; Isgandarova, S.; Yang, Y.; Zhou, Y.; Rao, A.; You, M. J.; Sun, D.; Huang, Y., Mutations in 5-methylcytosine oxidase TET2 and RhoA cooperatively disrupt T cell homeostasis. *J Clin Invest* 2017, *127* (8), 2998-3012.

64. Pan, W.; Zhu, S.; Qu, K.; Meeth, K.; Cheng, J.; He, K.; Ma, H.; Liao, Y.; Wen, X.; Roden, C.; Tobiasova, Z.; Wei, Z.; Zhao, J.; Liu, J.; Zheng, J.; Guo, B.; Khan, S. A.; Bosenberg, M.; Flavell, R. A.; Lu, J., The DNA Methylcytosine Dioxygenase Tet2 Sustains Immunosuppressive Function of Tumor-Infiltrating Myeloid Cells to Promote Melanoma Progression. *Immunity* 2017, *47* (2), 284-297.e5.

65. Tahiliani, M.; Koh, K. P.; Shen, Y.; Pastor, W. A.; Bandukwala, H.; Brudno, Y.; Agarwal, S.; Iyer, L. M.; Liu, D. R.; Aravind, L.; Rao, A., Conversion of 5-methylcytosine to 5-hydroxymethylcytosine in mammalian DNA by MLL partner TET1. *Science* 2009, *324* (5929), 930-5.

66. He, Y. F.; Li, B. Z.; Li, Z.; Liu, P.; Wang, Y.; Tang, Q.; Ding, J.; Jia, Y.; Chen, Z.; Li, L.; Sun, Y.; Li, X.; Dai, Q.; Song, C. X.; Zhang, K.; He, C.; Xu, G. L., Tet-mediated formation of 5-carboxylcytosine and its excision by TDG in mammalian DNA. *Science* 2011, *333* (6047), 1303-7.

67. Ito, S.; Shen, L.; Dai, Q.; Wu, S. C.; Collins, L. B.; Swenberg, J. A.; He, C.; Zhang, Y., Tet proteins can convert 5-methylcytosine to 5-formylcytosine and 5-carboxylcytosine. *Science* 2011, *333* (6047), 1300-3.

68. Spruijt, C. G.; Gnerlich, F.; Smits, A. H.; Pfaffeneder, T.; Jansen, P. W.; Bauer, C.; Munzel, M.; Wagner, M.; Muller, M.; Khan, F.; Eberl, H. C.; Mensinga, A.; Brinkman, A. B.; Lephikov, K.; Muller, U.; Walter, J.; Boelens, R.; van Ingen, H.; Leonhardt, H.; Carell, T.; Vermeulen, M., Dynamic readers for 5-(hydroxy)methylcytosine and its oxidized derivatives. *Cell* 2013, *152* (5), 1146-59.

69. Lio, C. W.; Zhang, J.; Gonzalez-Avalos, E.; Hogan, P. G.; Chang, X.; Rao, A., Tet2 and Tet3 cooperate with B-lineage transcription factors to regulate DNA modification and chromatin accessibility. *Elife* 2016, *5*.

70. Kellinger, M. W.; Song, C. X.; Chong, J.; Lu, X. Y.; He, C.; Wang, D., 5-formylcytosine and 5-carboxylcytosine reduce the rate and substrate specificity of RNA polymerase II transcription. *Nat Struct Mol Biol* 2012, *19* (8), 831-3.

71. Su, M.; Kirchner, A.; Stazzoni, S.; Muller, M.; Wagner, M.; Schroder, A.; Carell, T., 5-Formylcytosine Could Be a Semipermanent Base in Specific Genome Sites. *Angew Chem Int Ed Engl* 2016, *55* (39), 11797-800.

72. Lu, X.; Zhao, B. S.; He, C., TET family proteins: oxidation activity, interacting molecules, and functions in diseases. *Chem Rev* 2015, *115* (6), 2225-39.

73. Busque, L.; Patel, J. P.; Figueroa, M. E.; Vasanthakumar, A.; Provost, S.; Hamilou, Z.; Mollica, L.; Li, J.; Viale, A.; Heguy, A.; Hassimi, M.; Socci, N.; Bhatt, P. K.; Gonen, M.; Mason, C. E.; Melnick, A.; Godley, L. A.; Brennan, C. W.; Abdel-Wahab, O.; Levine, R. L., Recurrent somatic TET2 mutations in normal elderly individuals with clonal hematopoiesis. *Nat Genet* 2012, *44* (11), 1179-81.

74. Shen, Q.; Zhang, Q.; Shi, Y.; Shi, Q.; Jiang, Y.; Gu, Y.; Li, Z.; Li, X.; Zhao, K.; Wang, C.; Li, N.; Cao, X., Tet2 promotes pathogen infection-induced myelopoiesis through mRNA oxidation. *Nature* 2018, *554* (7690), 123-127.

75. Huang, Y.; Pastor, W. A.; Shen, Y.; Tahiliani, M.; Liu, D. R.; Rao, A., The behaviour of 5-hydroxymethylcytosine in bisulfite sequencing. *PLoS One* 2010, *5* (1), e8888.

76. Buenrostro, J. D.; Giresi, P. G.; Zaba, L. C.; Chang, H. Y.; Greenleaf, W. J., Transposition of native chromatin for fast and sensitive epigenomic profiling of open chromatin, DNA-binding proteins and nucleosome position. *Nat Methods* 2013, *10* (12), 1213-8.

77. Zhang, Y.; Liu, T.; Meyer, C. A.; Eeckhoute, J.; Johnson, D. S.; Bernstein, B. E.; Nusbaum, C.; Myers, R. M.; Brown, M.; Li, W.; Liu, X. S., Model-based analysis of ChIP-Seq (MACS). *Genome Biol* 2008, *9* (9), R137.

78. Love, M. I.; Huber, W.; Anders, S., Moderated estimation of fold change and dispersion for RNA-seq data with DESeq2. *Genome Biol* 2014, *15* (12), 550.

79. McLean, C. Y.; Bristor, D.; Hiller, M.; Clarke, S. L.; Schaar, B. T.; Lowe, C. B.; Wenger, A. M.; Bejerano, G., GREAT improves functional interpretation of cis-regulatory regions. *Nat Biotechnol* 2010, *28* (5), 495-501.

80. Langemeijer, S. M.; Kuiper, R. P.; Berends, M.; Knops, R.; Aslanyan, M. G.; Massop, M.; Stevens-Linders, E.; van Hoogen, P.; van Kessel, A. G.; Raymakers, R. A.; Kamping, E. J.; Verhoef, G. E.; Verburgh, E.; Hagemeijer, A.; Vandenberghe, P.; de Witte, T.; van der Reijden, B. A.; Jansen, J. H., Acquired mutations in TET2 are common in myelodysplastic syndromes. *Nat Genet* 2009, *41* (7), 838-42.

81. Hashimoto, H.; Pais, J. E.; Zhang, X.; Saleh, L.; Fu, Z. Q.; Dai, N.; Corrêa, I. R.; Zheng, Y.; Cheng, X., Structure of a Naegleria Tet-like dioxygenase in complex with 5-methylcytosine DNA. *Nature* 2014, *506* (7488), 391-5.

82. Hu, L.; Li, Z.; Cheng, J.; Rao, Q.; Gong, W.; Liu, M.; Shi, Y. G.; Zhu, J.; Wang, P.; Xu, Y., Crystal structure of TET2-DNA complex: insight into TET-mediated 5mC oxidation. *Cell* 2013, *155* (7), 1545-55.

83. Banaszynski, L. A.; Liu, C. W.; Wandless, T. J., Characterization of the FKBP.rapamycin.FRB ternary complex. *J Am Chem Soc* 2005, *127* (13), 4715-21.

84. Clackson, T.; Yang, W.; Rozamus, L. W.; Hatada, M.; Amara, J. F.; Rollins, C. T.; Stevenson, L. F.; Magari, S. R.; Wood, S. A.; Courage, N. L.; Lu, X.; Cerasoli, F.; Gilman, M.; Holt, D. A., Redesigning an FKBP-ligand interface to generate chemical dimerizers with novel specificity. *Proc Natl Acad Sci U S A* 1998, *95* (18), 10437-42.

85. Ibrahimi, A.; Vande Velde, G.; Reumers, V.; Toelen, J.; Thiry, I.; Vandeputte, C.; Vets, S.; Deroose, C.; Bormans, G.; Baekelandt, V.; Debyser, Z.; Gijsbers, R., Highly efficient multicistronic lentiviral vectors with peptide 2A sequences. *Hum Gene Ther* 2009, *20* (8), 845-60.

86. Kim, J. H.; Lee, S. R.; Li, L. H.; Park, H. J.; Park, J. H.; Lee, K. Y.; Kim, M. K.; Shin, B. A.; Choi, S. Y., High cleavage efficiency of a 2A peptide derived from porcine teschovirus-1 in human cell lines, zebrafish and mice. *PLoS One* 2011, *6* (4), e18556.

87. Bogdanović, O.; Smits, A. H.; de la Calle Mustienes, E.; Tena, J. J.; Ford, E.; Williams, R.; Senanayake, U.; Schultz, M. D.; Hontelez, S.; van Kruijsbergen, I.; Rayon, T.; Gnerlich, F.; Carell, T.; Veenstra, G. J.; Manzanares, M.; Sauka-Spengler, T.; Ecker, J. R.; Vermeulen, M.; Gómez-Skarmeta, J. L.; Lister, R., Active DNA demethylation at enhancers during the vertebrate phylotypic period. *Nat Genet* 2016, *48* (4), 417-26.

88. Szulwach, K. E.; Li, X.; Li, Y.; Song, C. X.; Han, J. W.; Kim, S.; Namburi, S.; Hermetz, K.; Kim, J. J.; Rudd, M. K.; Yoon, Y. S.; Ren, B.; He, C.; Jin, P., Integrating 5-hydroxymethylcytosine into the epigenomic landscape of human embryonic stem cells. *PLoS Genet* 2011, *7* (6), e1002154.

89. Pastor, W. A.; Huang, Y.; Henderson, H. R.; Agarwal, S.; Rao, A., The GLIB technique for genome-wide mapping of 5-hydroxymethylcytosine. *Nat Protoc* 2012, *7* (10), 1909-17.

90. Ghoneim, H. E.; Fan, Y.; Moustaki, A.; Abdelsamed, H. A.; Dash, P.; Dogra, P.; Carter, R.; Awad, W.; Neale, G.; Thomas, P. G.; Youngblood, B., De Novo Epigenetic Programs Inhibit PD-1 Blockade-Mediated T Cell Rejuvenation. *Cell* 2017, *170* (1), 142-157.e19.

91. Jung, H.; Kim, H. S.; Kim, J. Y.; Sun, J. M.; Ahn, J. S.; Ahn, M. J.; Park, K.; Esteller, M.; Lee, S. H.; Choi, J. K., DNA methylation loss promotes immune evasion of tumours with high mutation and copy number load. *Nat Commun* 2019, *10* (1), 4278.

92. Fang, S.; Li, J.; Xiao, Y.; Lee, M.; Guo, L.; Han, W.; Li, T.; Hill, M. C.; Hong, T.; Mo, W.; Xu, R.; Zhang, P.; Wang, F.; Chang, J.; Zhou, Y.; Sun, D.; Martin, J. F.; Huang, Y., Tet inactivation disrupts YY1 binding and long-range chromatin interactions during embryonic heart development. *Nat Commun* 2019, *10* (1), 4297.

93. Rasmussen, K. D.; Berest, I.; Keβler, S.; Nishimura, K.; Simón-Carrasco, L.; Vassiliou, G. S.; Pedersen, M. T.; Christensen, J.; Zaugg, J. B.; Helin, K., TET2 binding to enhancers facilitates transcription factor recruitment in hematopoietic cells. *Genome Res* 2019, *29* (4), 564-575.

94. Koh, K. P.; Rao, A., DNA methylation and methylcytosine oxidation in cell fate decisions. *Curr Opin Cell Biol* 2013, *25* (2), 152-61.

95. Sohni, A.; Bartoccetti, M.; Khoueiry, R.; Spans, L.; Vande Velde, J.; De Troyer, L.; Pulakanti, K.; Claessens, F.; Rao, S.; Koh, K. P., Dynamic switching of active promoter and enhancer domains regulates Tet1 and Tet2 expression during cell state transitions between pluripotency and differentiation. *Mol Cell Biol* 2015, *35* (6), 1026-42.

96. Li, Z.; Cai, X.; Cai, C. L.; Wang, J.; Zhang, W.; Petersen, B. E.; Yang, F. C.; Xu, M., Deletion of Tet2 in mice leads to dysregulated hematopoietic stem cells and subsequent development of myeloid malignancies. *Blood* 2011, *118* (17), 4509-18.

97. Mognol, G. P.; Spreafico, R.; Wong, V.; Scott-Browne, J. P.; Togher, S.; Hoffmann, A.; Hogan, P. G.; Rao, A.; Trifari, S., Exhaustion-associated regulatory regions in CD8. *Proc Natl Acad Sci U S A* 2017, *114* (13), E2776-E2785.

98. Falo, L. D.; Kovacsovics-Bankowski, M.; Thompson, K.; Rock, K. L., Targeting antigen into the phagocytic pathway in vivo induces protective tumour immunity. *Nat Med* 1995, *1* (7), 649-53.

99. Schoenborn, J. R.; Wilson, C. B., Regulation of interferon-gamma during innate and adaptive immune responses. *Adv Immunol* 2007, *96*, 41-101.

100. Sheppard, K. A.; Fitz, L. J.; Lee, J. M.; Benander, C.; George, J. A.; Wooters, J.; Qiu, Y.; Jussif, J. M.; Carter, L. L.; Wood, C. R.; Chaudhary, D., PD-1 inhibits T-cell receptor induced phosphorylation of the ZAP70/CD3zeta signalosome and downstream signaling to PKCtheta. *FEBS Lett* 2004, *574* (1-3), 37-41.

101. Topalian, S. L.; Hodi, F. S.; Brahmer, J. R.; Gettinger, S. N.; Smith, D. C.; McDermott, D. F.; Powderly, J. D.; Carvajal, R. D.; Sosman, J. A.; Atkins, M. B.; Leming, P. D.; Spigel, D. R.; Antonia, S. J.; Horn, L.; Drake, C. G.; Pardoll, D. M.; Chen, L.; Sharfman, W. H.; Anders, R. A.; Taube, J. M.; McMiller, T. L.; Xu, H.; Korman, A. J.; Jure-Kunkel, M.; Agrawal, S.; McDonald, D.; Kollia, G. D.; Gupta, A.; Wigginton, J. M.; Sznol, M., Safety, activity, and immune correlates of anti-PD-1 antibody in cancer. *N Engl J Med* 2012, *366* (26), 2443-54.

102. Hamid, O.; Robert, C.; Daud, A.; Hodi, F. S.; Hwu, W. J.; Kefford, R.; Wolchok, J. D.; Hersey, P.; Joseph, R. W.; Weber, J. S.; Dronca, R.; Gangadhar, T. C.; Patnaik, A.; Zarour, H.; Joshua, A. M.; Gergich, K.; Elassaiss-Schaap, J.; Algazi, A.; Mateus, C.; Boasberg, P.; Tumeh, P. C.; Chmielowski, B.; Ebbinghaus, S. W.; Li, X. N.; Kang, S. P.; Ribas, A., Safety and tumor responses with lambrolizumab (anti-PD-1) in melanoma. *N Engl J Med* 2013, *369* (2), 134-44.

103. Ishida, Y.; Agata, Y.; Shibahara, K.; Honjo, T., Induced expression of PD-1, a novel member of the immunoglobulin gene superfamily, upon programmed cell death. *EMBO J* 1992, *11* (11), 3887-95.

104. Bardhan, K.; Anagnostou, T.; Boussiotis, V. A., The PD1:PD-L1/2 Pathway from Discovery to Clinical Implementation. *Front Immunol* 2016, *7*, 550.

105. Atsaves, V.; Leventaki, V.; Rassidakis, G. Z.; Claret, F. X., AP-1 Transcription Factors as Regulators of Immune Responses in Cancer. *Cancers (Basel)* 2019, *11* (7).

106. Gallant, S.; Gilkeson, G., ETS transcription factors and regulation of immunity. *Arch Immunol Ther Exp (Warsz)* 2006, *54* (3), 149-63.

107. Philip, M.; Fairchild, L.; Sun, L.; Horste, E. L.; Camara, S.; Shakiba, M.; Scott, A. C.; Viale, A.; Lauer, P.; Merghoub, T.; Hellmann, M. D.; Wolchok, J. D.; Leslie, C. S.; Schietinger, A., Chromatin states define tumour-specific T cell dysfunction and reprogramming. *Nature* 2017, *545* (7655), 452-456.

108. Ko, M.; An, J.; Pastor, W. A.; Koralov, S. B.; Rajewsky, K.; Rao, A., TET proteins and 5-methylcytosine oxidation in hematological cancers. *Immunol Rev* 2015, *263* (1), 6-21.

109. Showalter, A.; Limaye, A.; Oyer, J. L.; Igarashi, R.; Kittipatarin, C.; Copik, A. J.; Khaled, A. R., Cytokines in immunogenic cell death: Applications for cancer immunotherapy. *Cytokine* 2017, *97*, 123-132.

110. Yang, J. C.; Rosenberg, S. A., Adoptive T-Cell Therapy for Cancer. *Adv Immunol* 2016, *130*, 279-94.

111. Gatti-Mays, M. E.; Redman, J. M.; Collins, J. M.; Bilusic, M., Cancer vaccines: Enhanced immunogenic modulation through therapeutic combinations. *Hum Vaccin Immunother* 2017, *13* (11), 2561-2574.

112. Rogers, L. M.; Veeramani, S.; Weiner, G. J., Complement in monoclonal antibody therapy of cancer. *Immunol Res* 2014, *59* (1-3), 203-10.